NASA/CR—2001–211045

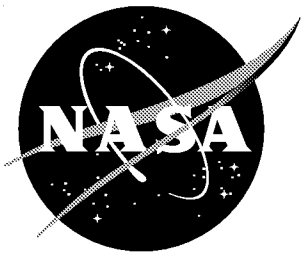

Experimental Structural Dynamic Response of Plate Specimens Due to Sonic Loads in a Progressive Wave Tube

Juan F. Betts
Lockheed Martin Corporation, Hampton, Virginia

August 2001

The NASA STI Program Office ... in Profile

Since its founding, NASA has been dedicated to the advancement of aeronautics and space science. The NASA Scientific and Technical Information (STI) Program Office plays a key part in helping NASA maintain this important role.

The NASA STI Program Office is operated by Langley Research Center, the lead center for NASA's scientific and technical information. The NASA STI Program Office provides access to the NASA STI Database, the largest collection of aeronautical and space science STI in the world. The Program Office is also NASA's institutional mechanism for disseminating the results of its research and development activities. These results are published by NASA in the NASA STI Report Series, which includes the following report types:

- TECHNICAL PUBLICATION. Reports of completed research or a major significant phase of research that present the results of NASA programs and include extensive data or theoretical analysis. Includes compilations of significant scientific and technical data and information deemed to be of continuing reference value. NASA counterpart of peer-reviewed formal professional papers, but having less stringent limitations on manuscript length and extent of graphic presentations.

- TECHNICAL MEMORANDUM. Scientific and technical findings that are preliminary or of specialized interest, e.g., quick release reports, working papers, and bibliographies that contain minimal annotation. Does not contain extensive analysis.

- CONTRACTOR REPORT. Scientific and technical findings by NASA-sponsored contractors and grantees.

- CONFERENCE PUBLICATION. Collected papers from scientific and technical conferences, symposia, seminars, or other meetings sponsored or co-sponsored by NASA.

- SPECIAL PUBLICATION. Scientific, technical, or historical information from NASA programs, projects, and missions, often concerned with subjects having substantial public interest.

- TECHNICAL TRANSLATION. English-language translations of foreign scientific and technical material pertinent to NASA's mission.

Specialized services that complement the STI Program Office's diverse offerings include creating custom thesauri, building customized databases, organizing and publishing research results ... even providing videos.

For more information about the NASA STI Program Office, see the following:

- Access the NASA STI Program Home Page at ***http://www.sti.nasa.gov***

- E-mail your question via the Internet to help@sti.nasa.gov

- Fax your question to the NASA STI Help Desk at (301) 621-0134

- Phone the NASA STI Help Desk at (301) 621-0390

- Write to:
  NASA STI Help Desk
  NASA Center for AeroSpace Information
  7121 Standard Drive
  Hanover, MD 21076-1320

NASA/CR—2001–211045

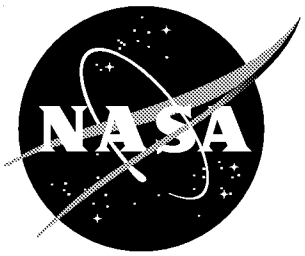

Experimental Structural Dynamic Response of Plate Specimens Due to Sonic Loads in a Progressive Wave Tube

Juan F. Betts
Lockheed Martin Corporation, Hampton, Virginia

National Aeronautics and
Space Administration

Langley Research Center
Hampton, Virginia 23681-2199

Prepared for Langley Research Center
under Contract NAS1-00135, Task Order DF26

August 2001

Acknowledgments

A special thanks to Mr. Jay Robinson and Dr. Steve Rizzi from the Structural Acoustic Branch at NASA Langley Research Center for their guidance and support of this effort. The author also wishes to acknowledge the efforts of Mr. John Swartzbaugh and Mr. Donald Smith of the Gas Fluid & Acoustic Research Support Branch at the NASA Langley Research Center for their work in configuring and operating the Thermal Acoustic Fatigue Apparatus (TAFA) during this activity. He also wishes to thank Mr. Carl Davis of Wyle Laboratories, Hampton for various instrumentation support.

Available from:

NASA Center for AeroSpace Information (CASI)
7121 Standard Drive
Hanover, MD 21076-1320
(301) 621-0390

National Technical Information Service (NTIS)
5285 Port Royal Road
Springfield, VA 22161-2171
(703) 605-6000

Abstract

The objective of the current study was to assess the repeatability of experiments at NASA Langley's Thermal Acoustic Fatigue Apparatus (TAFA) facility and to use these experiments to validate numerical models. To this end experiments were conducted in this progressive wave tube (PWT) facility's four-modulator configuration.

Experiments show that power spectral density (PSD) curves were repeatable except at the resonant frequencies, which tended to vary between 5Hz to 15Hz. Results show that the thinner specimen had more variability in the resonant frequency location than the thicker sample, especially for modes higher than the first mode in the frequency range.

Absolute Percent Errors (APEs) and Mean Absolute Percent Errors (MAPEs) were calculated to increase to normalize the error results and increase the statistical population size. MAPE results indicated that errors were largely insensitive to the location in the sample, but were very sensitive to the magnitude of the response. Therefore, resonant frequencies and higher OASPL tended to produce higher MAPEs.

The time of the day (morning or afternoon) that the plate specimens were tested affected their dynamic resonant response. The only change between morning and afternoon tests was possibly the air temperature in the PWT. Therefore, it stands to reason, that the air being fed to the PWT warmed up during day affecting the dynamic response of the plates at the resonant frequencies. The torquing sequence used to clamp the plates was changed from day to day, and yet the resonant responses were repeatable for the thicker 0.125in (0.318cm) plate. Therefore, torquing sequence did not affect the dynamic response of the thicker plate. The thinner 0.062in (0.1588cm) plate's resonant dynamic response was affected by torquing sequence.

Root Mean Square (RMS) (the area under the PSD curves) tended to be more repeatable. The RMS accelerations increased with SPL and the specimen tended to behave "linearly" through the SPL range of 135 to 153dB. Standard Deviations (STDs) of the results tended to be relatively low constant up to about 147dB.

Comparing the variability of the RMS vs. PSD results, the RMS results were more repeatable. The STD results were less than 10% of the RMS results for both the 0.125in (0.318cm) and 0.062in (0.1588cm) thick plate. The STD of the PSD results were

around 20% to 100% of the mean PSD results for non-resonant and resonant frequencies, respectively, for the 0.125in (0.318cm) thicker plate and between 25% to 125% of the mean PSD results, for nonresonant and resonant frequencies, respectively, for the thinner plate.

Table of Contents

List of Figures and Tables

List of Variables and Abbreviations

APE	absolute percent error
cm	centimeters
dB	decibel
f	frequency
g	$9.8 m/s^2$ (the acceleration due to gravity)
G_{xx}	double-sided frequency domain autocorrelation function or PSD function
In	inches
lb	pounds
m	meters
MAPE	mean absolute percent error
N	Newtons
OASPL	Overall Sound Pressure Level
Pa	Pascals
PSD	power spectral density
PWT	progressive wave tube
RMS	root mean square
R_{xx}	single sided time domain autocorrelation function
s	seconds
SPL	sound pressure level
STD	standard deviation
S_{xx}	single-sided frequency domain autocorrelation function or PSD function
S_{xy}	single-sided frequency domain crosscorrelation function
T	period
TAFA	Thermal Acoustic Fatigue Apparatus
γ^2	coherence function
ω	circular frequency (equals $2\pi f$)
π	pie (equals 3.14159265…)
μ	mean of data
σ	standard deviation of data

Throughout this report both English and SI units are used. English units are followed by the equivalent SI value and unit in parenthesis. The report follows an $e^{+i\omega t}$ convention unless otherwise indicated. References are located at the end of each chapter for reader's ease.

1. Introduction

The Thermal Acoustic Fatigue Apparatus (TAFA) is a progressive wave tube (PWT) facility at the NASA Langley Research Center. This facility is used to test specimens dynamic response under high intensity acoustic noise environment with or without a high temperature option. The overall sound pressure level (SPL) incident on the tested specimen is maintained through a closed loop control system.[1,2] The dynamic response of the specimen can be acquired with accelerometers, scanning laser vibrometer, and strain gages, or a combination of these transducers. In this report acoustic measurements were acquired with a leading and trailing edge microphone, and the plate dynamic response was acquired using five accelerometers.

The experimental assessment of the dynamic response of plate specimens at TAFA documented in this report, follows last year's documentation of improvements to the facility through the use of closed-loop control by Rizzi.[1] Rizzi documents the performance of the newly installed acoustic source controller to a variety of desired control signals.

The object of the report was to assess the repeatability of the experimental dynamic response of specimens at TAFA and provide a quality database to validate numerical models. To this end experiments were conducted in the facility's four-modulator reduced configuration.[3] A schematic and picture of the facility is shown in Figs. 1-1 and 1-2, respectively.

This report utilizes the analysis of the first (mean) and second (variance) moment statistical characteristics of power spectral density (PSD) and the root mean square (RMS) of the experimental acceleration results as a framework to document several important findings. The report investigates such things as the "linear" range of dynamic response, bolt torque effects when mounting specimens to the test section (boundary condition effects), and the effect of source deviation to the desired control signal.

Prior to 1994 the facility supported the development of thermal protection system for the Space Shuttle and the National Aerospace Plane. After 1994 the facility underwent several improvements and supported sonic fatigue studies of the wing strake subcomponents on the High Speed Civil Transport.

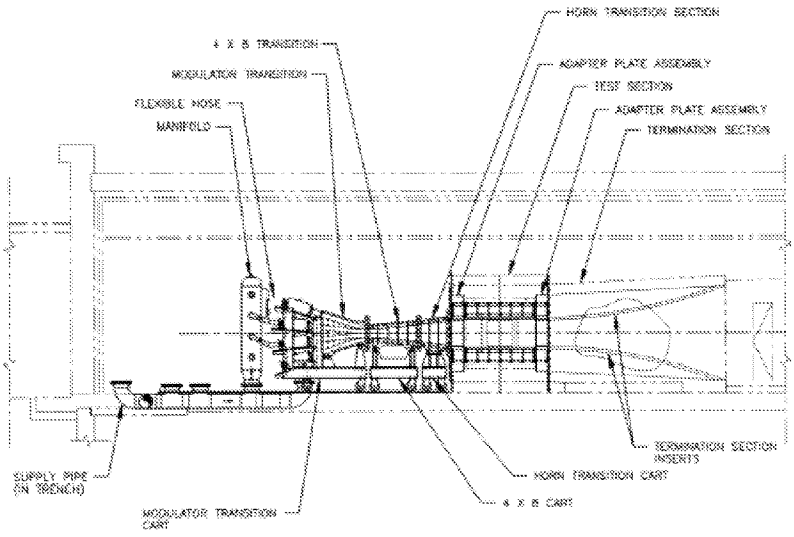

Figure 1-1. Schematic of TAFA in the four-modulator reduced configuration.

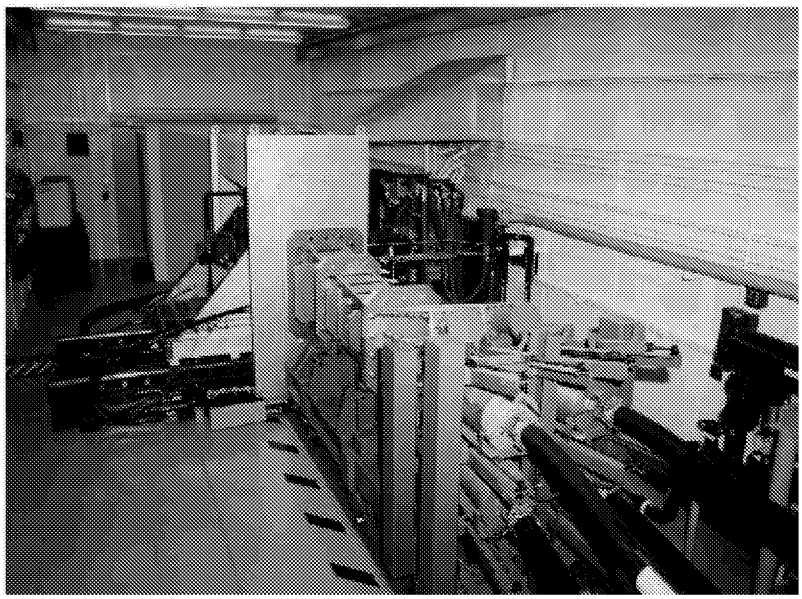

Figure 1-2. Picture of TAFA in the four-modulator reduced configuration.

References

1. Rizzi, S.A., "Improvements To Progressive Wave Tube Performance Through Closed-Loop Control," NASA/TM-2000-210623, October 2000.
2. "VibControl/NT, revision 2.4.0 Manual," M+P International, Inc. 1999.

3. Rizzi,S.A., and Turner,T.L., "Enhanced Capabilities of The NASA Langley Thermal Acoustic Fatigue Apparatus," Sixth International Conference on Recent Advances in Structural Dynamics, Southampton, England, July 1997, pp. 15.

2. Experimental Setup

2.1 TAFA Characteristics and Experimental Matrix

In order to produce the acoustic signal, a signal generator in the control system generated a prescribed acoustic spectrum. Characteristics of the acoustic source and control mechanism are addressed in Section 3.1. For the tests evaluated in this report the signal was a broadband white noise spectrum signal with a frequency range of 50 to 450Hz. The signal from the signal generator is amplified with Crown amplifiers[1], and acoustic modulators generate the acoustic signal.[2] Air is fed through hoses attached to the modulators at 14 lb/s (62.27 N/s) and the acoustic wave with mean flow travels down the PWT.

Two microphones are located along the wall of the PWT one on the leading edge before the specimen to be tested and one at the trailing edge after the specimen. These microphone signals become the control reference signal. For the experiments in this report, the spectrums from the two microphones were averaged and the overall desired control SPL was specified. The specified OASPL started at 135dB (the facility noise floor) and incremented in 6dB increments until 159dB. The maximum OASPL range prescribed by the manufacturer for the microphone amplitude signal is 165dB[3] or 6dB higher than the maximum OASPL used for the tests in this report.[4]

Five tests were conducted for the 0.125 inch (0.318 cm) plate and four tests were conducted for the 0.0625 inch (0.1588 cm) plate, for a total of nine tests. The plates were rigidly clamped to the mounting fixture. To assess the clamping plate-fixture boundary condition effect on the dynamic response, two torque patterns were used.

Torque pattern one started torquing the bolts from the lower left corner up and right simultaneously and ending at the upper right corner of the plate. Torque pattern two also started in the lower left hand corner of the plate and bolts were torqued counter clockwise. Bolts were torqued to 100 in-lb (1129.84 cm-N) for both torque patterns. Figure 2-1 shows a schematic of these two torque patterns. Two tests were conducted on each day, with the same torque pattern. The same test was then repeated the next day with the torque pattern changed. This same procedure was then repeated for the next plate

thickness.

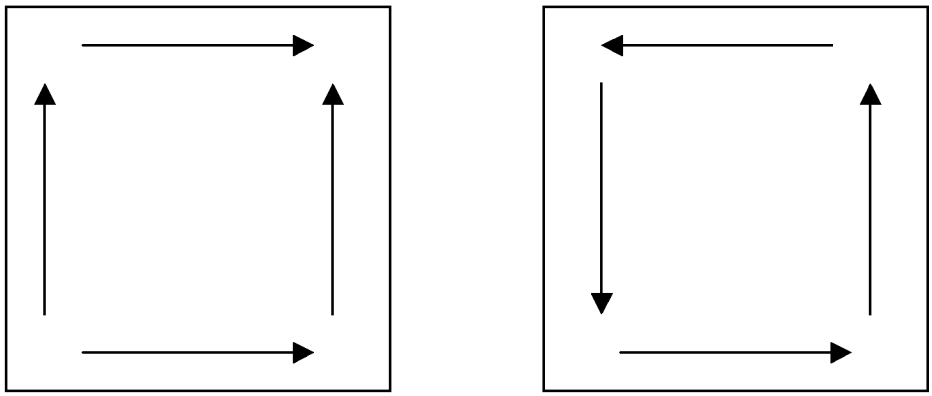

Figure 2-1. Torquing pattern 1 and 2 respectively used to clamp the plates.

Table 2-1. Experimental Schedule

Date	Thickness (in.)	Torque Sequence	Run Number
1-Morning	0.125 (0.3175 cm)	1	1
1-Afternoon	0.125 (0.3175 cm)	Not changed	2
2-Morning	0.125 (0.3175 cm)	2	3
2-Afternoon	0.125 (0.3175 cm)	Not changed	4
3-Morning	0.062 (0.15875 cm)	1	1
3-Afternoon	0.062 (0.15875 cm)	Not changed	2
4-Morning	0.062 (0.15875 cm)	2	3
4-Afternoon	0.062 (0.15875 cm)	Not changed	4
5-Morning	0.125 (0.3175 cm)	1	5

Table 2-1 shows the experimental schedule for the plate specimens. It is assumed for the purpose of this section, that time of the test and torque sequence used have no appreciable effects on the experimental results. Therefore the experiments performed belong to two statistical populations, one for the 0.125 inch (0.3175 cm) specimen and

the other for the 0.062 inch (0.15875 cm) specimen. Consequently, there were five and four repeat runs for the 0.125in (0.3175 cm) and 0.062 inch (0.15875 cm) thick specimens, respectively.

The run numbers are numbered according to the schedule in Table 2-1. For example, Run 1 and 2 for the 0.125inch (0.3175 cm) specimen would be the experiments performed on Date 1 morning and afternoon, respectively, and for the 0.062 inch (0.15875 cm) specimen Run 1 and 2 would he the tests performed on Date 3 morning and afternoon, respectively.

To determine the dynamic response of the plate, five 353B15 PCB accelerometers were used to measure the acceleration response of the plate to the excitation acoustic spectrum. The PSD was used as the basis for analyzing the repeatability of the dynamic response of the plate. Figure 2-2 and Table 2-2 show the accelerometer locations in the plate specimen. The x and y location in Table 2-2 refers to the horizontal and vertical distance, respectively, from the bottom left corner of the plate specimens. The maximum allowed acceleration for the accelerometers determined by the manufacturer is 500gs.[5]

Table 2-2. Accelerometer locations in the plate specimens.

Accelerometer	x-location (in)	y-location (in)
1	16.44 (41.76 cm)	16.44 (41.76 cm)
2	12.75 (32.39 cm)	16.44 (41.76 cm)
3	16.44 (41.76 cm)	12.75 (32.39 cm)
4	8.56 (21.74 cm)	12.75 (32.39 cm)
5	8.56 (21.74 cm)	8.56 (21.74 cm)

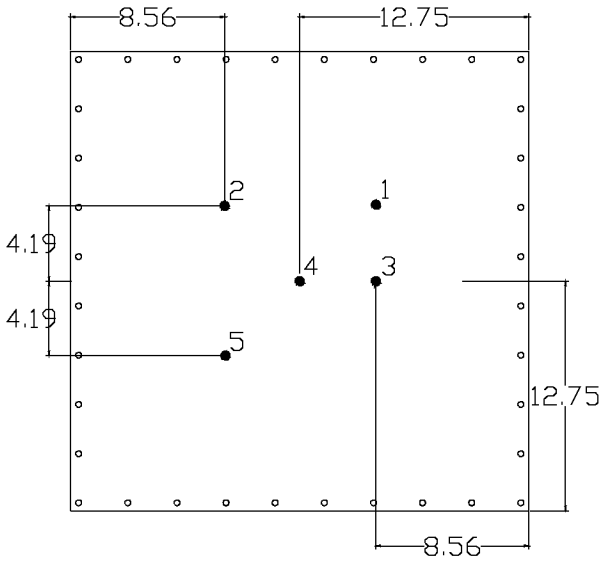

Figure 2-2. Accelerometer placement on the plate.

2.2 Specimen and Support Characteristics

Experiments were performed on 2024 T3 Aluminum plates specimens. These plates were 25.5 x 25.5 inches (64.77 x 64.77 cm) with thicknesses of 0.0625 (0.1587 cm) and 0.125 inches (0.3175 cm), respectively as seen in Fig. 2-3. The plates have 0.33inch (0.838 cm) holes 0.42 inches (1.067 cm) from the sides to allow bolt screws to go through the plate and secure it to mounting fixtures.

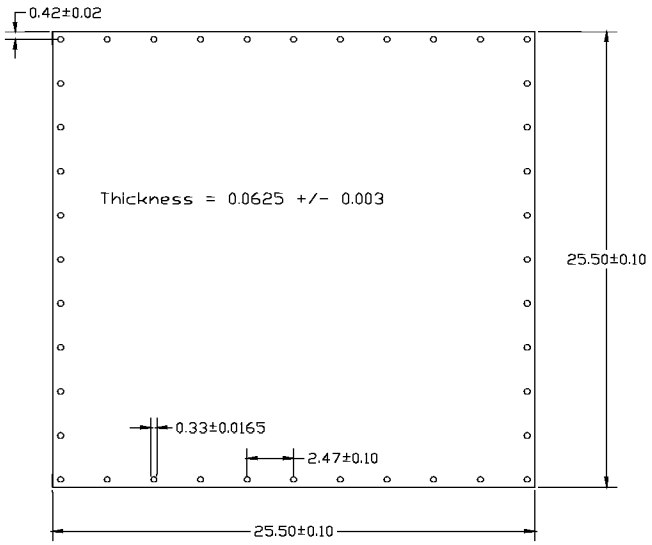

Figure 2-3. Sample test specimen with dimensions and tolerances.

The plates were supported using two mounting square fixtures. These fixtures sandwiched the test specimen, and bolts went through the two fixtures and the test specimen securing it to the test section wall. Figures 2-4 and 2-5 show the dimension of the two mounting fixtures. The upper mounting fixture was 25.5 x 25.5 inches (64.77 x 64.77 cm) in horizontal and vertical length and 20 x 20 inch (50.8 x 50.8 cm) middle cut out area. Therefore the exposed surface area of the plate specimen was 20 x 20 inches (50.8 x 50.8 cm). The thickness of this mounting fixture was 0.5 inches (1.27 cm).

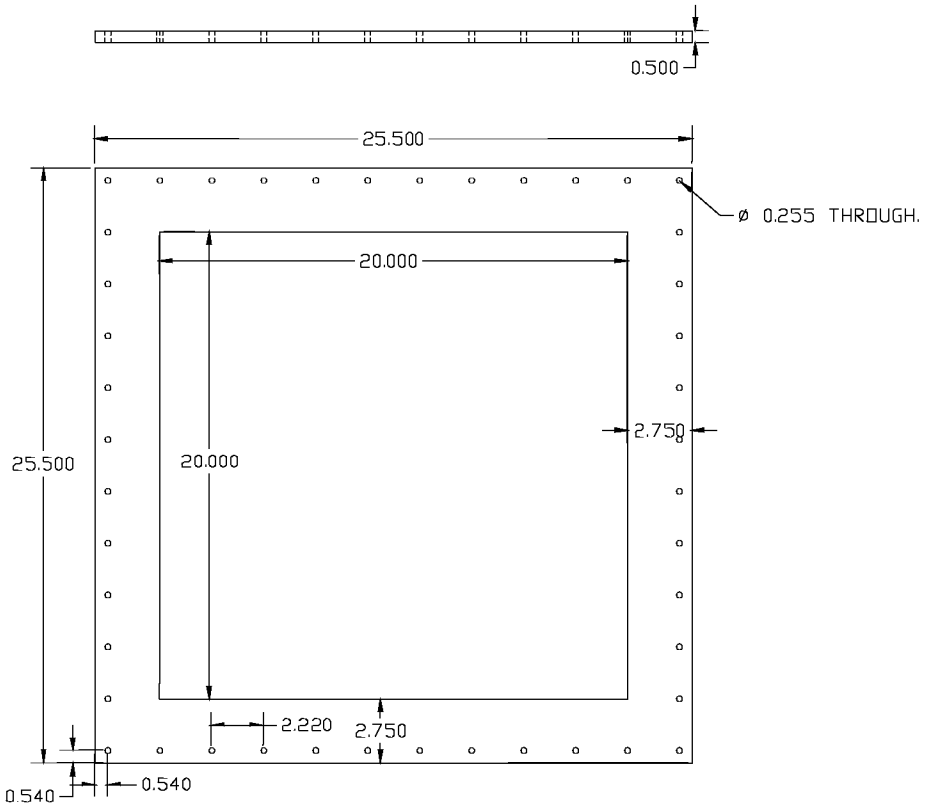

Figure 2-4. Test mounting fixtures (upper).

The bottom mounting fixture was 35.0 x 35.0 inches (88.90 x 88.90 cm) in horizontal and vertical length and 20 x 20 inch (50.8 x 50.8 cm) middle cut out area as shown in Fig. 2-5. The thickness of this mounting fixture was 1.0 inch (2.54 cm) with a stepped 0.5 inch (1.27 cm) thick 25 x 25 (64.77 x 64.77 cm) area to fit the upper mounting fixture.

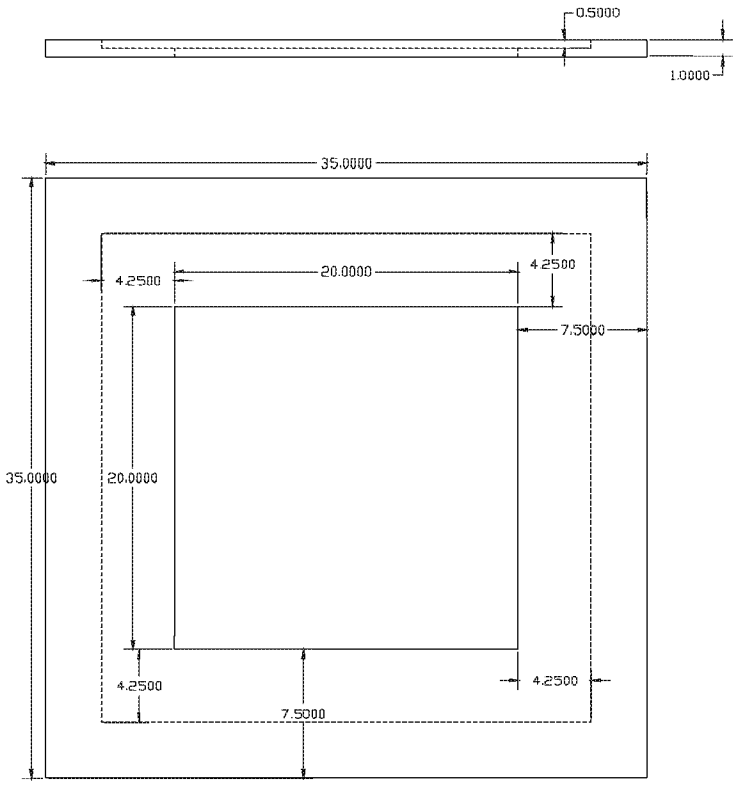

Figure 2-5. Test mounting fixtures (lower).

References

1. "Macro-Tech 600/1200/2400 Professional Power Amplifiers," Owner's Manual, Crown International Inc., 1995.
2. "Wyle Laboratories WAS 3000 Airstream Modulators," Operational Manual, Wyle Laboratories Scientific Services and Systems Group, January 1992.
3. "1/4 inch Condenser Microphones Type 4135/4136," Instructions and Applications, Brüel & Kjaer, February 1974.
4. "Dual Microphone Supply Type 5935," Technical Documentation, Brüel & Kjaer, February 1993.
5. "Shock and Vibration Catalog," PCB Piezotronics Inc., 1999.

3. Results

The layout of this chapter is divided into three sections. In broad terms section 3.1 addresses the acoustic source characteristics, while sections 3.2 and 3.3 address the dynamic response of the tested plate specimens. Section 3.1 describes some of the spectral characteristics of the acoustic source and its control software producing the grazing incident acoustic wave propagating along the progressive wave tube (PWT) to the plate specimen tested.

Section 3.2 and 3.3 describe power spectral density (PSD) and root mean square (RMS), respectively, of the dynamic response of the plate specimen. These sections use the analysis of the first (mean) and second (variance) moment statistical characteristics of PSD and the RMS of the experimental results as a framework to document several important findings of the experimental results. The PSD and RMS results provide frequency dependence, and magnitude response, respectively, repeatability assessment of the experimental results.

3.1 Acoustic Source Characteristics and Control

In order to characterize the source spectrum and control system an experiment with a "blank" specimen was performed. Figure 3-1 shows a picture of the "blank" specimen in the facility. A "blank" is a hard fixed specimen that acts as if it was the tunnel wall. The leading and trailing edge microphone spectrums, respectively, were acquired to ensure the repeatability of previous published results.[1]

The leading edge, trailing edge, control spectrum (average of leading and trailing edge microphone spectrums), and the drive signal spectrum from the controller, is shown in Figs. 3-2 through 3-6, respectively. The specified control signal had a frequency range between 50 to 500 Hz creating plane traveling waves down the PWT. There are several source spectral characteristics evident from these figures that had not previously been reported.

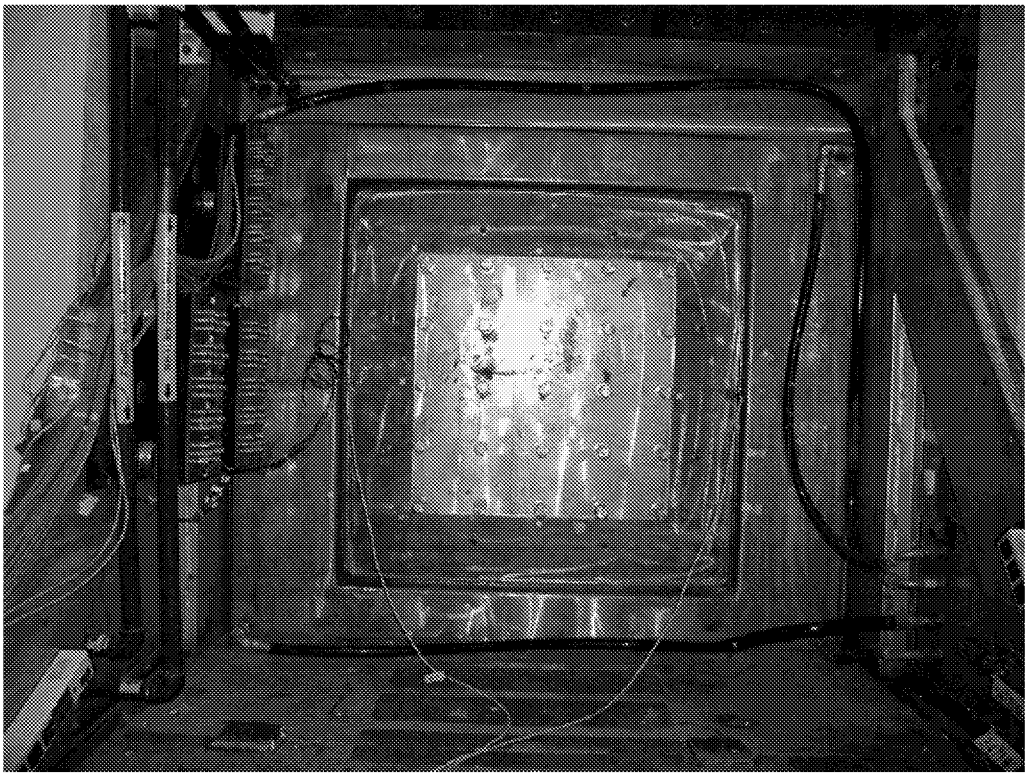

Figure 3-1. Picture of Blank Specimen.

From the plots it is evident that there was spectral energy below 50Hz and above 500 Hz even though there was no output by the drive signal at these frequencies. It is important to note from Fig. 3-3 that although the drive signal has a sharp dropoff outside the specified frequency range, the floor outside the specified range increased as the sound pressure level was increased.

The low frequency energy below the specified 50Hz, high pass cut-off, increased slightly as the OASPL was increased. Therefore it is plausible that the drive signal enhanced the low frequency energy but was not its the root cause. The low frequency spectral energy component was present even when the drive signal was not turned on, and only background air was running in the facility. Therefore, the energy at these frequencies seems to be a facility characteristic spectrum and not due to the drive signal. The low frequency energy become less important as the OASPL was increased.

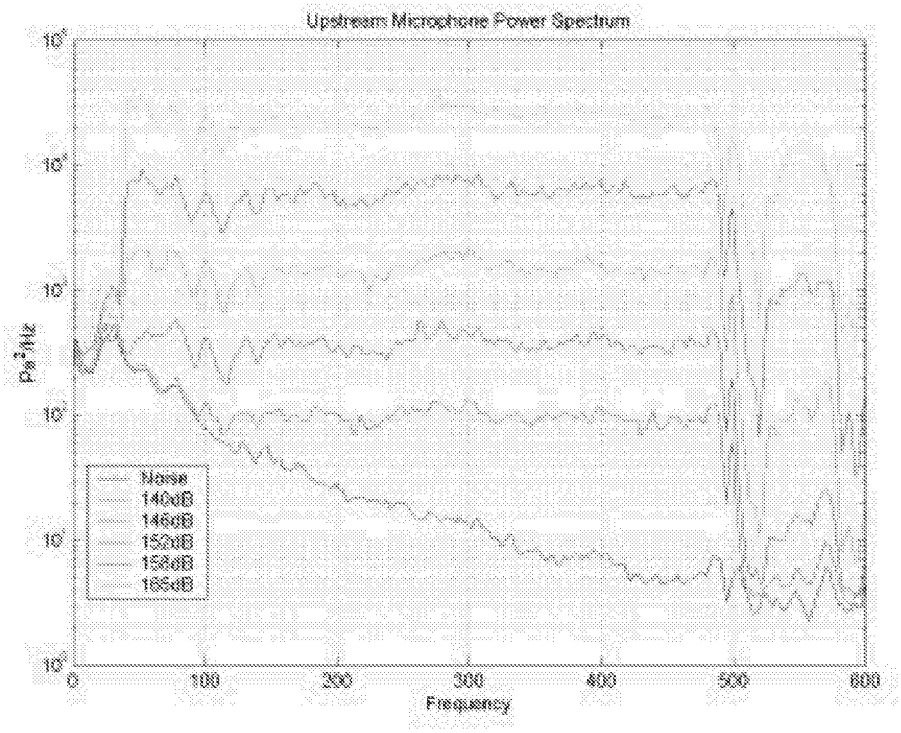

Figure 3-2. Upstream microphone power spectrum.

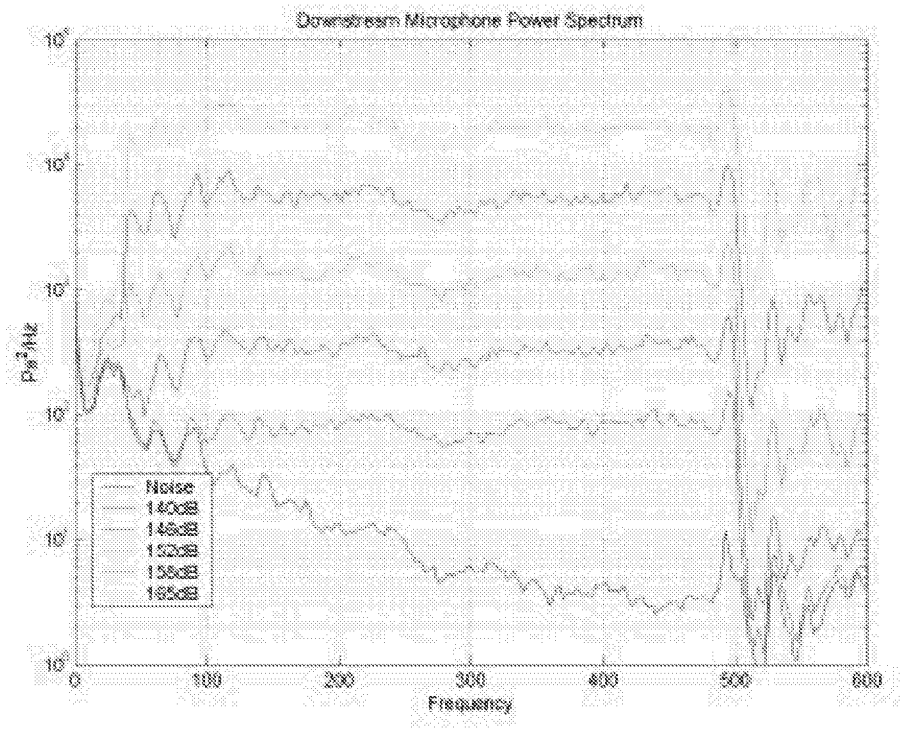

Figure 3-3. Downstream microphone power spectrum.

The measured spectral energy above 500 Hz increased as the OASPL was increased. Contrary to the lower frequency energy, the high frequency energy increased as OASPL was increased, and therefore did not remain much lower than the drive spectrum. Since one of the characteristics of nonlinear systems is the excitation of higher frequency components, one possible explanation for this high frequency noise, is that nonlinearities in the acoustics of the facility became more prevalent as OASPL was increased.

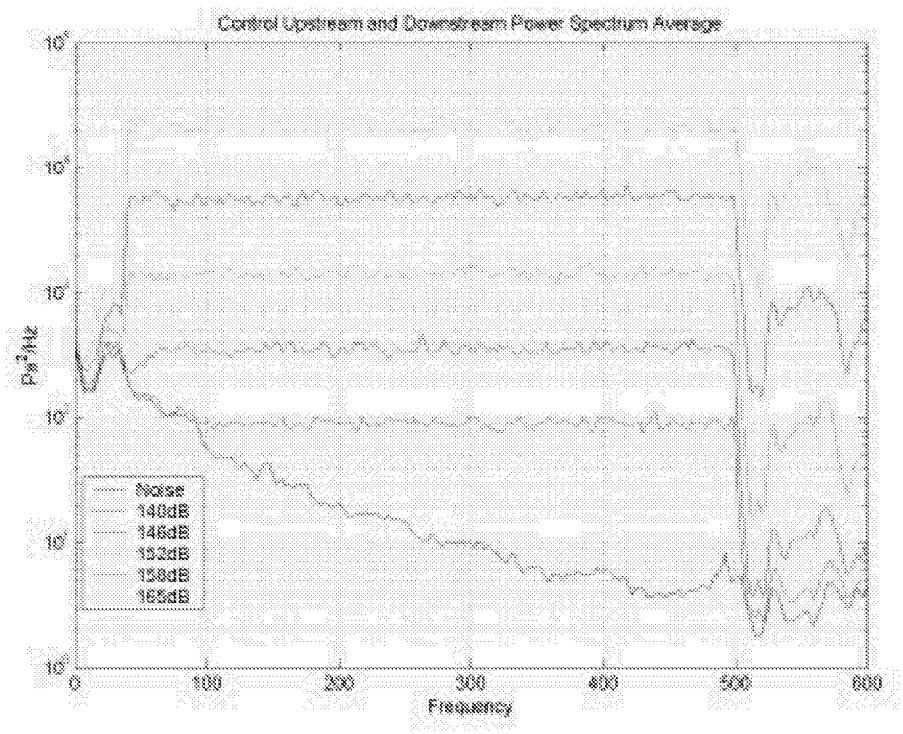

Figure 3-4. Control Power Spectrum.

Comparing the leading and trailing edge autospectra (Fig. 3-2 and 3-3) with the control spectra (Fig. 3-4), some characteristics are noted. The control spectra was flatter than either the leading or trailing edge spectra in the specified frequency range. A flat input spectra is desirable to prevent the structural dynamic response of the specimen to reflect input conditions.

Figure 3-5 shows the coherence plot between the upstream and downstream microphone. The coherence between the microphones shows improvements as both OASPL and frequency are increased. The coherence function (γ^2) is defined as

$$\gamma^2(f) = \frac{|S_{xx}|^2}{S_{xx}S_{yy}} \tag{3-1}$$

where S_{xy}, is the crosspectrum between the leading and trailing edge microphones and S_{xx}, and S_{yy} are the autospectrum of the leading and trailing microphones, repectively.

The coherence function can take values from 0 to 1, where 0 indicates no correlation and perfect linear correlation, respectively, between signals x (leading edge microphone) and y (trailing edge microphone). Previous published results[1] do not show the trend shown in Fig. 3-5, since those plots only showed the coherence, between upstream and downstream microphones, for the higher OASPLs,

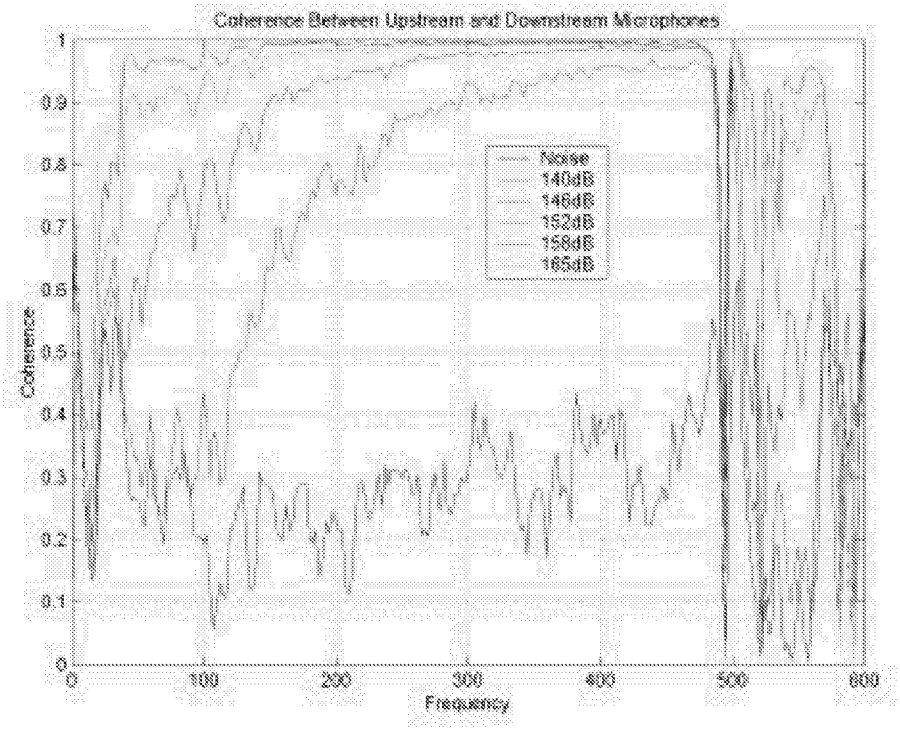

Figure 3-5. Coherence Between Upstream and Downstream Microphones.

Figure 3-6 shows the controller drive signal. The figure shows that the drive signal spectrum had more variability in voltage at the lower frequencies and OASPLs. Therefore, part of the spectral variation seen in the leading and trailing edge microphones as seen in Figs. 3-2 and 3-3, respectively, is due to this spectral variation in the drive signal. More information on the controller details refer to References 1 and 2.

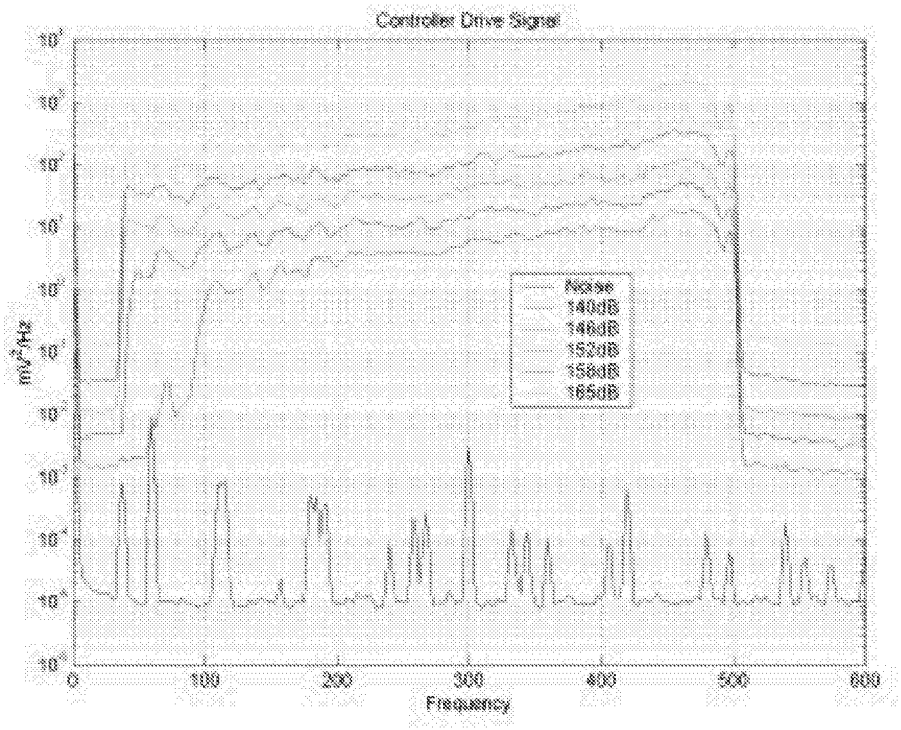

Figure 3-6. Controller Drive Signal.

3.2 Power Spectral Density (PSD) Results

3.2.1 Thicker Plate Results

Experimental PSD results were acquired at TAFA for different OASPLs for the 2024 T3 Plate Aluminum specimens. Figures 3-7 through 3-10 show the PSD Accelerometer 4 results for 0.125in (0.318cm) specimen and OASPLs 135, 141, 147, and 153dB, respectively. Accelerometer 4 is located in the middle of the plate specimen as shown in Fig. 2-2. PSD results for the accelerometers can be found in Appendix A.

PSD results in Figs. 3-7 through 3-10 show two distinct resonant peaks at around 110Hz and 390Hz, respectively. The general shape of the PSD curves were the same from run to run, and the resonant frequencies shifted 5 to 10Hz for the different runs. These figures also show, as expected, that level of the PSD curves increased as OASPL was increased.

Figures 3-7, 3-8, and 3-9 shows what appear to be two distinct first and second resonant results about 5 to 10 Hz apart. Runs 2 and 4 appear to be at lower resonant mode frequencies than runs 1, 3, and 5. This result is significant since runs 2 and 4 were afternoon tests, while runs 1,3, and 5 were morning tests. Therefore, the time of the day the plates were tested affected their dynamic resonant response. Since the only change between morning and afternoon tests was possibly the air temperature in the PWT, it stands to reason, that the air being fed to the PWT warmed up during day, affecting the dynamic response of the plates and evident by the resonant frequencies shift.

Another important conclusion of this result is that although the modes seem to be slightly affected by the time of the day they are tested, they were repeatable from day to day as long as they are tested at the same time of the day. Since the torquing sequence used to clamp the plates was changed from day to day, it stand to reason, that torquing sequence did not affect the dynamic response of the plate.

The PSD results also show a broadening of the resonant frequency peaks as OASPL is increased rather than the sharper spikes at the lower OASPLs. Note that Fig. 3-10 shows a flat PSD. This result is due to the accelerometer coming off the specimen due to the high acceleration levels in the plate and is not a valid result. Note that the PSD level increased with OASPL not only at the excitation frequency range of 50 to 450Hz,

but all the way to plotted range of 600Hz. This result occurred due to the characteristic tunnel noise energy present outside the excitation frequency range discussed in Section 3.1.

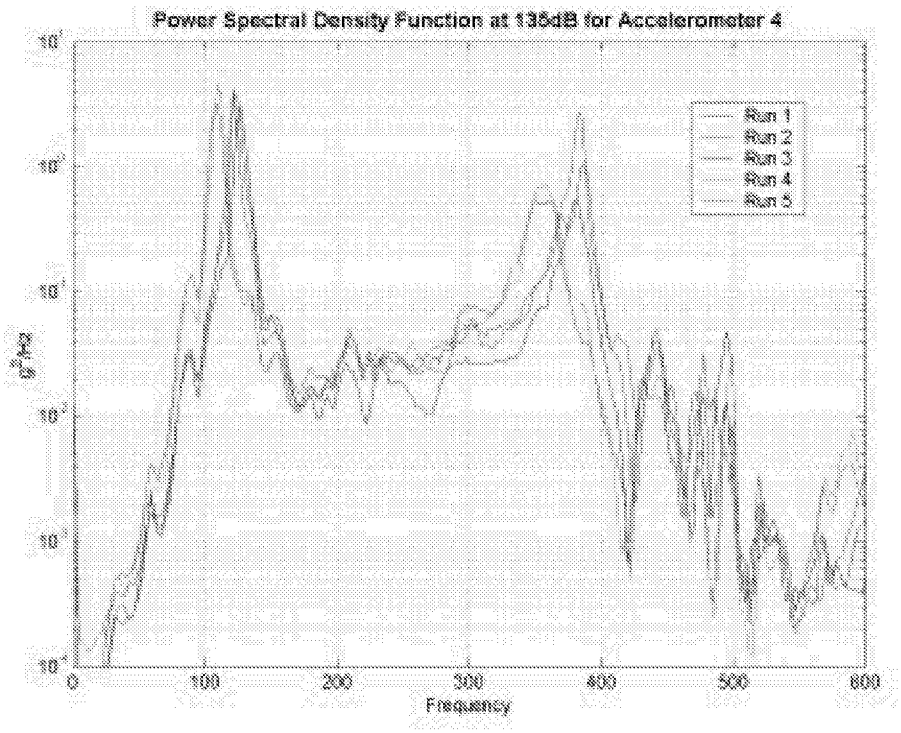

Figure 3-7. PSD at 135dB for Accelerometer 4 and 0.125in (0.318cm) thick plate.

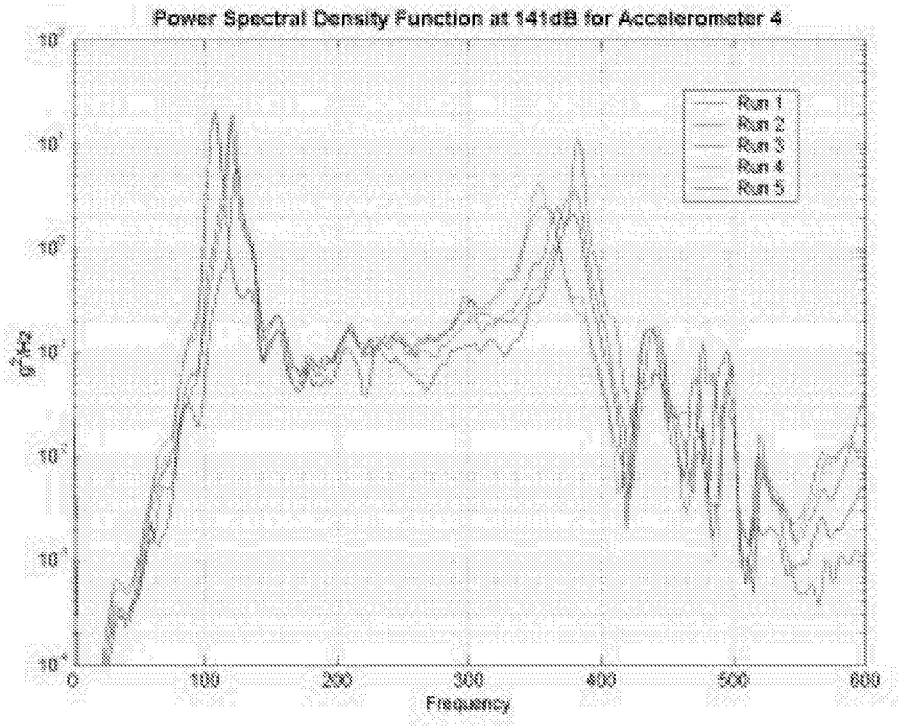

Figure 3-8. PSD at 141dB for Accelerometer 4 and 0.125in (0.318cm) thick plate.

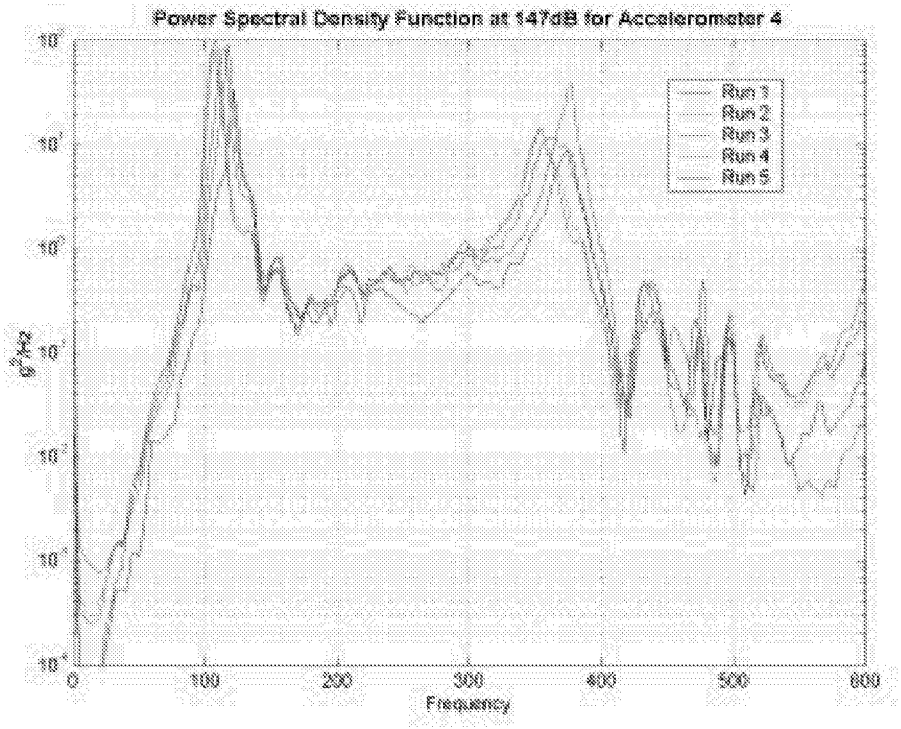

Figure 3-9. PSD at 147dB for Accelerometer 4 and 0.125in (0.318cm) thick plate.

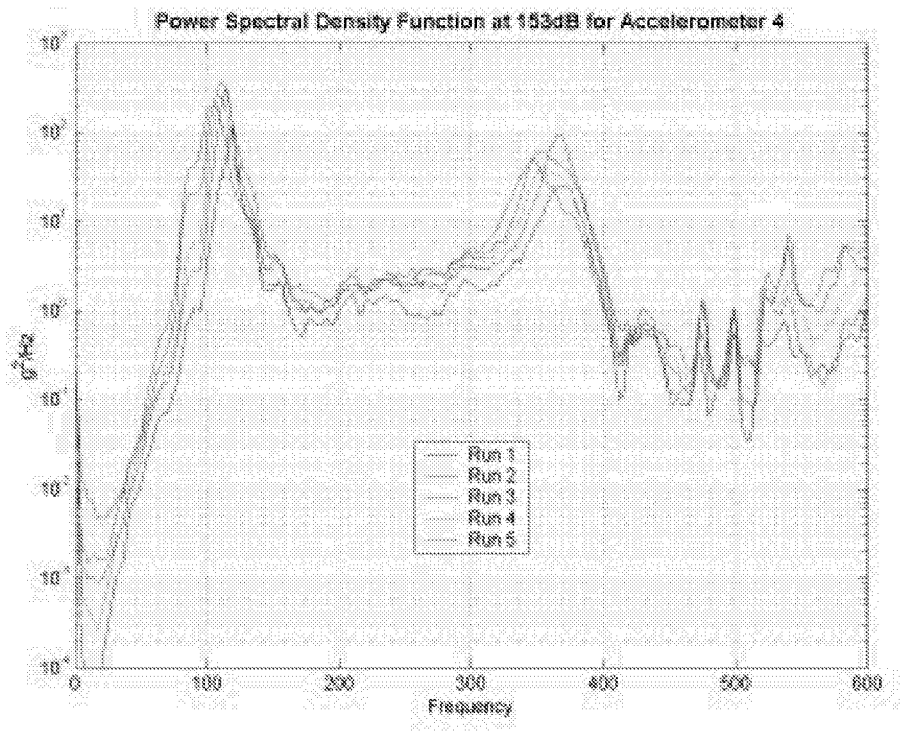

Figure 3-10. PSD at 153dB for Accelerometer 4 and 0.125in (0.318cm) thick plate.

Figures 3-11, 3-12, and 3-13 show the mean and standard deviation (STD) of the PSD at various OASPLs for Accelerometer 4 and 0.125in (0.318cm) specimen. The mean PSD results show a broadening of the two resonant peak regions due to the variability in values for each of the experimental runs. This broadening in the resonant PSD level also increases as the OASPL is increased. The STD of the PSD results show increased variance with increasing OASPL. The STD curves follow the same shape as the mean curves, where the peaks are located at the resonant frequencies.

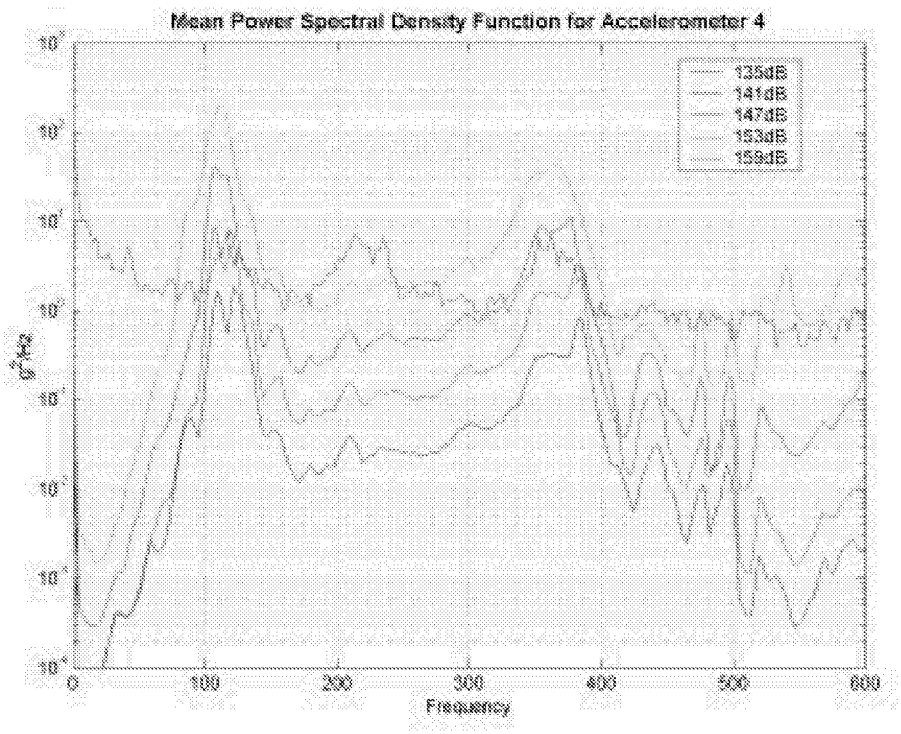

Figure 3-11. Mean PSD for Accelerometer 4 and 0.125in (0.318cm) thick plate.

Note that log plots can be deceptive, and many times engineers use this deceptiveness to make their results "look better." For example, Fig. 3-13 shows the mean PSD results with plus/minus one STD. To an untrained eye, it appears from the plot that the one STD results were very close to the mean PSD curves, indicating very repeatable experiments. Nevertheless, when the STD results are plotted by themselves, as in Fig. 3-12, a different picture emerges. At 110Hz resonant frequency, the standard deviation at 153dB is roughly 10^2 g^2/Hz. This is the same order of magnitude as the mean PSD value for this OASPL and frequency. For a normally distributed population 66%, 95%, and 99% of the population samples lie within one, two, and three standard deviations respectively. Therefore, such a large standard deviation provides very little confidence into what the true mean PSD curve was for this given OASPL and frequency.

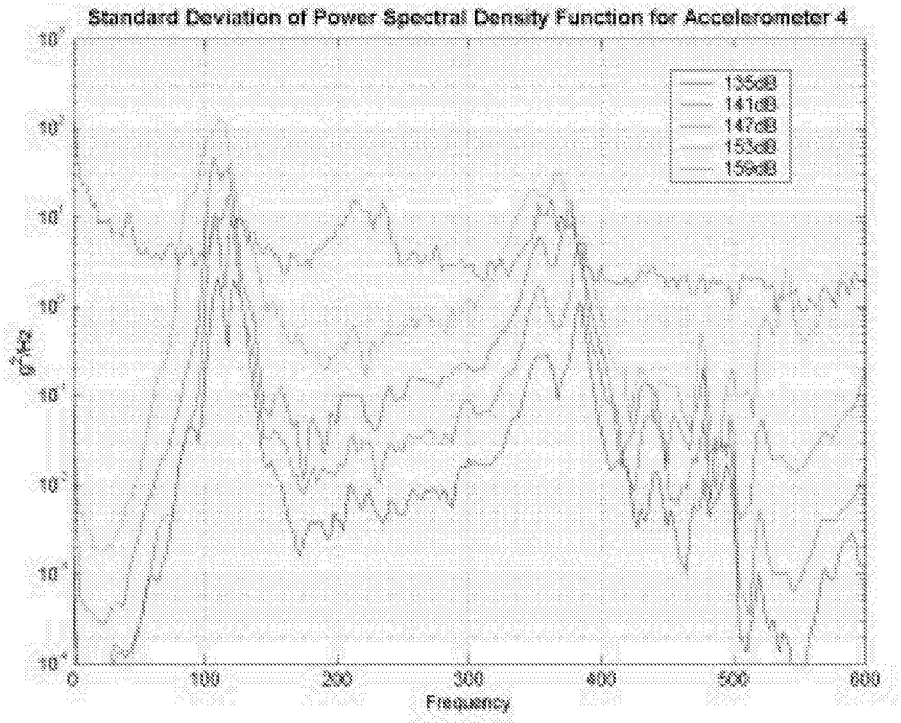

Figure 3-12. STD of PSD for Accelerometer 4 and 0.125in (0.318cm) thick plate.

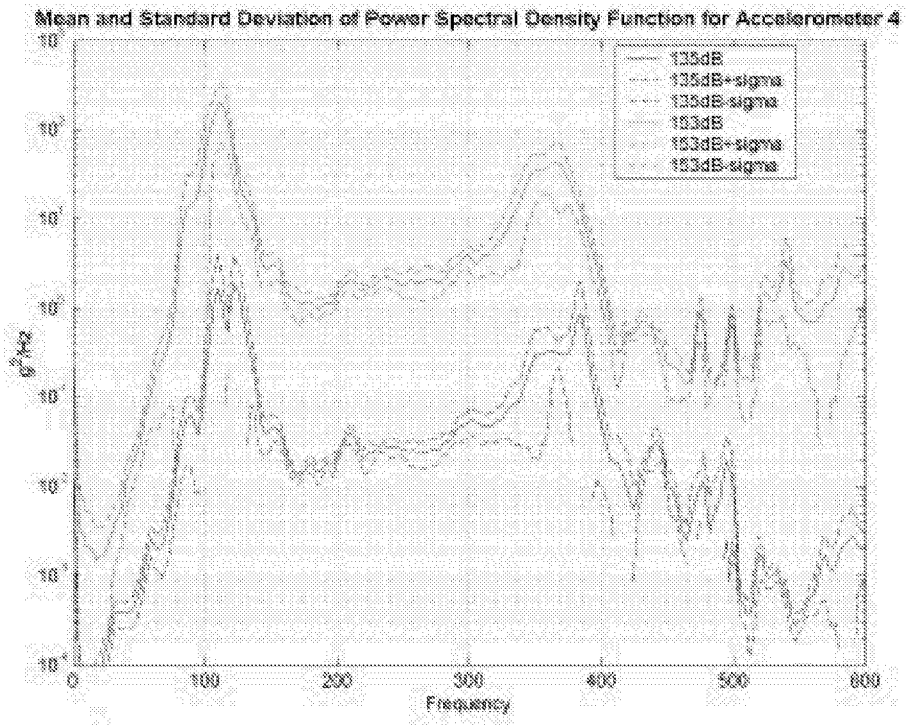

Figure 3-13. Mean and STD of PSD for Accelerometer 4 and 0.125in (0.318cm) thick plate.

The estimates of the mean and STD statistics plotted in Figs. 3-11, 3-12, and 3-13 were calculated based on five test runs. This was a relatively small sample size to draw reliable population mean and variance estimates. In order to increase the sample size a new standardized variable was calculated called the Absolute Percent Error (APE) defined as[3]

$$APE_{ij} = \left| \frac{\bar{x} - x_{ij}}{\bar{x}} \right| * 100 \tag{3-2}$$

where $\bar{x}$ is the mean value of the PSD function at a given frequency, and x_{ij} is the value of the PSD function at some accelerometer location (i) and OASPL (j) at the same frequency.

From these APEs, Mean Absolute Percent Errors (MAPEs) can be calculated. $MAPE_i$ and $MAPE_j$ given by

$$MAPE_i = \frac{\sum_j APE_{ij}}{n_j - 1}$$
$$MAPE_j = \frac{\sum_i APE_{ij}}{n_i - 1} \tag{3-3}$$

MAPEs also roughly equal the percentage of the ratio of STD to the mean result given by

$$MAPE \approx \frac{STD}{Mean} * 100 \tag{3-4}$$

Figure 3-14 shows the MAPE function for the different accelerometer ($MAPE_i$). The MAPE function for all accelerometers increased at frequencies where the PSD

function was small (remember you are dividing by $\bar{x}$) and at the resonant frequencies. The errors were independent of location and more dependent on the magnitude of the response. Therefore, resonant locations produced higher MAPEs. Note that all accelometers pick up the first mode (1,1) at around 110Hz, but Accelerometer 4 located in the middle of the plate does not pick mode (1,2) at 200 to 210 Hz, since it was located in a node line for this mode. Appendiz A shows the 200 to 210Hz resonant mode in the PSD plots for Accelerometers 1,2,3, and 5.

Figure 3-15 shows the MAPE function for different OASPLs ($MAPE_i$). The plot shows the same general trend as in Fig. 3-14, where frequency dependence and the location of structural modes dominated the error. Nevertheless, OASPL had a more significant effect than accelerometer location. Figure 3-15 also shows, that as OASPL was increased, the MAPE also increased. Finally, since the MAPE roughly equals the ratio STD of the PSD to the mean of the PSD results, it can be seen from Figs. 3-14 and 3-15 that on average this ratio oscillated between 20% to 100% for non-resonant and resonant frequencies, respectively.

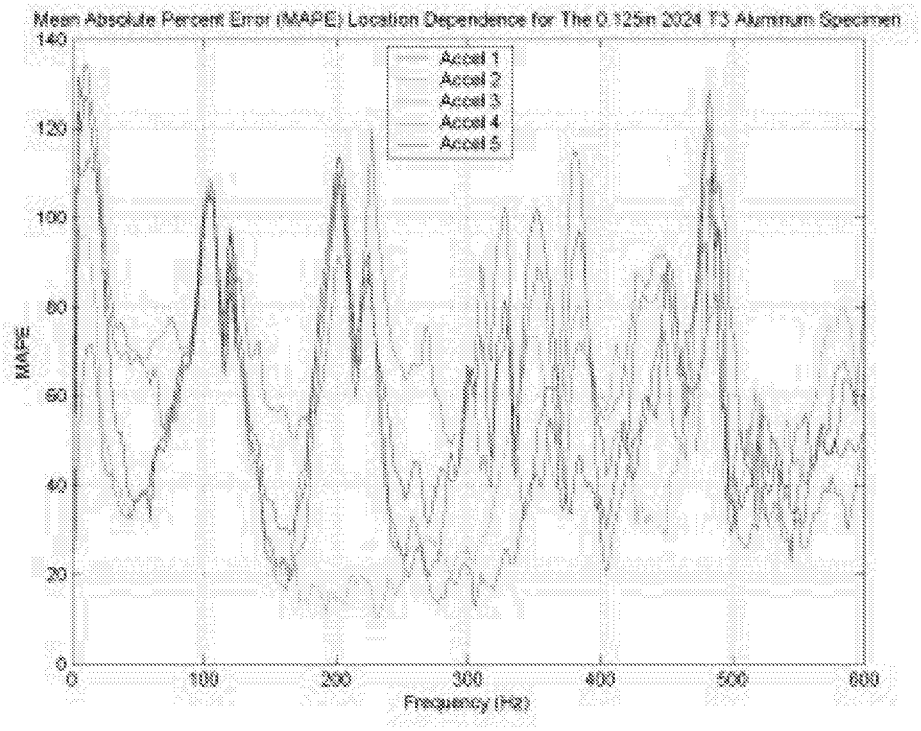

Figure 3-14. MAPE Location Dependence for the 0.125in (0.318cm) plate.

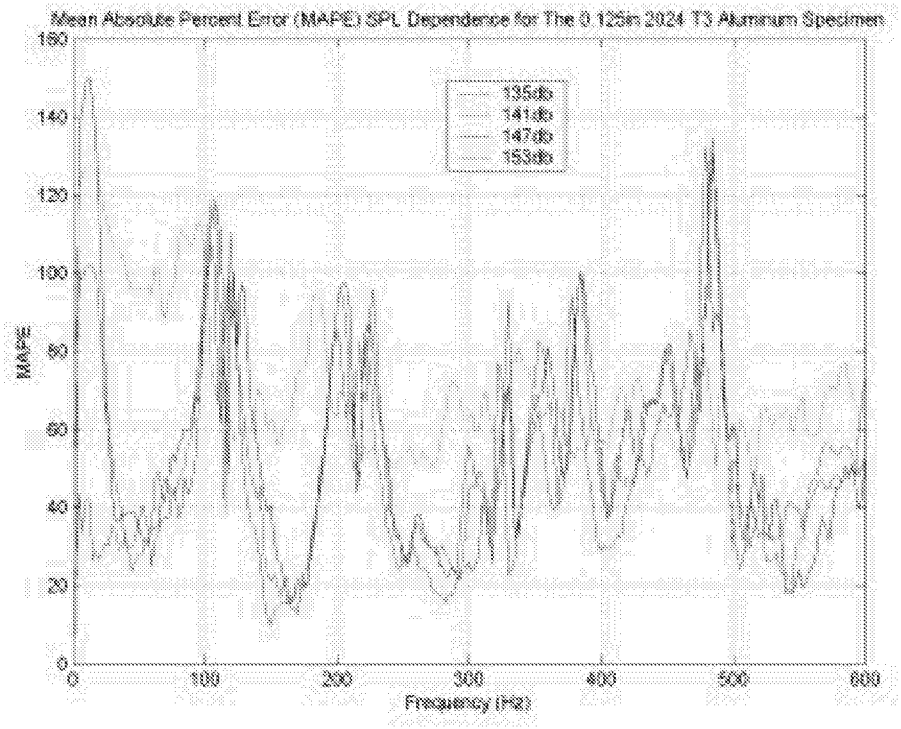

Figure 3-15. MAPE OASPL Dependence for the 0.125in (0.318cm) plate.

3.2.2 Thinner Plate Results

Figures 3-16 through 3-19 show PSD results for the 0.062in (0.1588cm) specimen for OASPLs 135, 141, 147, and 153dB, respectively. Numerically the first mode of this plate appears at around 50Hz if rigidly clamped conditions are assumed. Experimentally, the boundary conditions were a combination of rigidly clamped and simply supported boundary conditions, and therefore the first resonant frequency was below 50Hz. Since the excitation acoustic energy had a frequency range of 50Hz to 450Hz this mode is not excited.

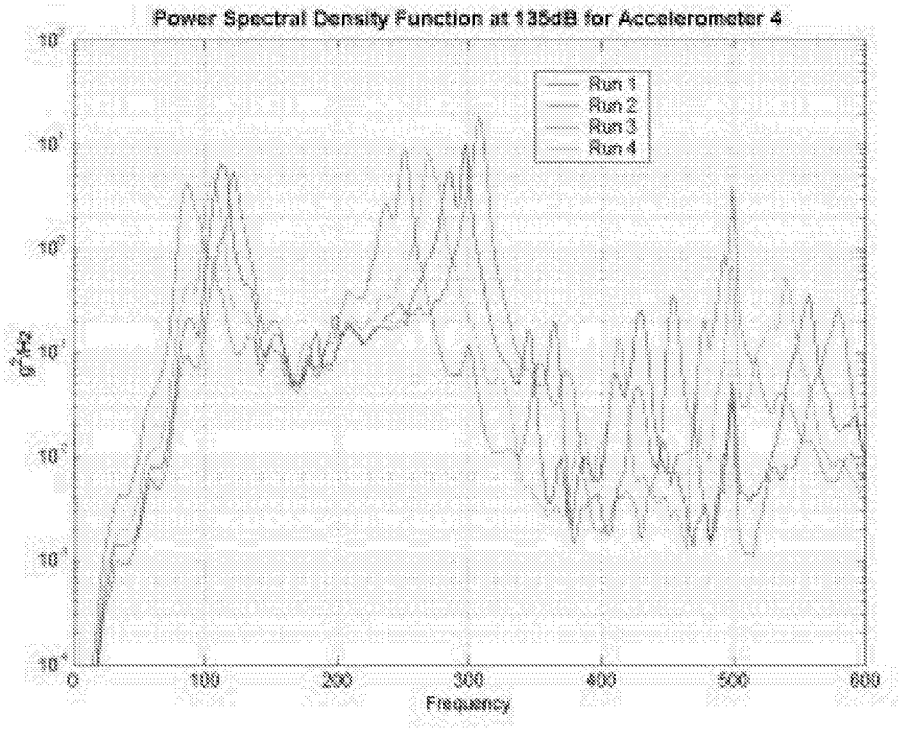

Figure 3-16. PSD at 135dB for Accelerometer 4 and 0.062in (0.1588cm) thick plate.

The PSD functions for the 0.062in (0.1588cm) thick specimen show two resonant peaks at around 100-110Hz and 250-310Hz. Both of these modes are repeated modes. There two other modes between these two frequencies at around 190Hz to 200Hz and

260Hz, respectively, that do not appear for Accelerometer 4. These resonant modes can be seen the PSD function plots in Appendix A for Accelerometers 1,2,3, and 5.

The PSD functions in Figs. 3-16 through 3-19 show that the resonant peaks for this sample tended to vary depending on the time of the day tested (morning or afternoon), and torque sequence used to secure the plate. Similar to the thicker 0.125in (0.318cm) plate results, runs 2 and 4 (afternoon runs) were at lower resonant frequencies than runs 1 and 3 (morning runs). Another important result that can be seen in these figures when comparing runs 1 and 2 against 3 and 4, is that torque sequence affected the dynamic response at the resonant frequencies. These figures show that torque sequence 1 and 2 produced lower and higher, respectively, resonant frequencies responses. Therefore, for this thinner 0.062in (0.1588cm) plate had its dynamic resonant response affected by air temperature and torquing pattern used to secure it to the test wall section of the PWT.

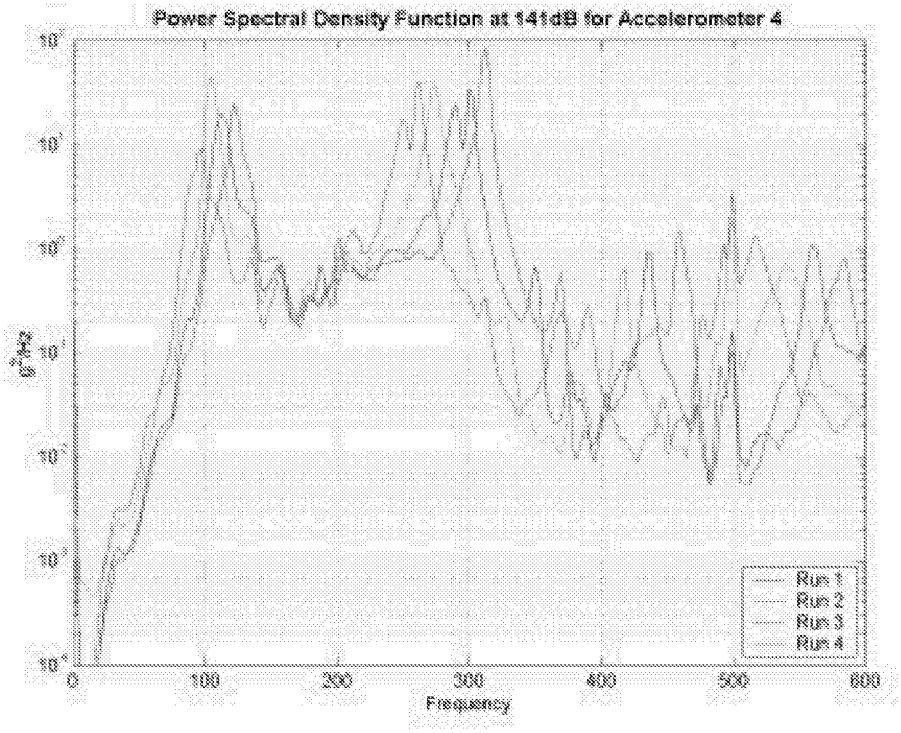

Figure 3-17. PSD at 141dB for Accelerometer 4 and 0.062in (0.1588cm) thick plate.

The PSD functions also show that with increasing frequency the peak resonant frequency variability increases. Comparing the 0.125in (0.318cm) and the 0.062in (0.1588cm) specimen, the variability in the resonant peaks was greater for the thinner specimen.

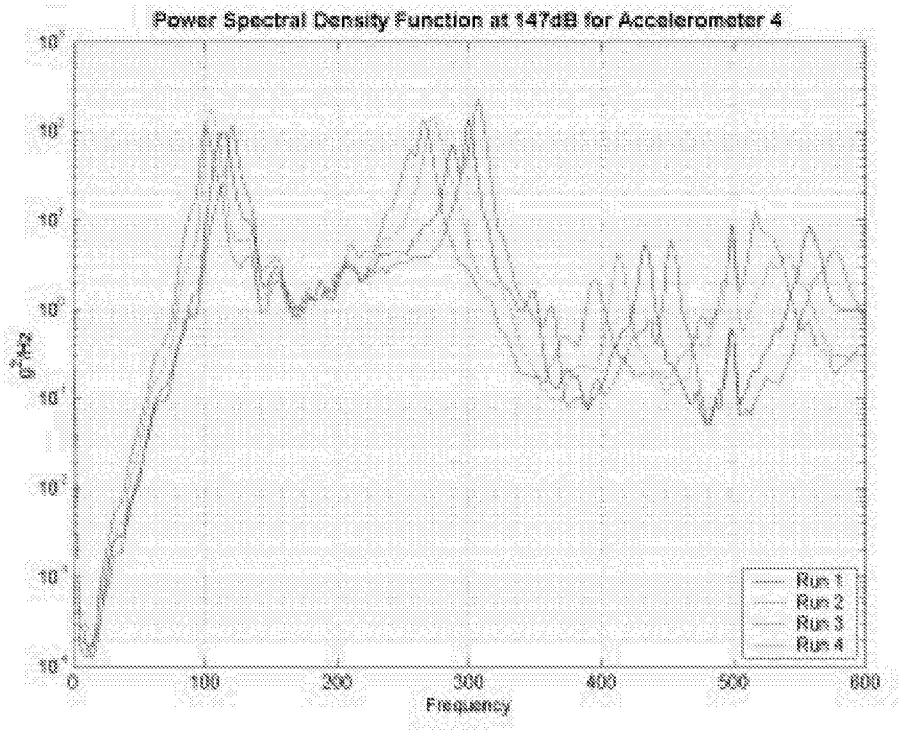

Figure 3-18. PSD at 147dB for Accelerometer 4 and 0.062in (0.1588cm) thick plate.

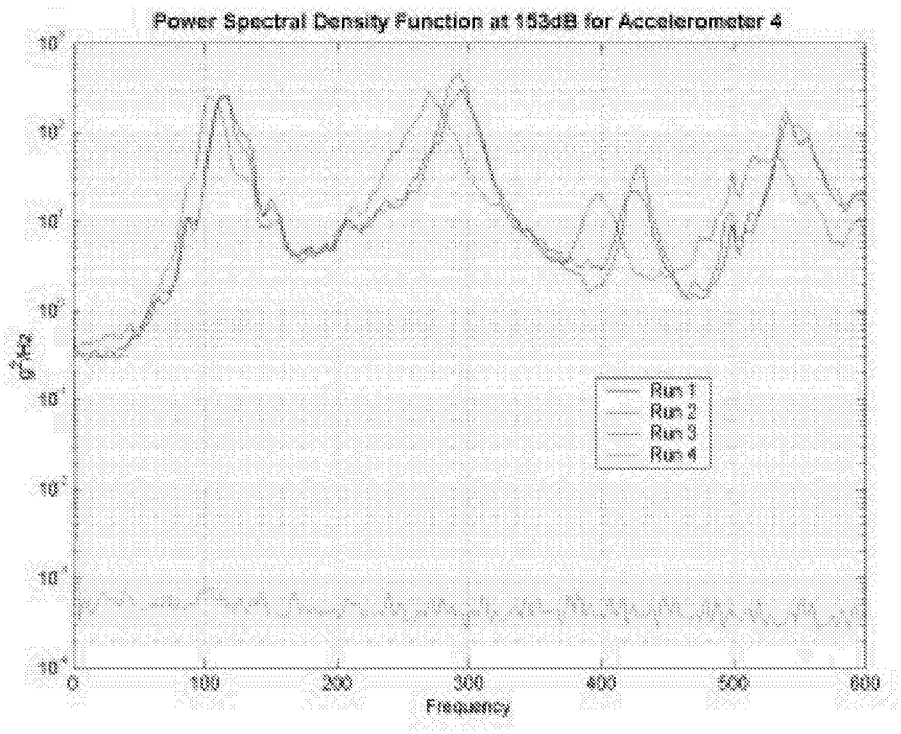

Figure 3-19. PSD at 153dB for Accelerometer 4 and 0.062in (0.1588cm) thick plate.

Figs. 3-20, 3-21, and 3-22 show the mean and standard deviation, respectively, of the PSD function for the 0.062in (0.1588cm) sample and Accelerometer 4 at various OASPLs. The mean PSD results show a broadening of the two resonant peak regions due to the variability in the experimental runs. This broadening in the resonant PSD level also increased as the OASPL was increased, although this effect seems to be less pronounced for this sample thickness when compared with the thicker 0.125in (0.318cm) sample.

The STD of the PSD results show increasing variance with increasing OASPL. The STD curves follow the same shape as the mean curves, where the peaks are located at the resonant frequencies. Comparing the thicker vs. thinner plate (0.125in (0.318cm) vs. 0.062in (0.1588cm)), Figs. 3-22 and 3-13 show that the variability in the PSD results was significantly greater for the thinner plate.

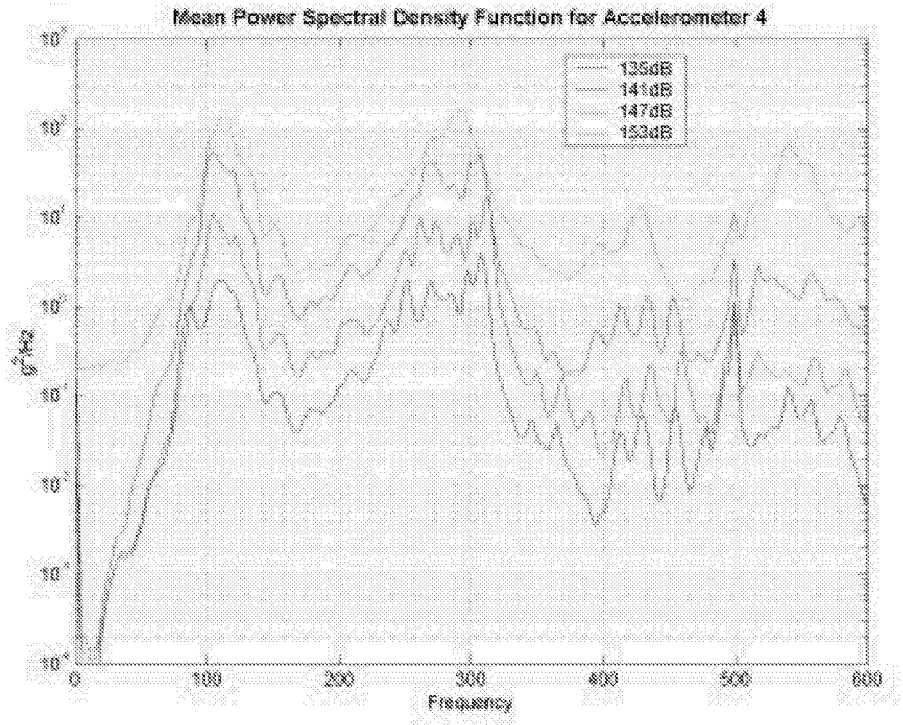

Figure 3-20. Mean PSD for Accelerometer 4 and 0.062in (0.1588cm) thick plate.

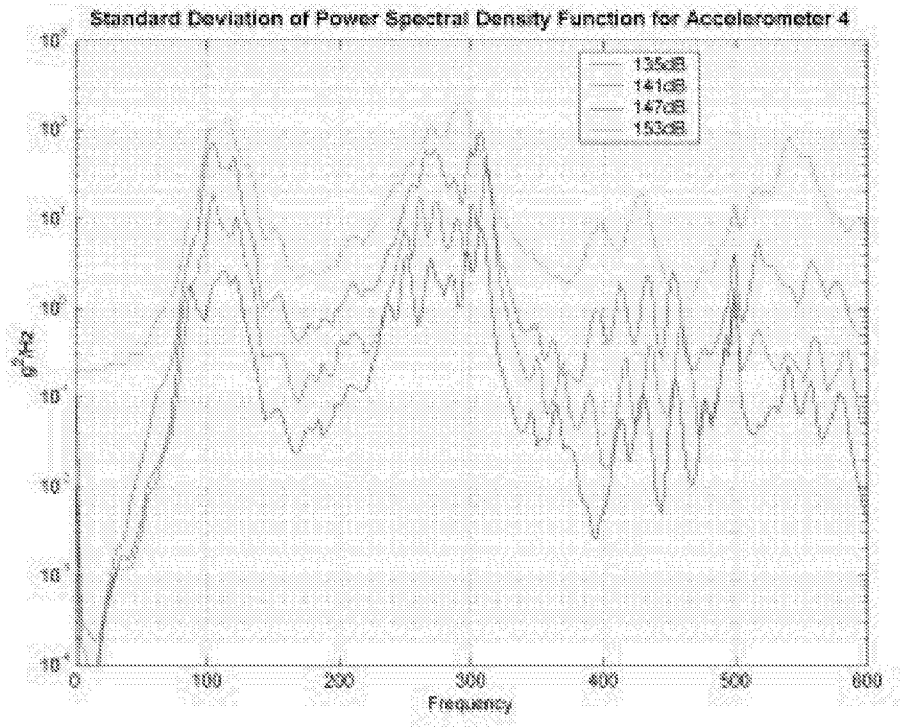

Figure 3-21. STD of PSD for Accelerometer 4 and 0.062in (0.1588cm) thick plate.

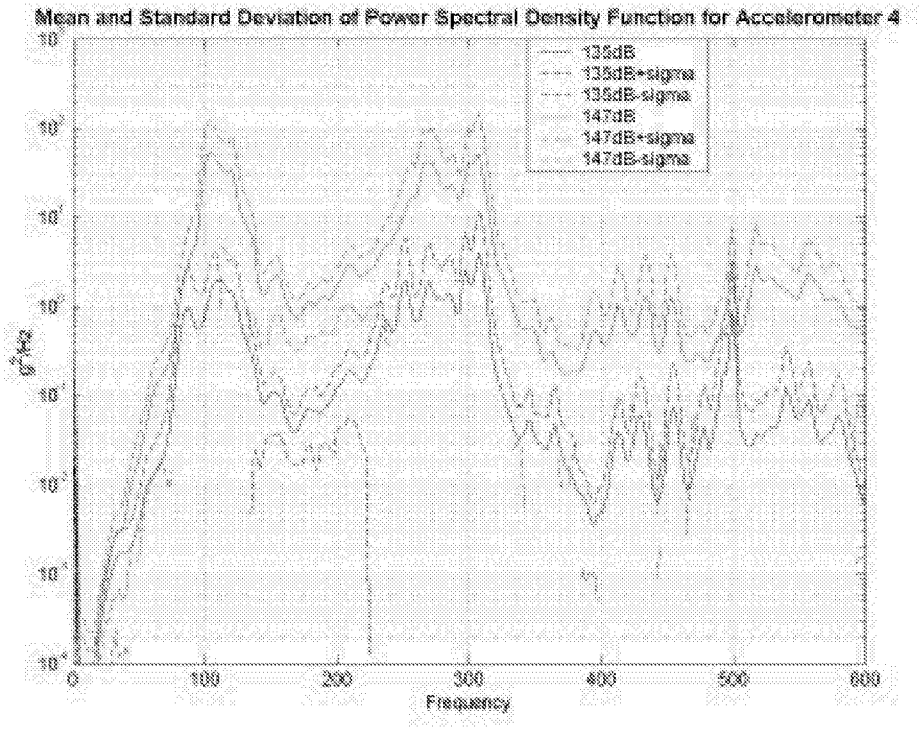

Figure 3-22. Mean and STD of PSD for Accelerometer 4 and 0.062in (0.1588cm) thick plate.

Figs. 3-23 and 3-24 show the MAPE location (MAPEi) and OASPL (MAPEj) dependence, respectively, for the 0.062in (0.1588cm) specimen. These figures show the MAPEs to be more erratic than the thicker 0.125in (0.318cm) plate. From Eq. (3-4), the MAPE roughly equals the ratio STD of the PSD to the mean of the PSD results. Therefore, on average this ratio oscillated between 25% to 125% for non-resonant and resonant frequencies, respectively.

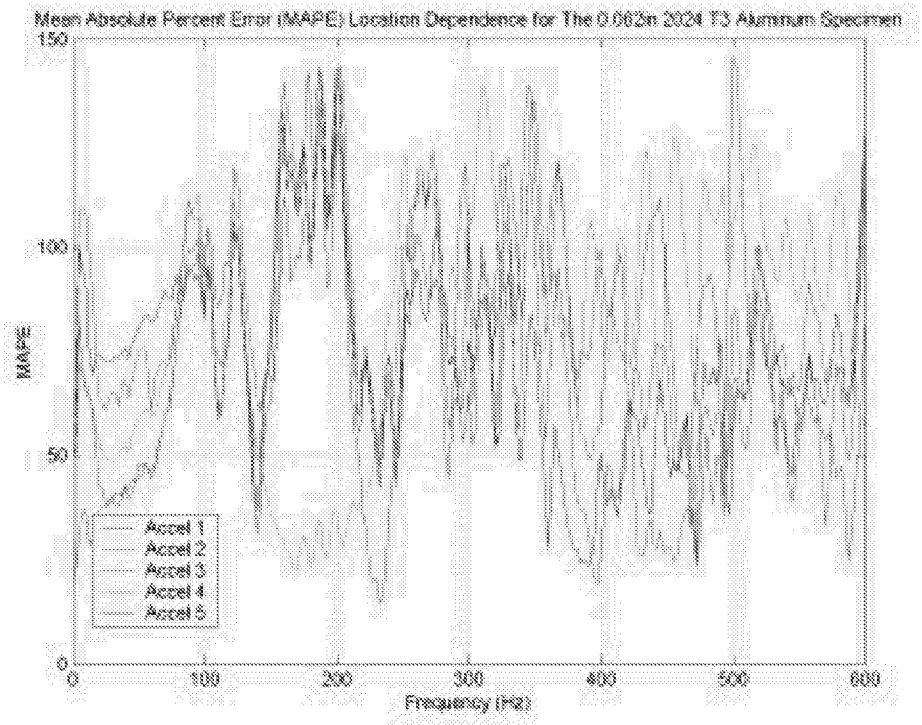

Figure 3-23. MAPE Location Dependence for the 0.062in (0.1588cm) Specimen.

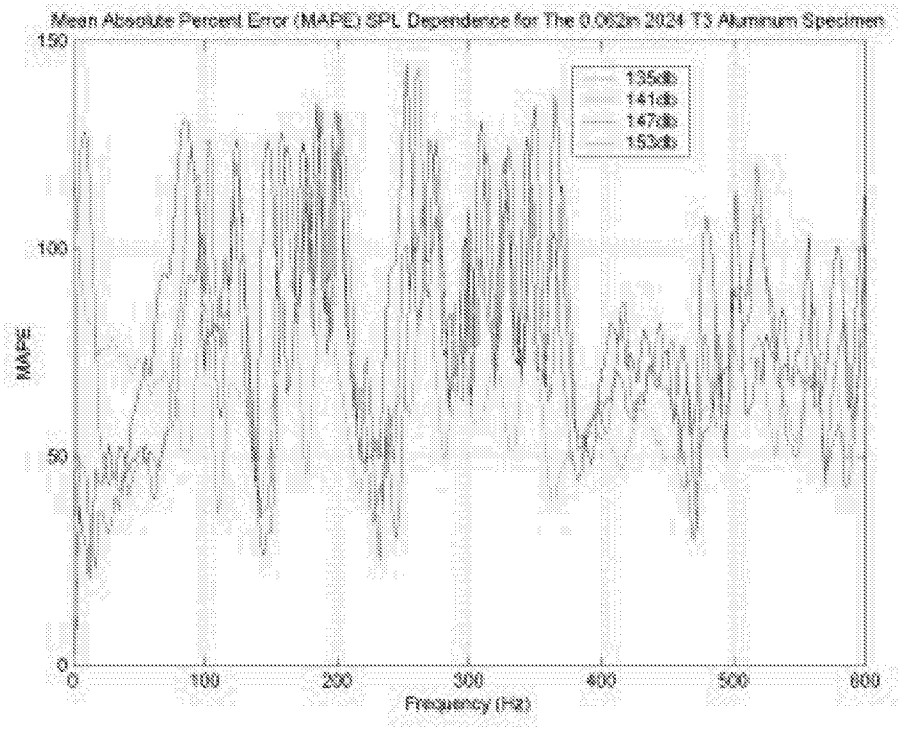

Figure 3-24. MAPE OASPL Dependence for the 0.125in (0.318cm) Specimen.

3.3 Root Mean Square (RMS) Statistic Results

The PSD results in the previous section provide a frequency dependence dynamic response of the plate specimens. In this section the acceleration magnitude response vs. input OASPL is of interest. The PSD function is the frequency domain autocorrelation function related to the time domain autocorrelation function by the Weiner-Khintchine Fourier transform pair given by[4]

$$R_{xx}(\tau) = \int_0^\infty S_{xx}(f)\cos(\omega\tau)df$$
$$S_{xx}(f) = \int_0^\infty R_{xx}(\tau)\cos(\omega\tau)d\tau \qquad (3\text{-}5)$$

where R_{xx} and S_{xx} are the time and frequency domain, respectively, single-sided autocorrelation functions, and $\omega=2\pi f$. Throughout this report the frequency domain autocorrelation function has been called the Power Spectral Density (PSD). The Root Mean Square (RMS) value is defined as[4]

$$RMS = \sqrt{R_{xx}(0)} = \sqrt{\lim_{T\to 0}\frac{1}{T}\int_0^T x^2(t)dt} = \sqrt{\int_0^\infty S_{xx}(f)df} \qquad (3\text{-}6)$$

Therefore, the square root of the areas under the PSD curve is the RMS value.

3.3.1 Thicker Plate Results

Figure 3-25 shows the RMS accelerations of different runs for Accelerometer 4 as a function of OASPL for the 0.125in (0.318cm) specimen. The plot shows a linear increase in acceleration RMS response with increasing OASPL. Divergence from this functional relationship starts around 150dB OASPL. Above 150dB, accelerometers come off the plate and the data is not valid. The accelerometers used to measure the dynamic response had a usable range of 500g RMS. Other RMS acceleration runs vs. OASPL can be found in Appendix B.

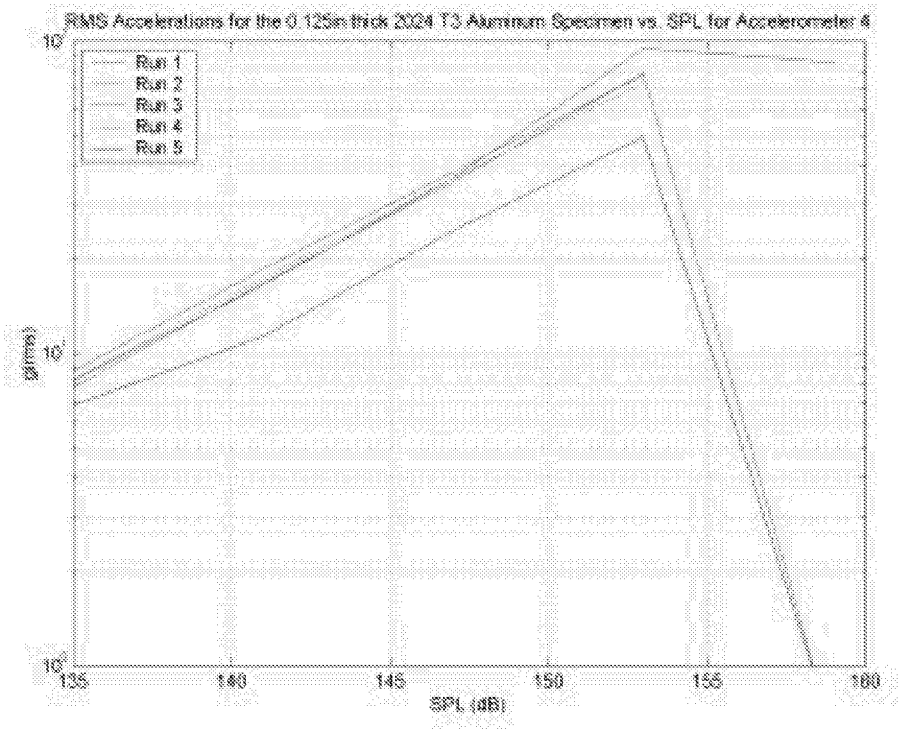

Figure 3-25. RMS Accelerations vs. OASPL for Accelerometer 4 and the 0.125in (0.318cm) plate.

Figures 3-26 and 3-27 show the mean (solid line) plus/minus one STD (dashed line) of the RMS acceleration for accelerometers 1 thru 5, for the 0.125in (0.318cm) plate. The plots show a linear relationship between RMS acceleration response vs. incident OASPL for accelerometers 1 thru 5. Given that the response of this plate is

strongly first mode dominated, it was expected for Accelerometer 4 (center of plate location) to have the highest acceleration followed by Accelerometer 3 (center leading edge location) and for Accelerometers 1, 2, and 5 to have about the same value (See Fig. 2-2 in Section 2.1). The plot shows this result experimentally up to 153dB. Above this value the reliability of the results deteriorates and the one STD envelopes for the different accelerometers overlap. The plots also show that below 147dB OASPL, the one STD envelope was fairly constant as OASPL is increased. This result indicates that the variability in the results was linearly increasing in magnitude with increasing OASPL.

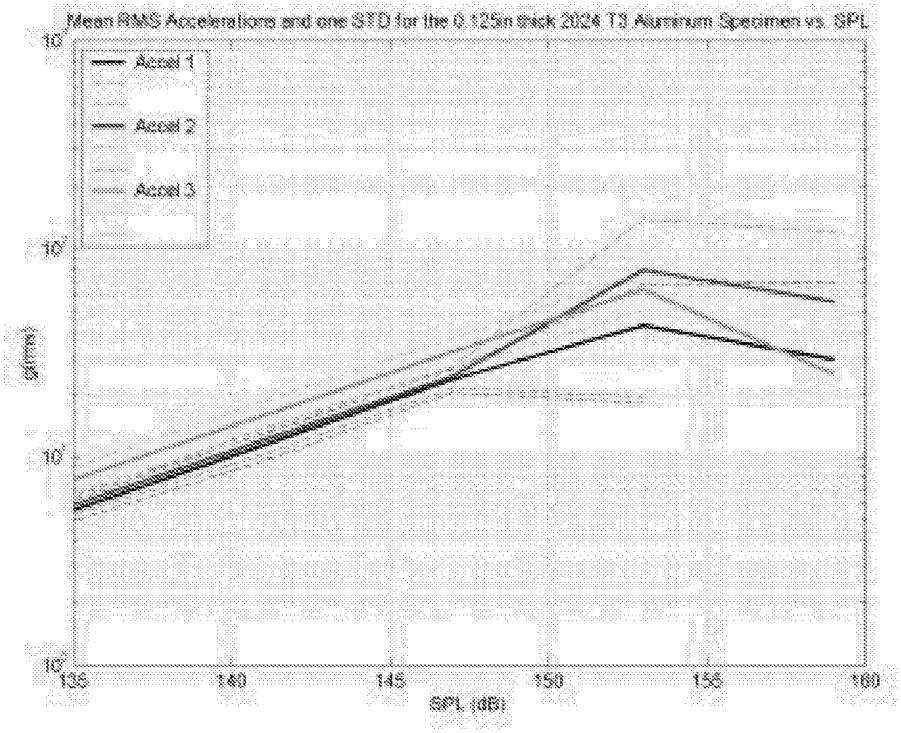

Figure 3-26. Mean and STD RMS Acceleration vs. OASPL for the 0.125in (0.318cm) plate.

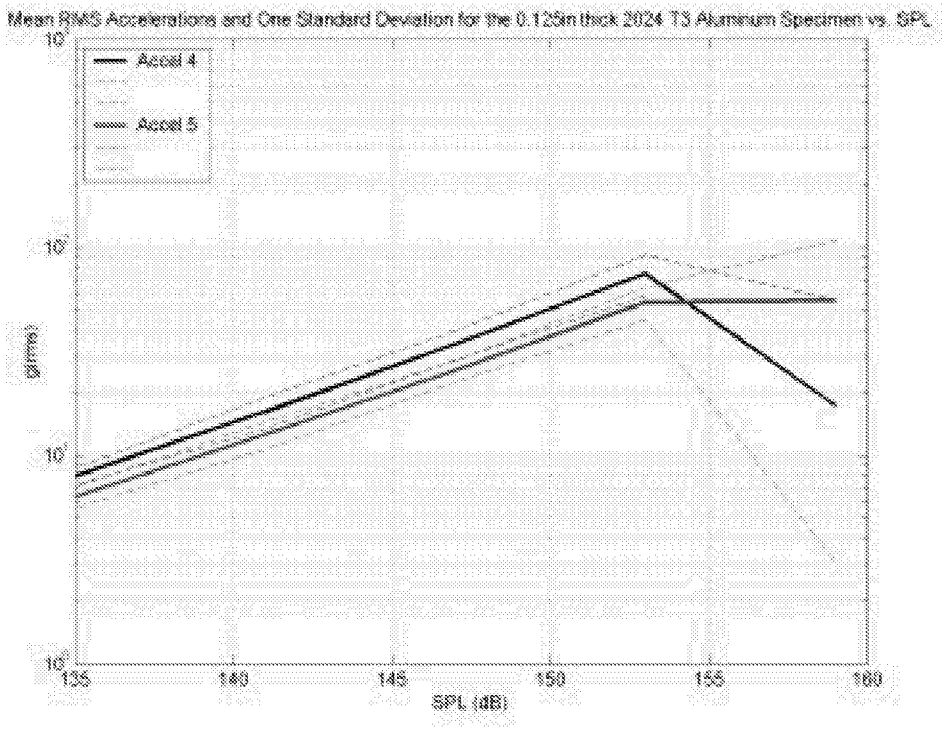

Figure 3-27. Mean and STD RMS Acceleration vs. OASPL for the 0.125in (0.318cm) plate.

Comparing the variability of the RMS vs. PSD results discussed in Section 3.2.1, the RMS results are far more repeatable. The STD results were less than 10% of the RMS results, while the STD of the PSD results were around 20% to 100% of the mean PSD results for non-resonant and resonant frequencies, respectively, for this thickness plate.

Figure 3-28 shows the overall mean and standard deviation vs. OASPL for 0.125in (0.318cm) specimen. The overall mean was computed by averaging all the accelerometer results. The STD was calculated by taking the square difference between each of the individual accelerometer run against this mean. Consequently, the STD in Fig. 3-28 is not the average of the STDs shown in Figs. 3-26 and 3-27.

The STD of the overall RMS, shown in Fig. 3-28, was on average below 20% of the overall mean RMS. There was an additional 10% more variability in the STD result, because of accelerometers response difference due to their locations on the plate.

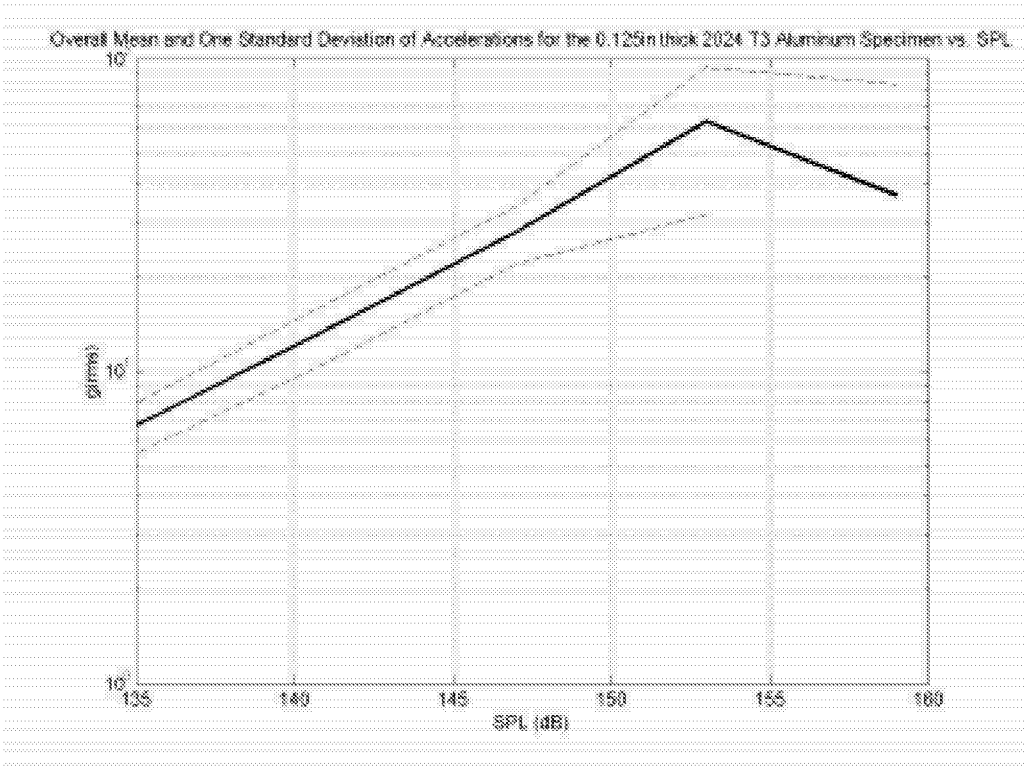

Figure 3-28. Overall Mean and STD of Accelerations vs. OASPL for the 0.125in (0.318cm) plate.

3.3.2 Thinner Plate Results

Figure 3-29 shows the RMS accelerations of different runs for Accelerometer 4 as a function of OASPL for the 0.062in (0.1588cm) plate. The plot shows a linear acceleration dynamic response vs. OASPL. Other RMS acceleration vs. OASPL for the other accelometers can be found in Appendix B.

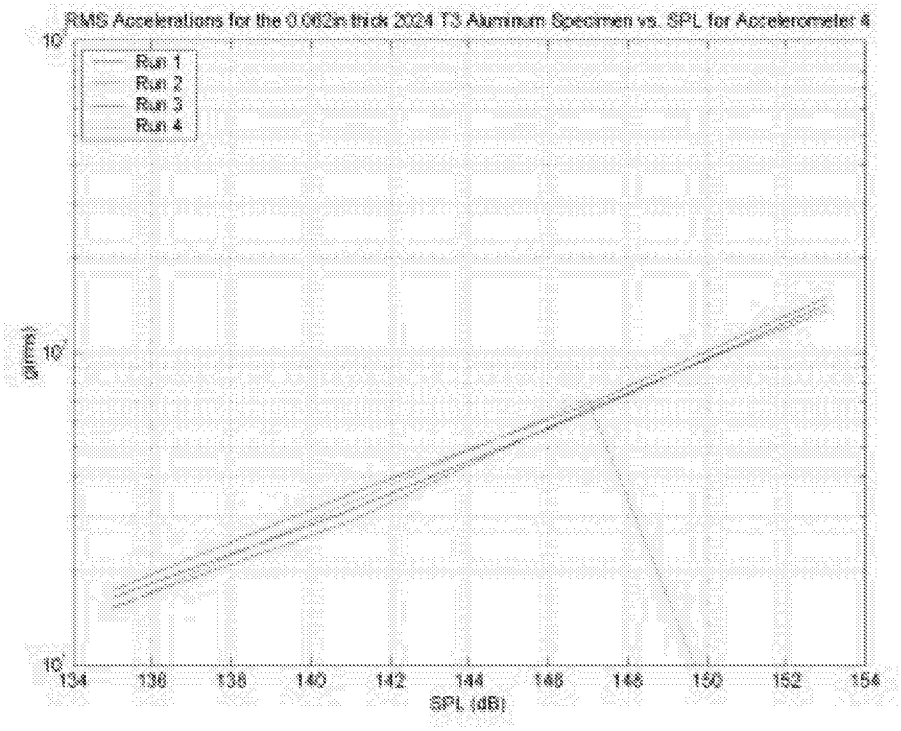

Figure 3-29. RMS Accelerations vs. OASPL for the 0.062in (0.1588cm) plate.

Figures 3-30 and 3-31 show the mean (solid line) plus/minus one STD (dashed line) of the RMS acceleration for accelerometers 1 thru 5, for the 0.062in (0.1588cm) plate. The plots show a linear relationship between RMS acceleration response vs. incident OASPL for accelerometers 1 thru 5. The plots also show that the one STD envelope had a fairly constant distance from its mean RMS results with increasing OASPL. This trend started to break down around 147dB, where the one STD envelope for accelerometers 2 and 4 start diverging from its mean RMS result.

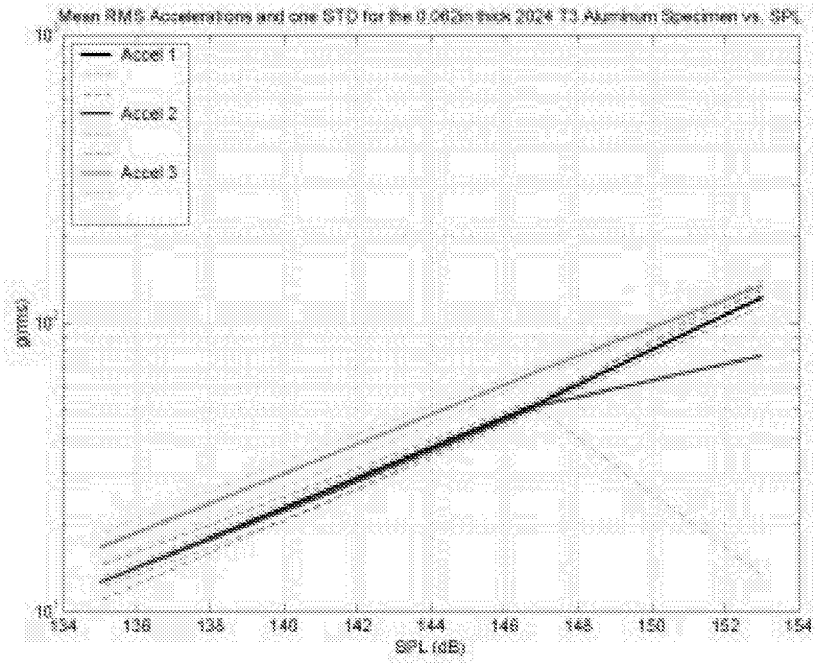

Figure 3-30. Mean and STD RMS Acceleration vs. OASPL for the 0.062in (0.1588cm) plate.

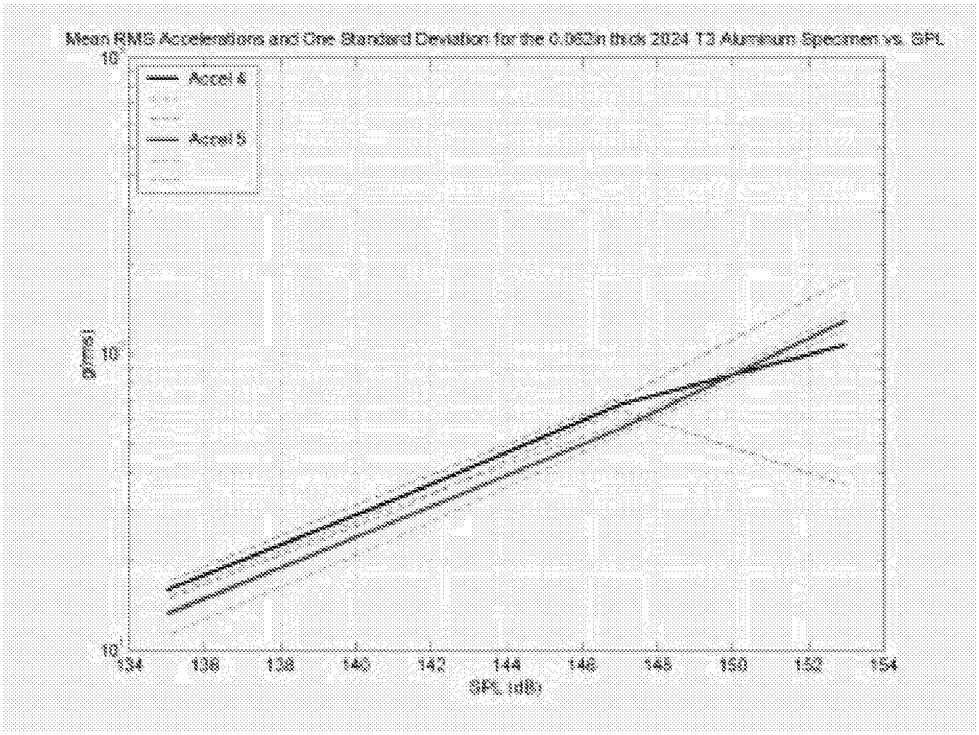

Figure 3-31. Mean and STD RMS Acceleration vs. OASPL for the 0.062in (0.1588cm) plate.

The variability comparison between RMS vs. PSD results (discussed in Section 3.2.2) for the 0.062in (0.1588cm) plate produced similar results as for the thicker 0.125in (0.318cm) plate. For the 0.062in (0.1588cm) plate, on average, the STD of the RMS results was less than 10% of the mean RMS results. In contrast, on average, the STD of the PSD results was between 25% to 125% of the mean PSD results, for nonresonant and resonant frequencies, respectively. Clearly, the RMS results were far more repeatable than the PSD results for both the thin and thick plate.

Figure 3-32 shows the overall mean and standard deviation vs. OASPL for the 0.062in (0.1588cm) plate. As stated previously for the thicker 0.125in plate, the mean was computed by averaging all the accelerometer results. The STD was calculated by taking the square difference between each of the individual accelerometer run against this mean. The STD for this plot was not calculated by averaging the square difference between each individual accelerometer runs against that accelerometer mean. Consequently, the STD in Fig. 3-32 is not the average of the STDs shown in Figs. 3-30 and 3-31.

The STD of the overall RMS, shown in Fig. 3-32, was on average 15% to 20% of the overall mean RMS. Therefore, there was an additional 5% to 10% more variability in the STD result, because of accelerometers response difference due to their location on the plate. This result was comparable to the thicker 0.125in (0.318cm) plate, which also experienced an additional 10% more variability in this STD results due to the same accelerometer location response differences reason.

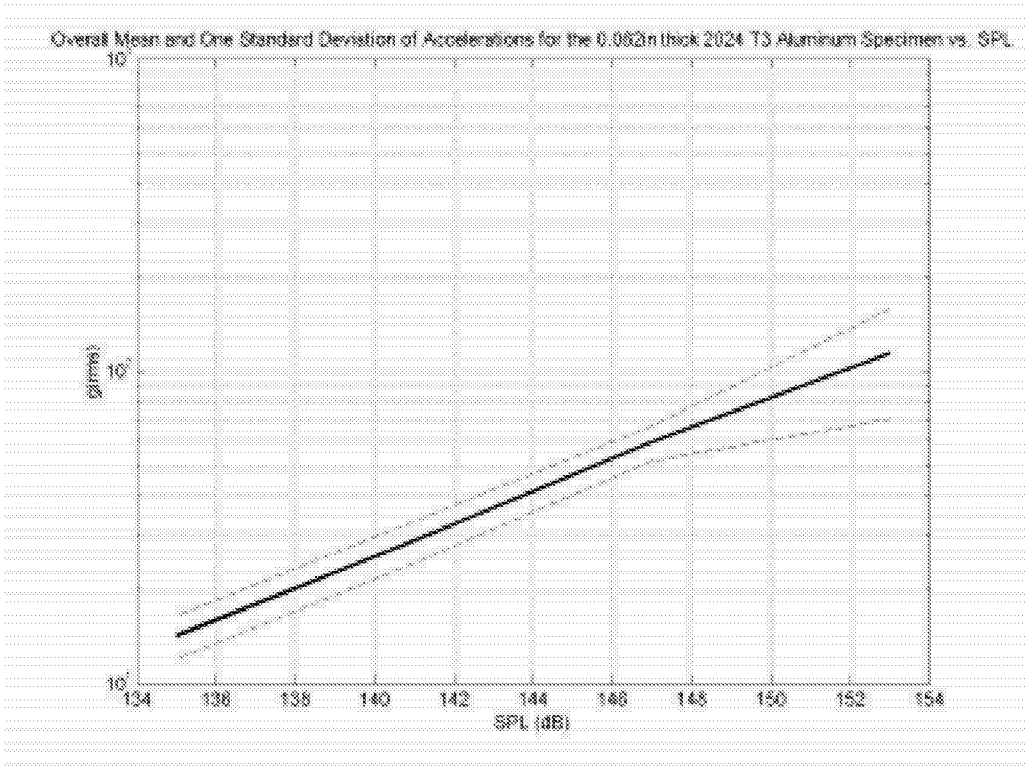

Figure 3-32. Overall Mean and STD of Accelerations vs. OASPL for the 0.125in (0.318cm) plate.

References

1. Rizzi, S.A., "Improvements To Progressive Wave Tube Performance Through Closed-Loop Control," NASA/TM-2000-210623, October 2000.
2. “VibControl/NT, revision 2.4.0 Manual,” M+P International, Inc. 1999.
3. Makridakis, S., Wheelwright, S.C., and Hyndman, R.J., Forecasting Methods and Applications, Wiley, New York, 1998.
4. McConnell, K.G., Vibration Testing Theory and Practice, Wiley, New York, 1995. pp. 49-50.

4. Conclusions

The objective of the current study was to assess the repeatability of experiments at NASA Langley's Thermal Acoustic Fatigue Apparatus (TAFA) facility and to use these experiments to validate numerical models. To this end experiments were conducted in this progressive wave tube (PWT) facility's four-modulator configuration.

Experiments show that power spectral density (PSD) curves were repeatable except at the resonant frequencies, which tended to vary between 5Hz to 15Hz. Results show that the thinner specimen had more variability in the resonant frequency location than the thicker sample, especially for modes higher than the first mode in the frequency range.

Absolute Percent Errors (APEs) and Mean Absolute Percent Errors (MAPEs) were calculated to increase to normalize the error results and increase the statistical population size. MAPE results indicated that errors were largely insensitive to the location in the sample, but were very sensitive to the magnitude of the response. Therefore, resonant frequencies and higher OASPL tended to produce higher MAPEs.

The time of the day (morning or afternoon) that the plate specimens were tested affected their dynamic resonant response. The only change between morning and afternoon tests was possibly the air temperature in the PWT. Therefore, it stands to reason, that the air being fed to the PWT warmed up during day affecting the dynamic response of the plates at the resonant frequencies. The torquing sequence used to clamp the plates was changed from day to day, and yet the resonant responses were repeatable for the thicker 0.125in (0.318cm) plate. Therefore, torquing sequence did not affect the dynamic response of the thicker plate. The thinner 0.062in (0.1588cm) plate's resonant dynamic response was affected by torquing sequence.

Root Mean Square (RMS) (the area under the PSD curves) tended to be more repeatable. The RMS accelerations increased with SPL and the specimen tended to behave "linearly" through the SPL range of 135 to 153dB. Standard Deviations (STDs) of the results tended to be relatively low constant up to about 147dB.

Comparing the variability of the RMS vs. PSD results, the RMS results were more repeatable. The STD results were less than 10% of the RMS results for both the

0.125in (0.318cm) and 0.062in (0.1588cm) thick plate. The STD of the PSD results were around 20% to 100% of the mean PSD results for non-resonant and resonant frequencies, respectively, for the 0.125in (0.318cm) thicker plate and between 25% to 125% of the mean PSD results, for nonresonant and resonant frequencies, respectively, for the thinner plate.

Appendix A: Complete PSD Results

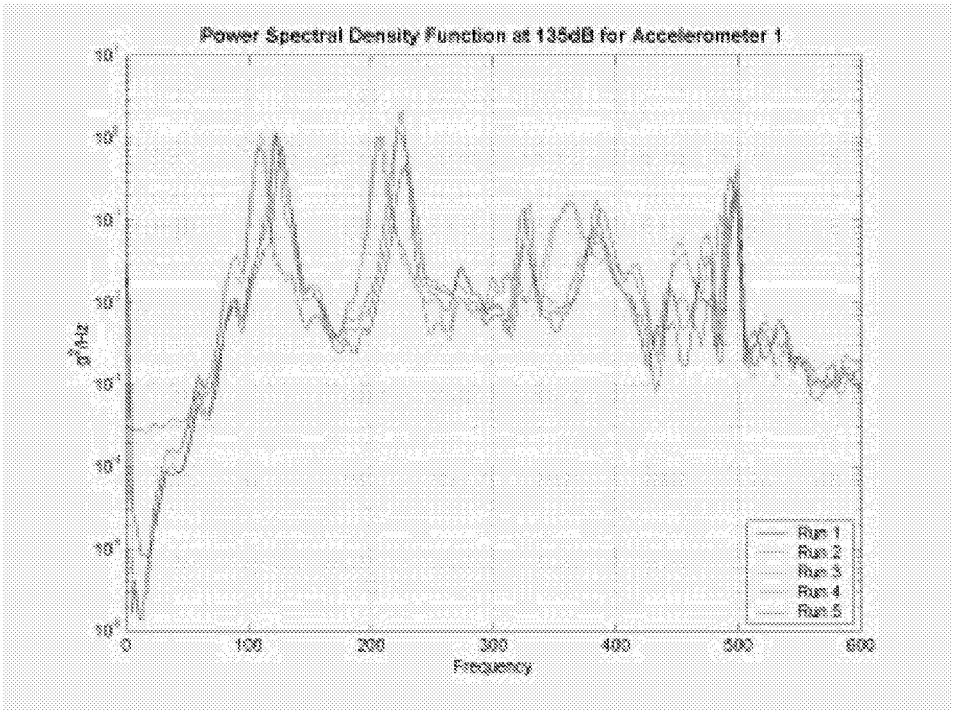

Figure A-1. PSD at 135dB for Accelerometer 1 and 0.125in thick plate.

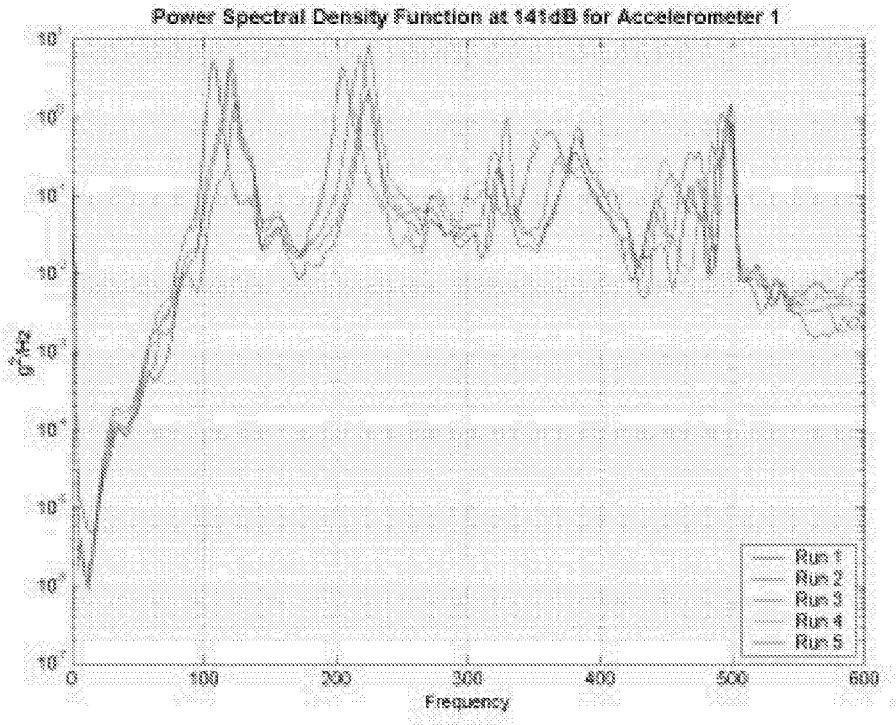

Figure A-2. PSD at 141dB for Accelerometer 1 and 0.125in thick plate.

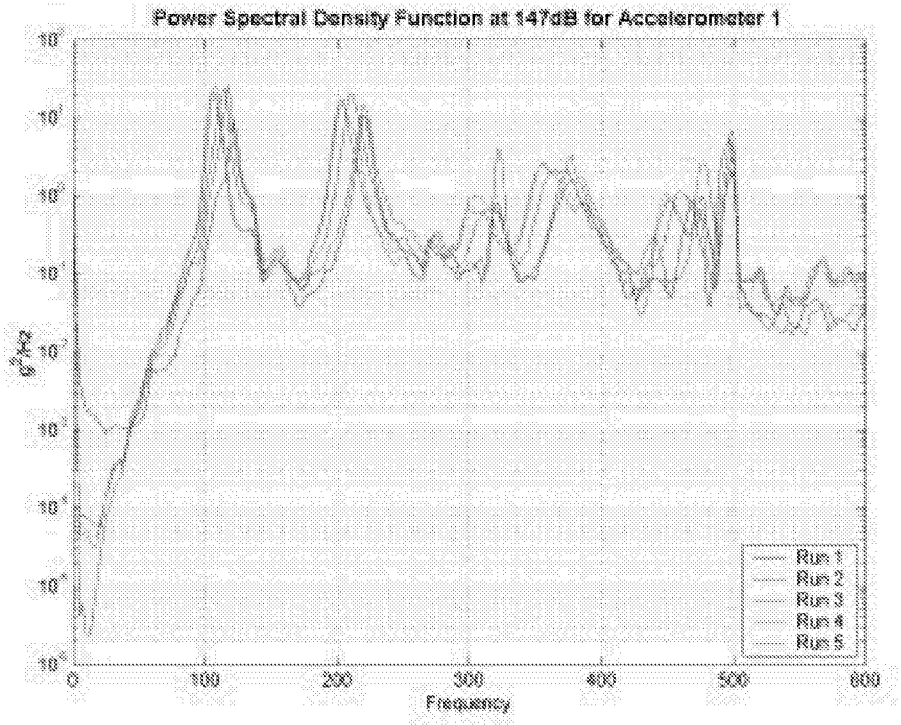

Figure A-3. PSD at 147dB for Accelerometer 1 and 0.125in thick plate.

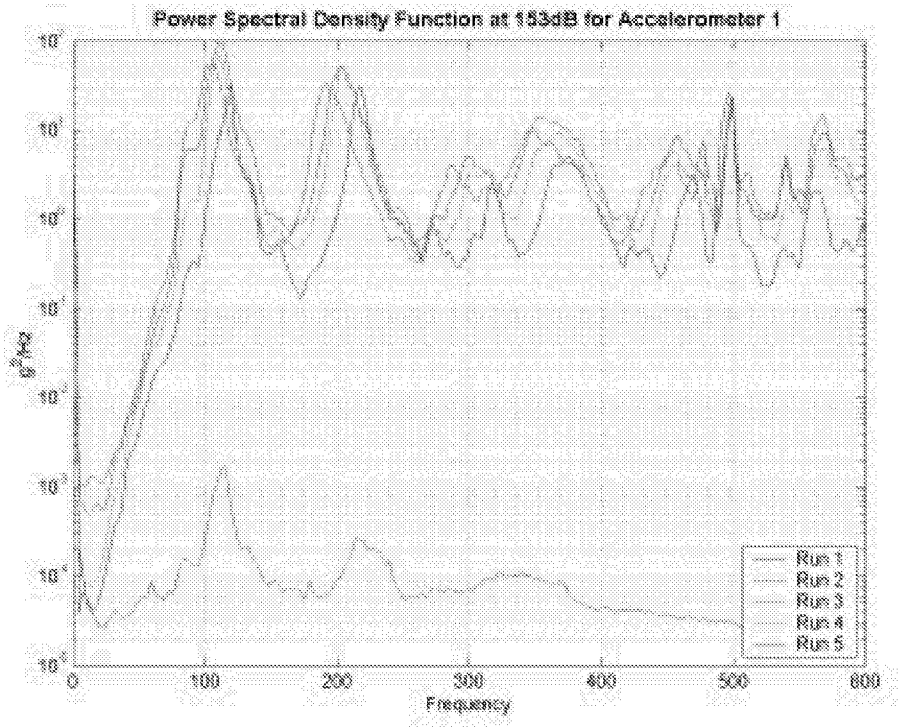

Figure A-4. PSD at 153dB for Accelerometer 1 and 0.125in thick plate.

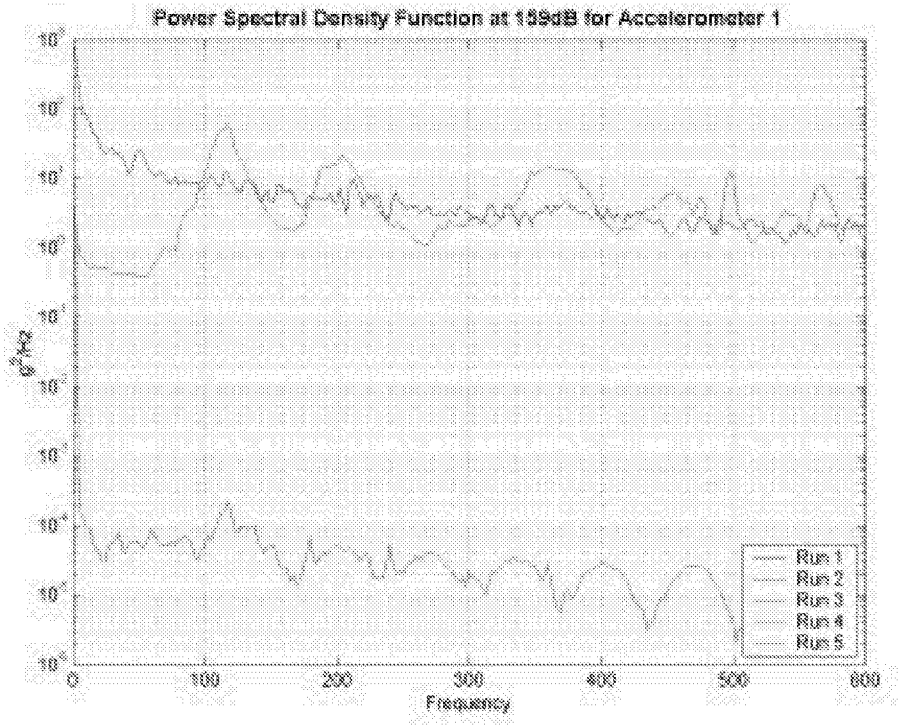

Figure A-5. PSD at 159dB for Accelerometer 1 and 0.125in thick plate.

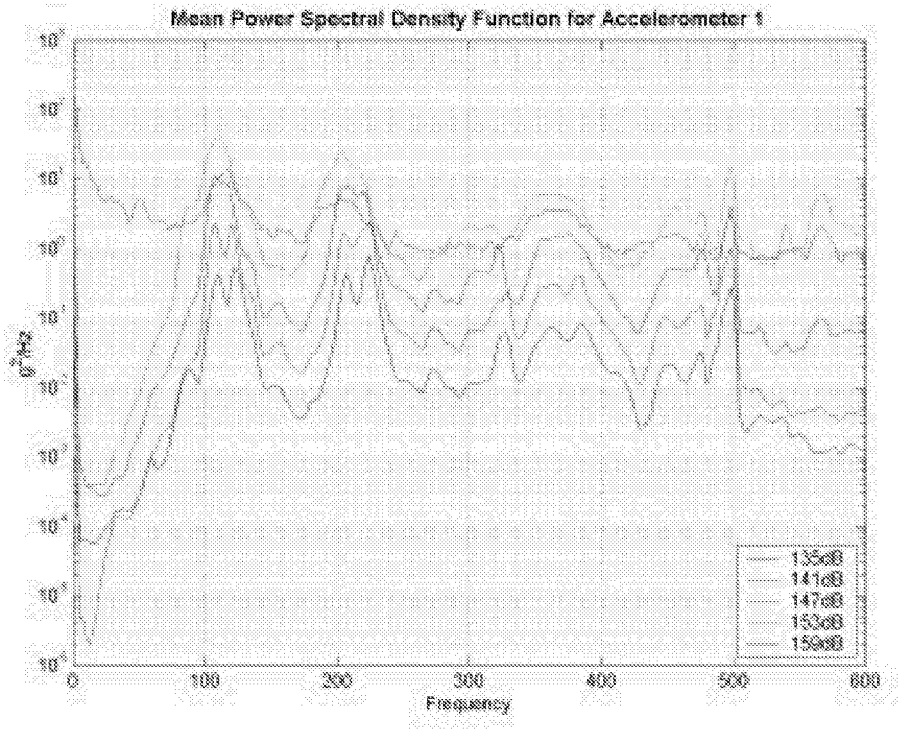

Figure A-6. Mean PSD for Accelerometer 1 and 0.125in thick plate.

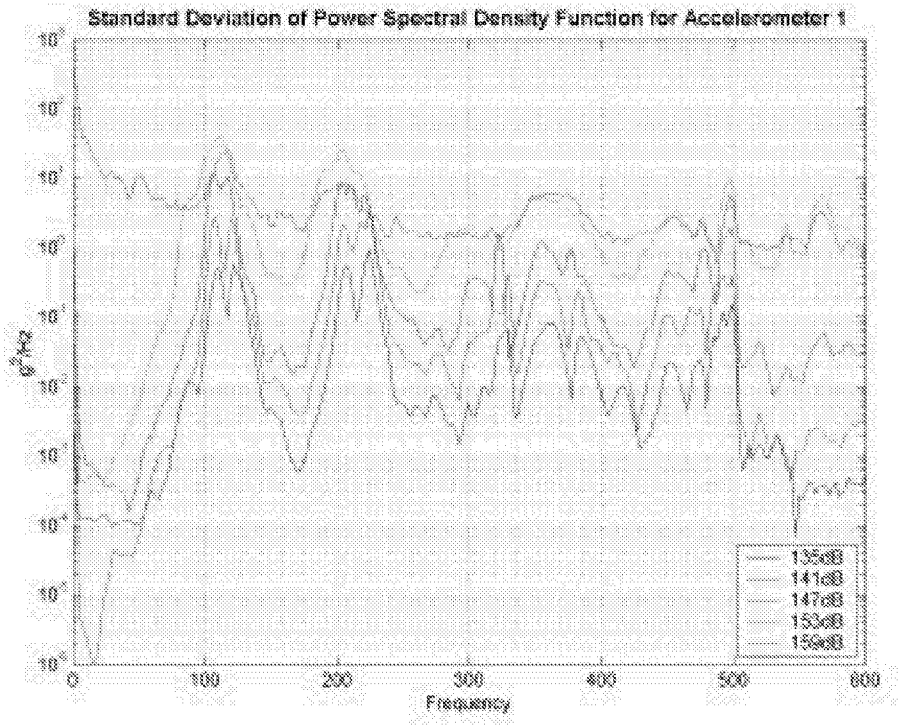

Figure A-7. STD of PSD for Accelerometer 1 and 0.125in thick plate.

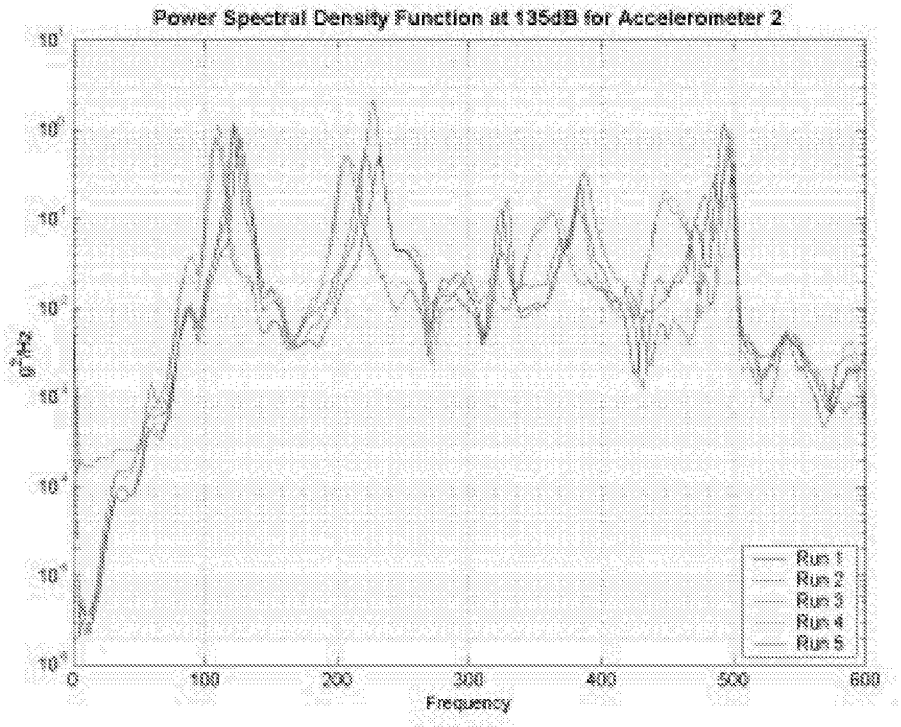

Figure A-8. PSD at 135dB for Accelerometer 2 and 0.125in thick plate.

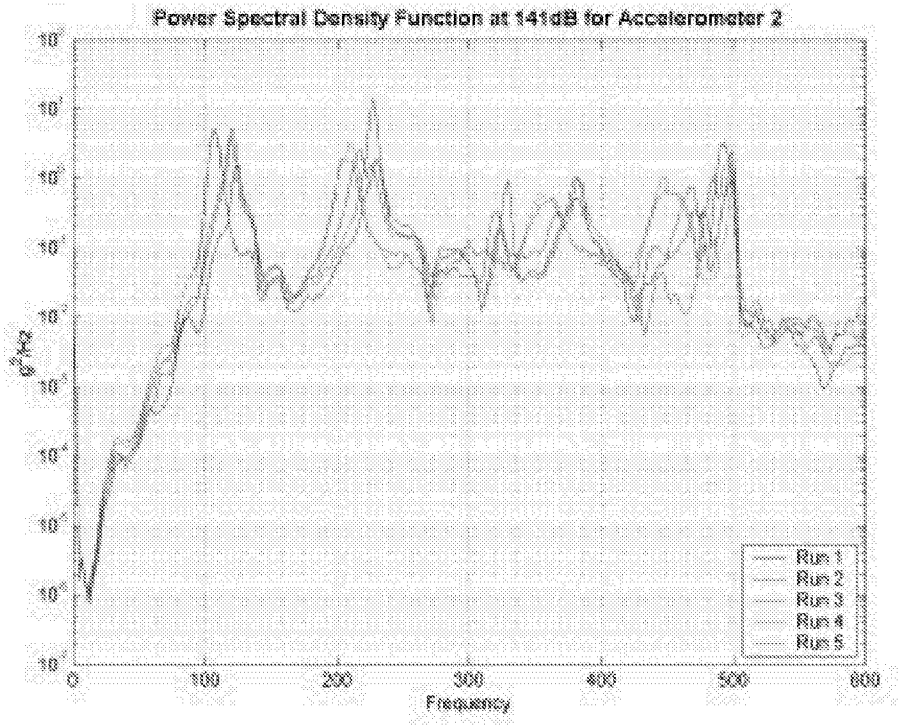

Figure A-9. PSD at 141dB for Accelerometer 2 and 0.125in thick plate.

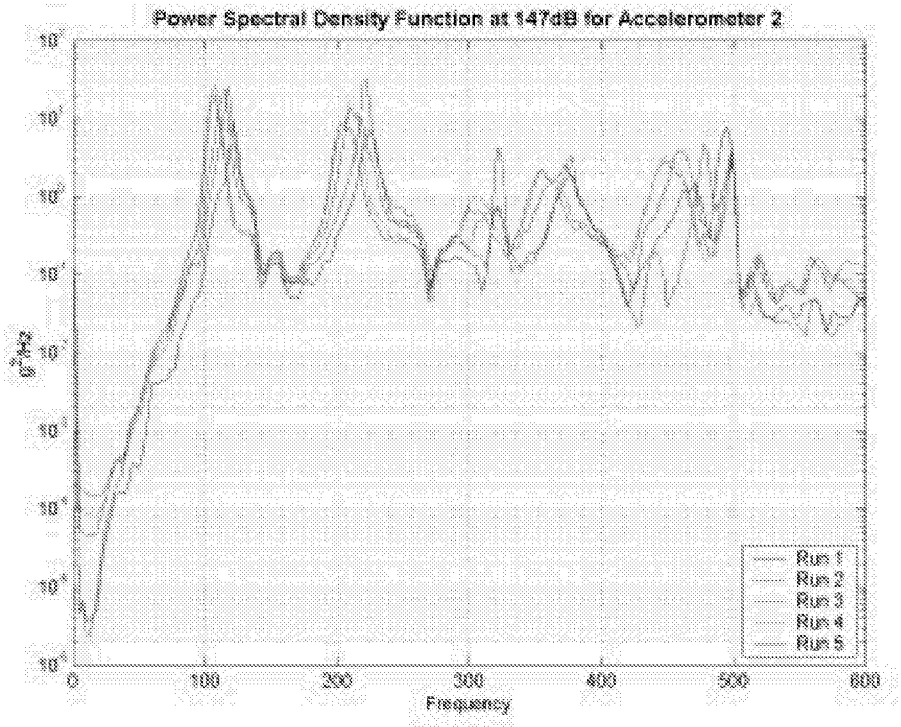

Figure A-10. PSD at 147dB for Accelerometer 2 and 0.125in thick plate.

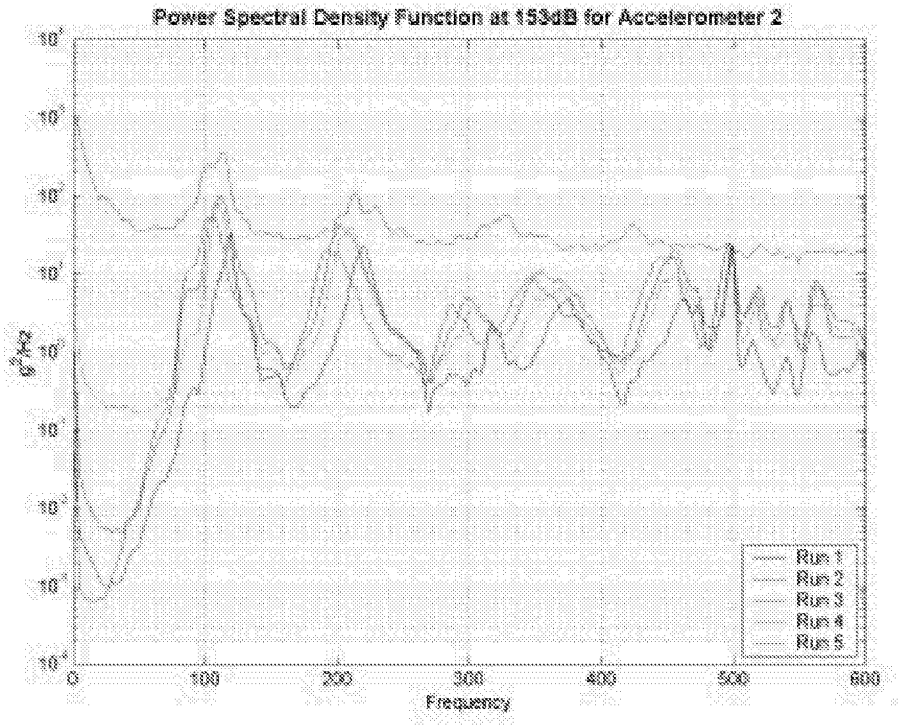

Figure A-11. PSD at 153dB for Accelerometer 2 and 0.125in thick plate.

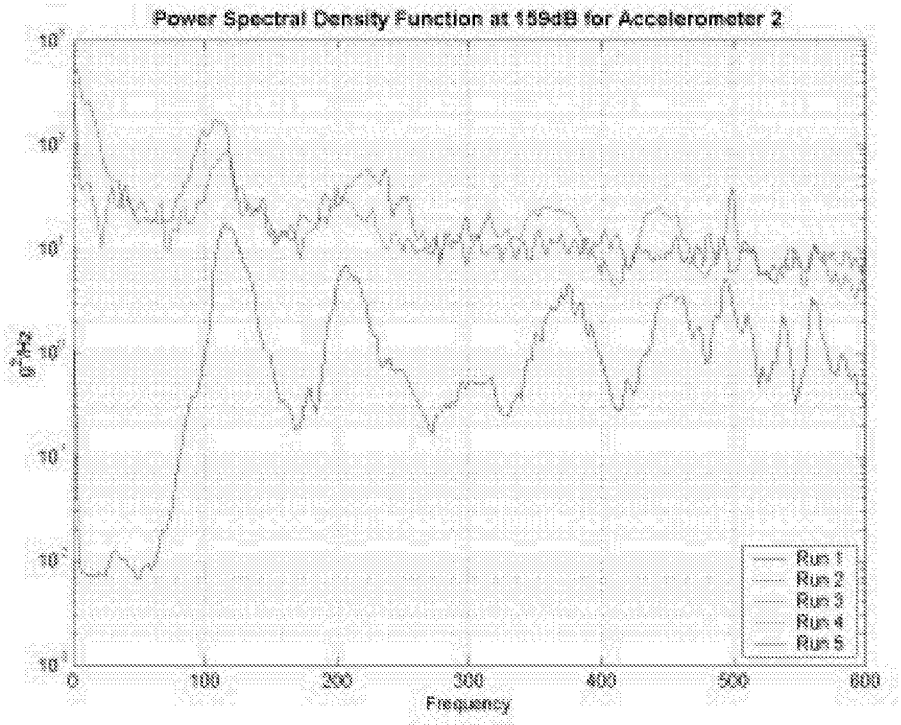

Figure A-12. PSD at 159dB for Accelerometer 2 and 0.125in thick plate.

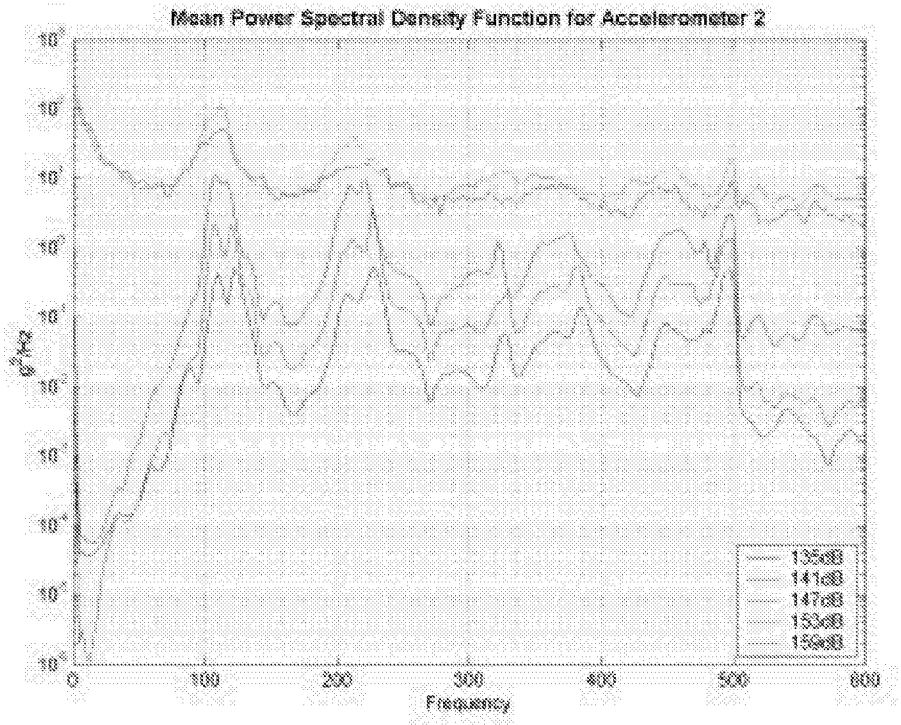

Figure A-13. Mean PSD for Accelerometer 2 and 0.125in thick plate.

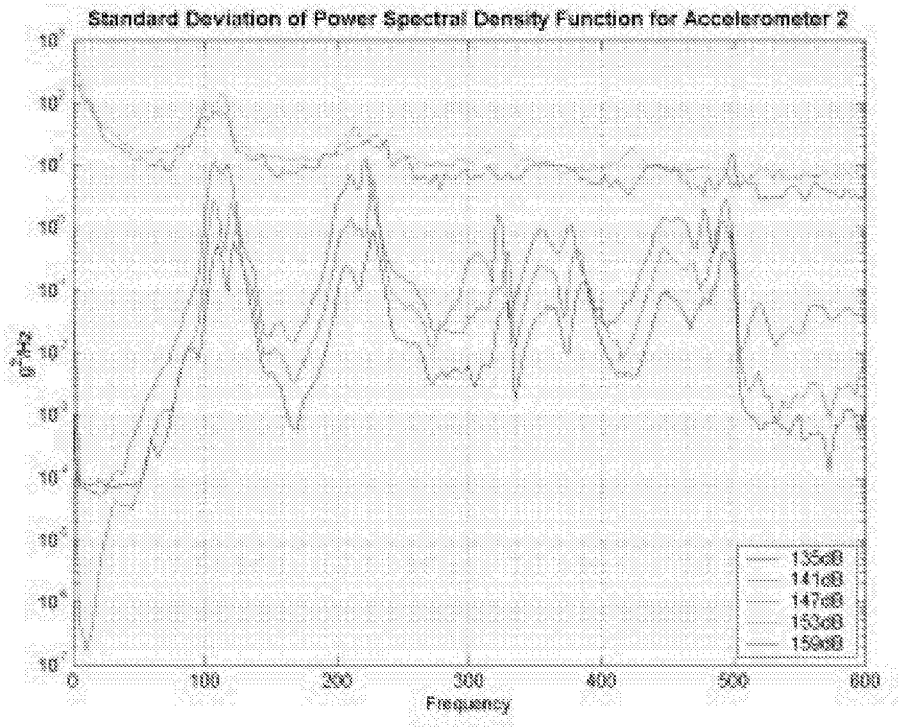

Figure A-14. STD of PSD for Accelerometer 2 and 0.125in thick plate.

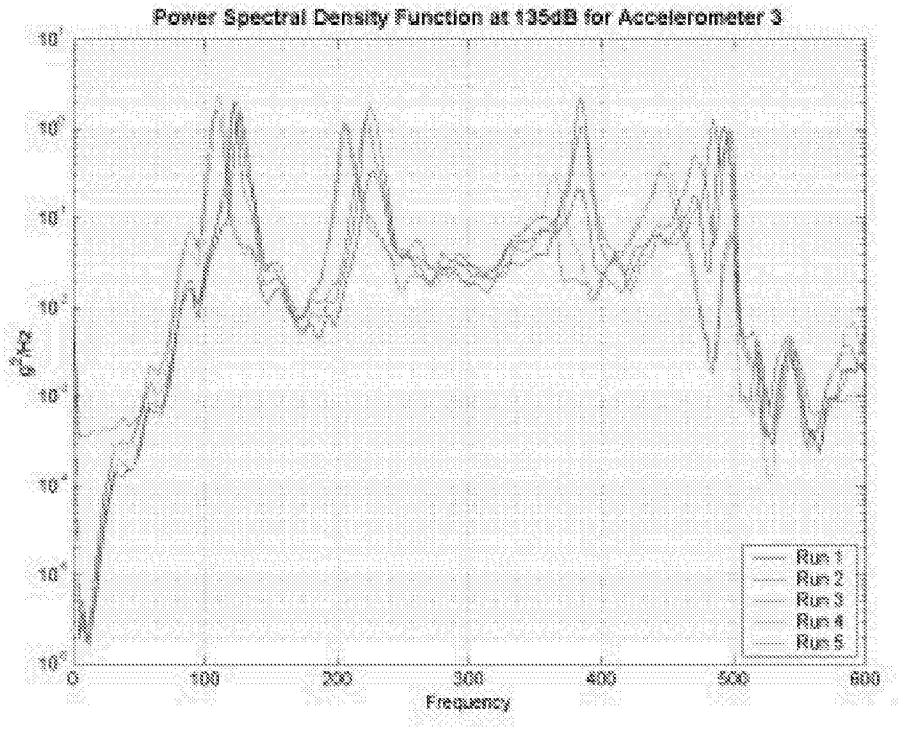

Figure A-15. PSD at 135dB for Accelerometer 3 and 0.125in thick plate.

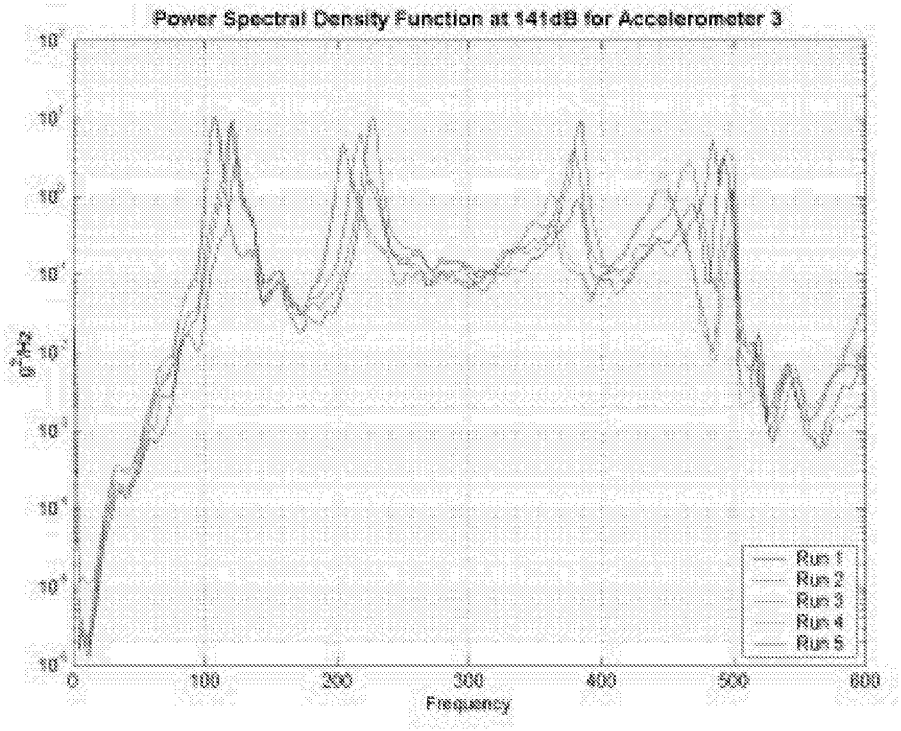

Figure A-16. PSD at 141dB for Accelerometer 3 and 0.125in thick plate.

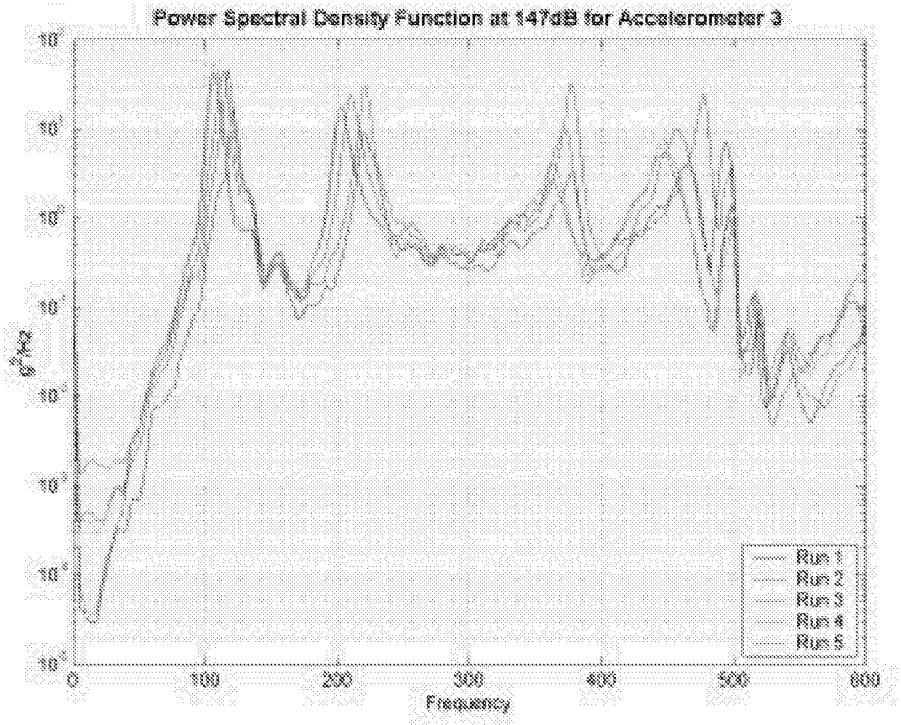

Figure A-17. PSD at 147dB for Accelerometer 3 and 0.125in thick plate.

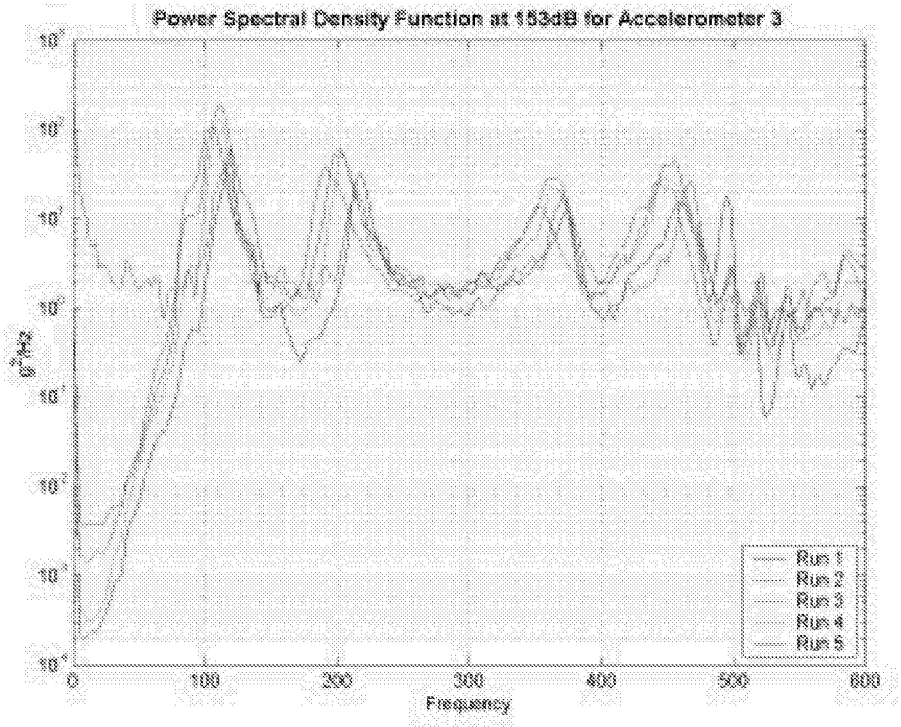

Figure A-18. PSD at 153dB for Accelerometer 3 and 0.125in thick plate.

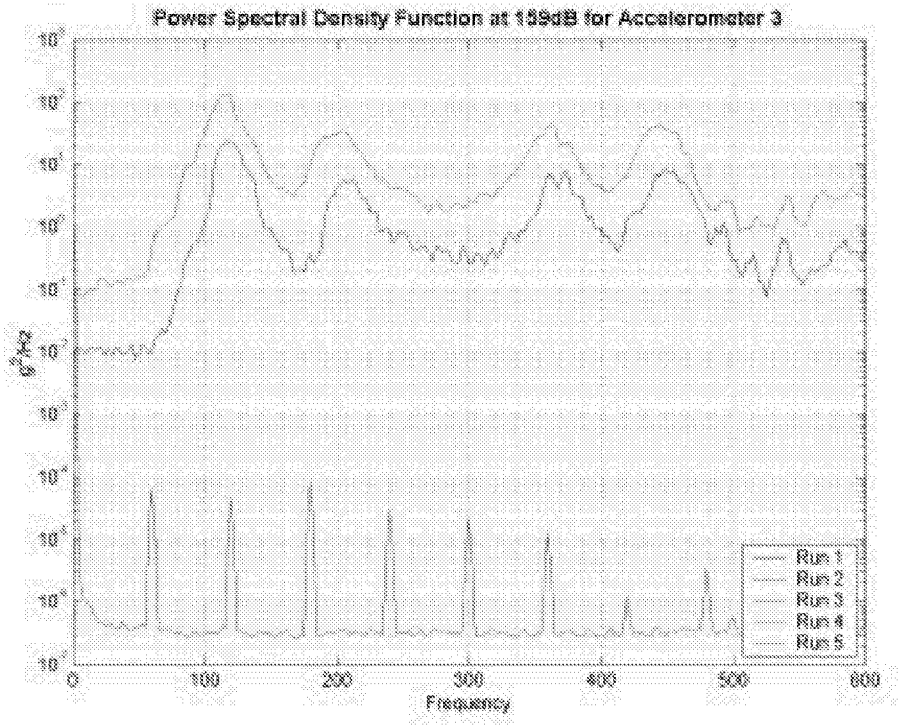

Figure A-19. PSD at 159dB for Accelerometer 3 and 0.125in thick plate.

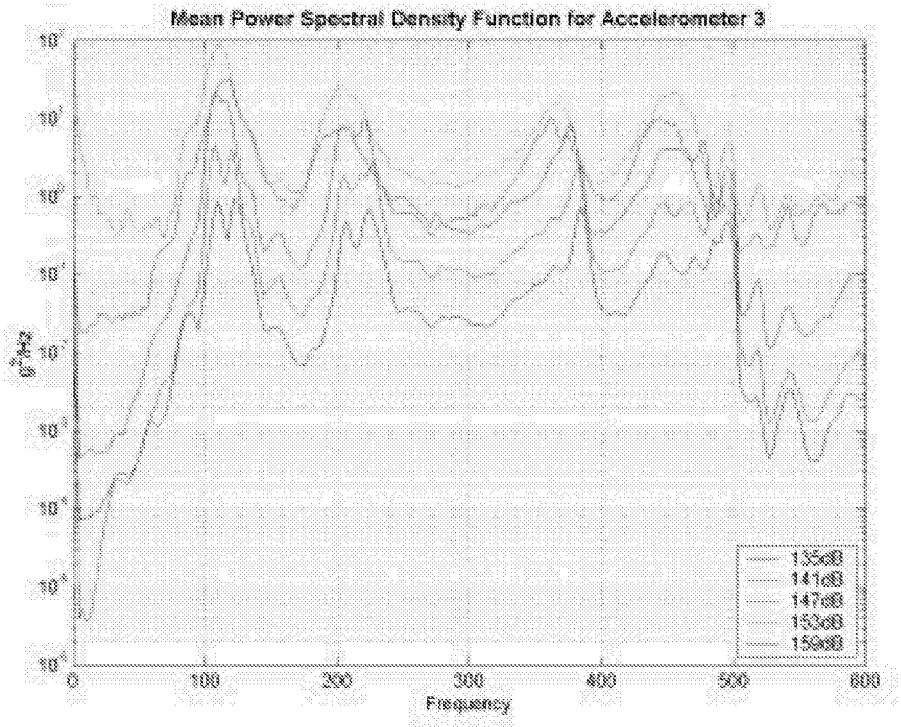

Figure A-20. Mean PSD for Accelerometer 3 and 0.125in thick plate.

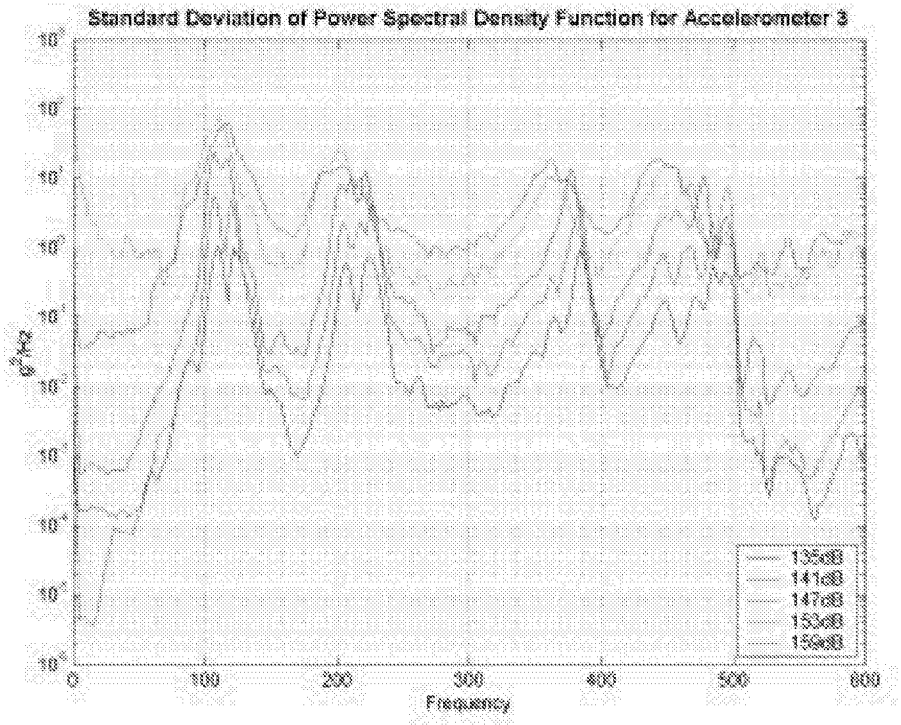

Figure A-21. STD of PSD for Accelerometer 3 and 0.125in thick plate.

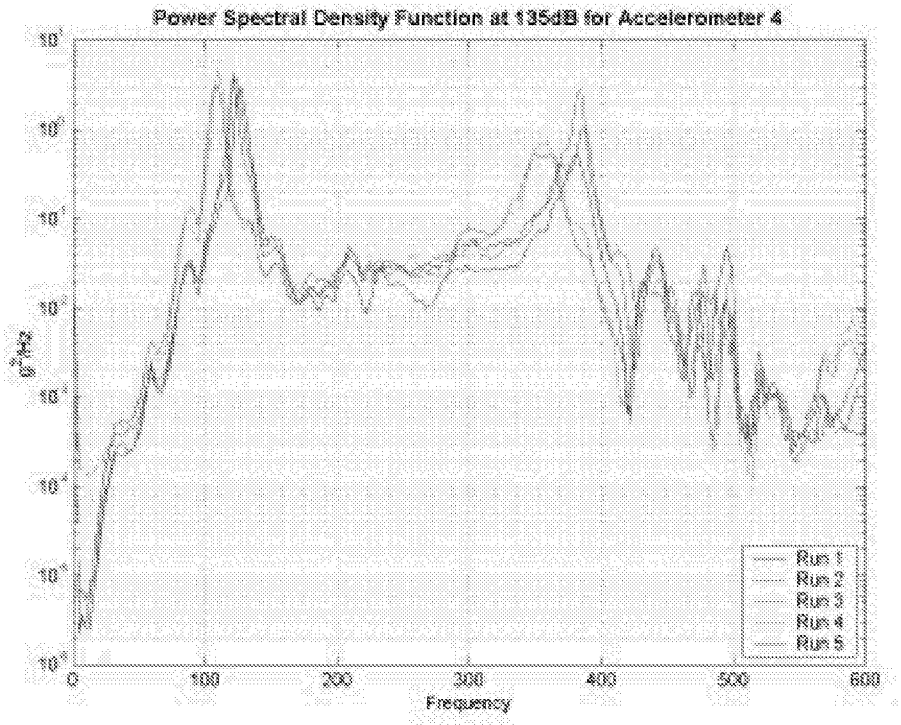

Figure A-22. PSD at 135dB for Accelerometer 4 and 0.125in thick plate.

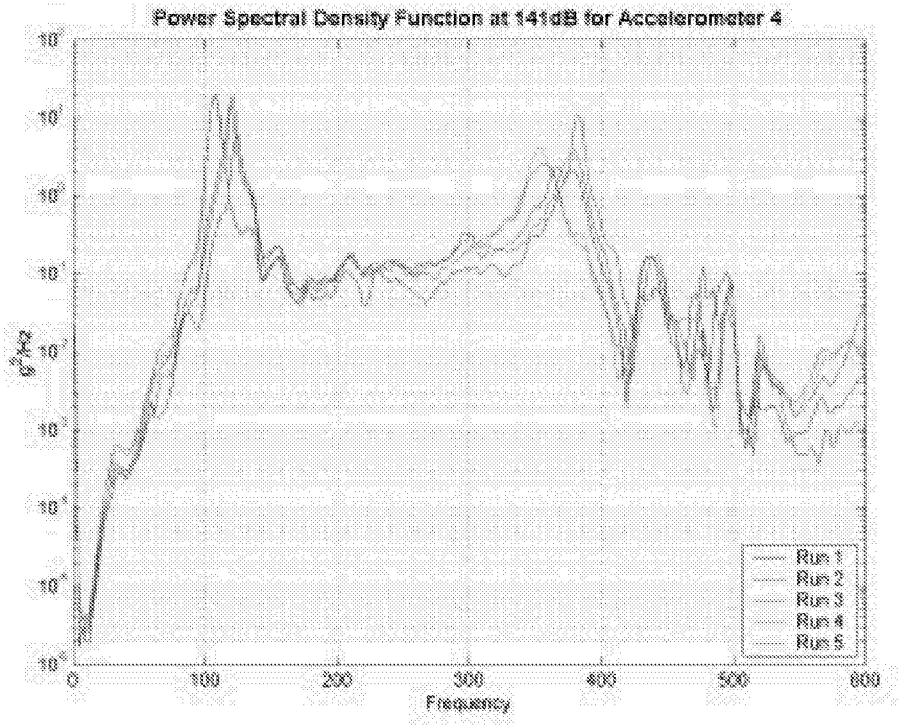

Figure A-23. PSD at 141dB for Accelerometer 4 and 0.125in thick plate.

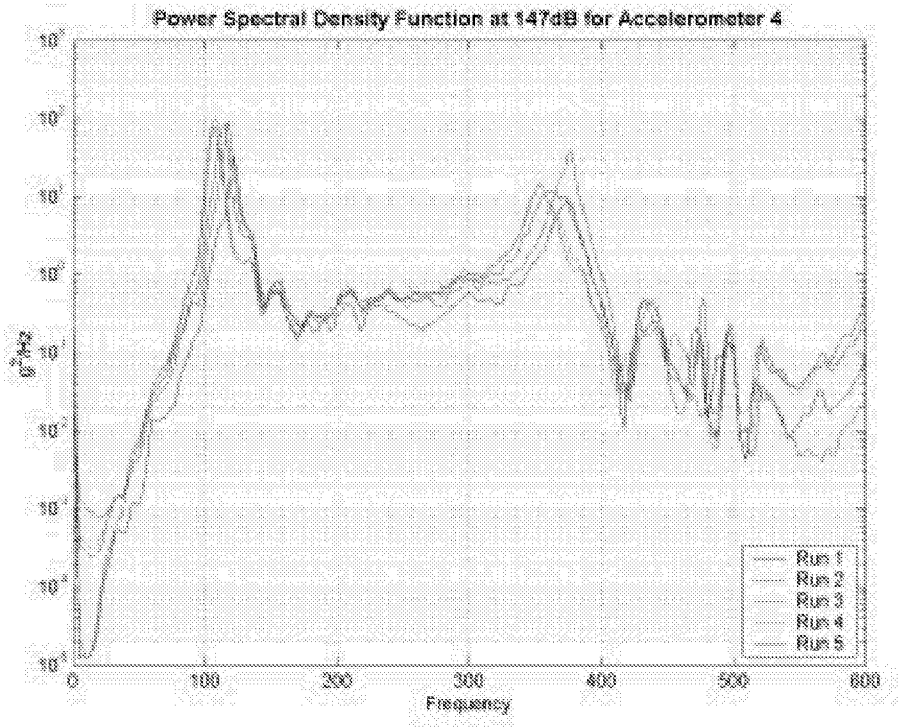

Figure A-24. PSD at 147dB for Accelerometer 4 and 0.125in thick plate.

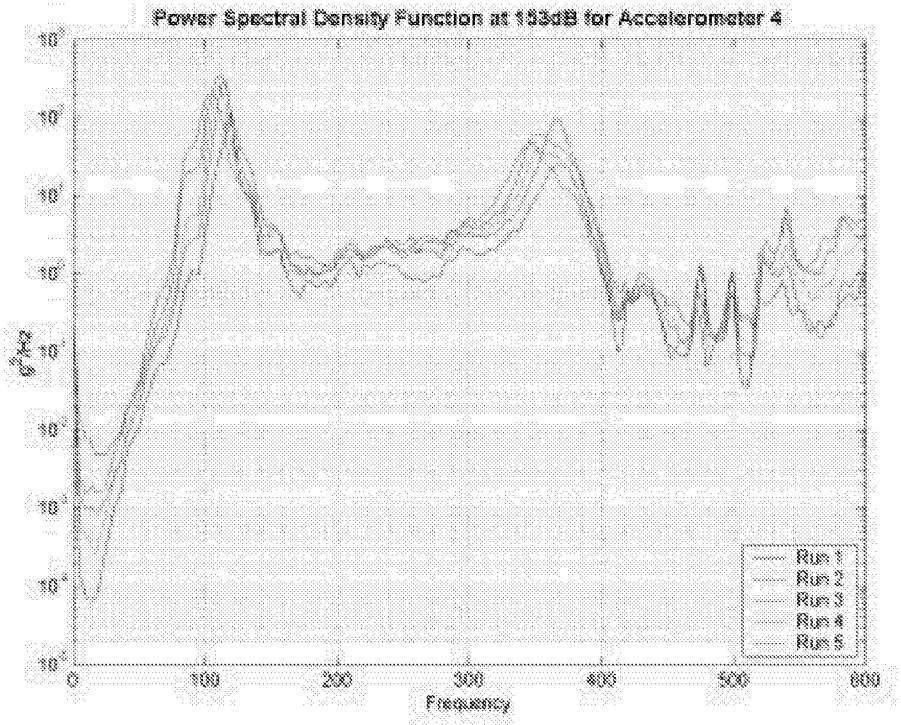

Figure A-25. PSD at 153dB for Accelerometer 4 and 0.125in thick plate.

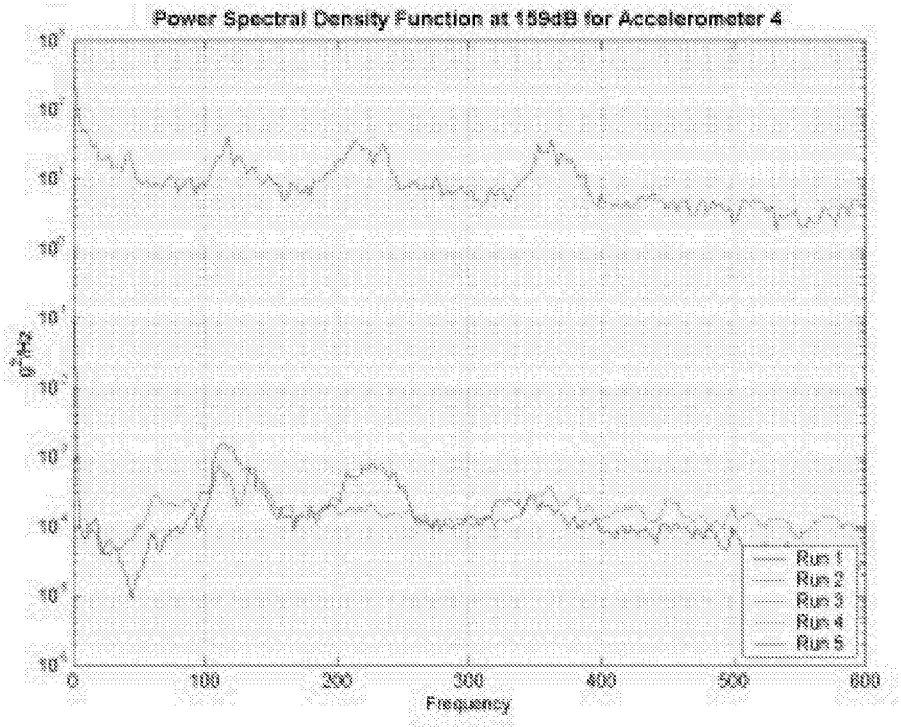

Figure A-26. PSD at 159dB for Accelerometer 4 and 0.125in thick plate.

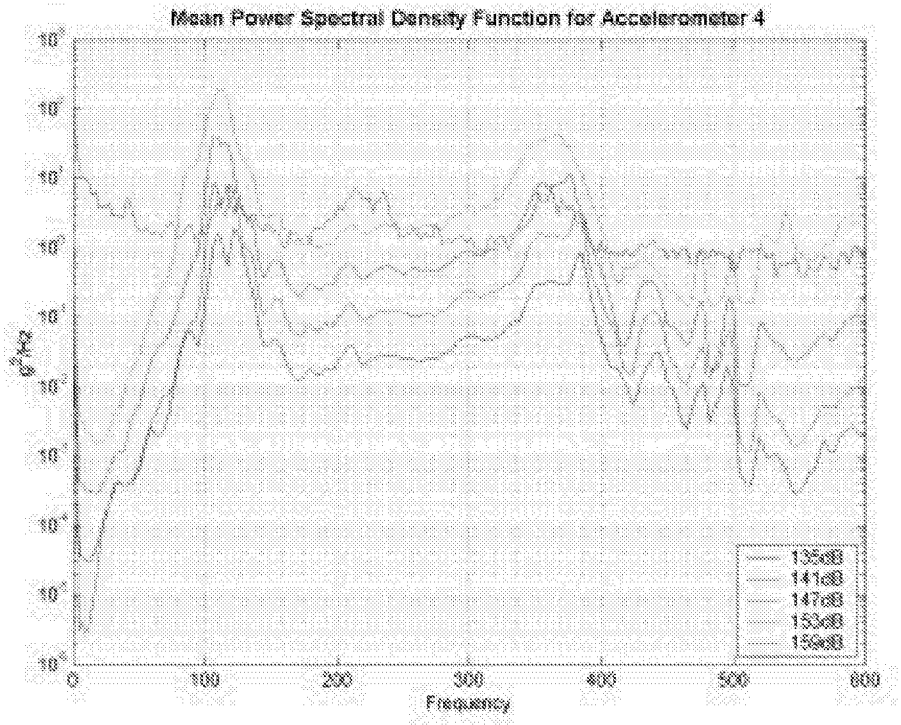

Figure A-27. Mean PSD for Accelerometer 4 and 0.125in thick plate.

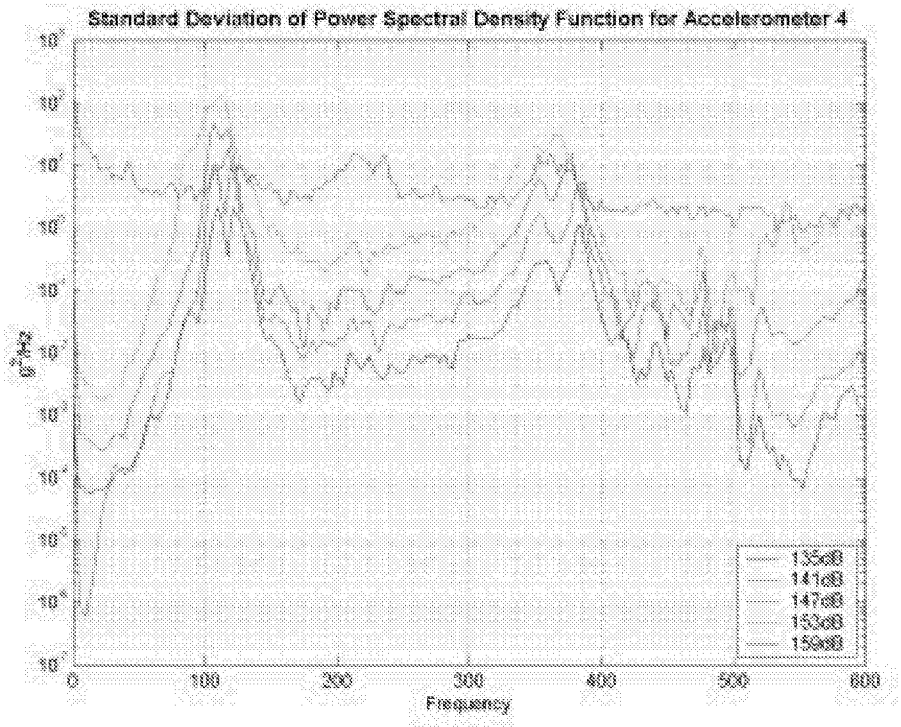

Figure A-28. STD of PSD for Accelerometer 4 and 0.125in thick plate.

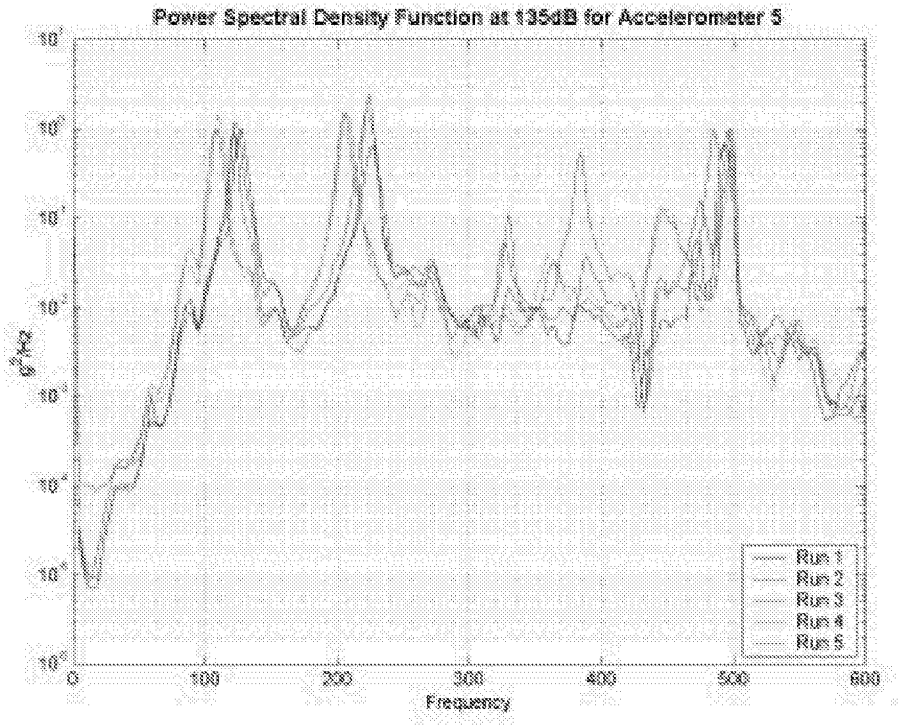

Figure A-29. PSD at 135dB for Accelerometer 5 and 0.125in thick plate.

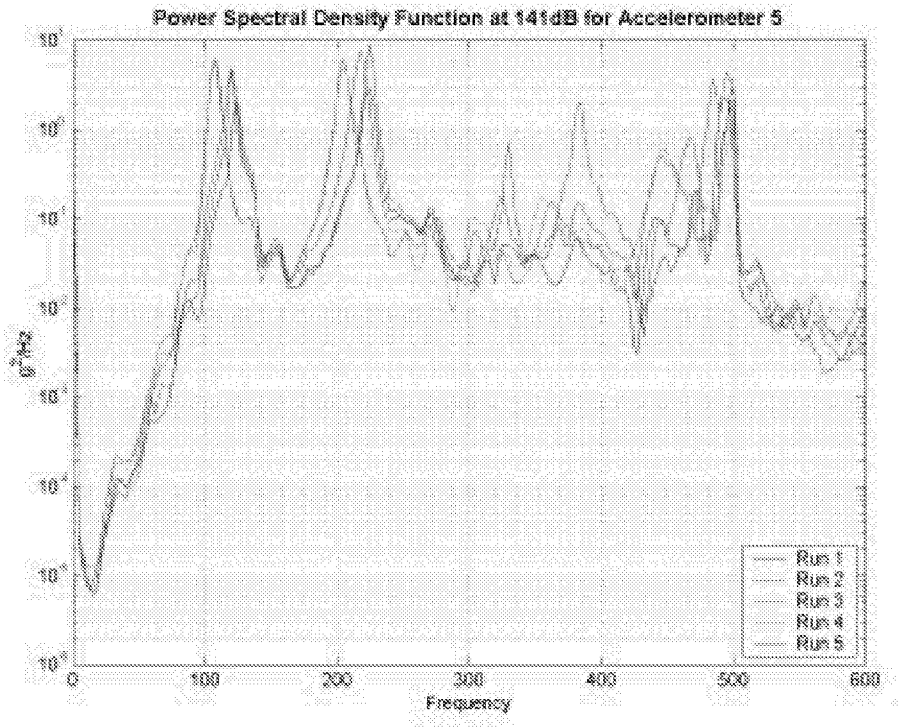

Figure A-30. PSD at 141dB for Accelerometer 5 and 0.125in thick plate.

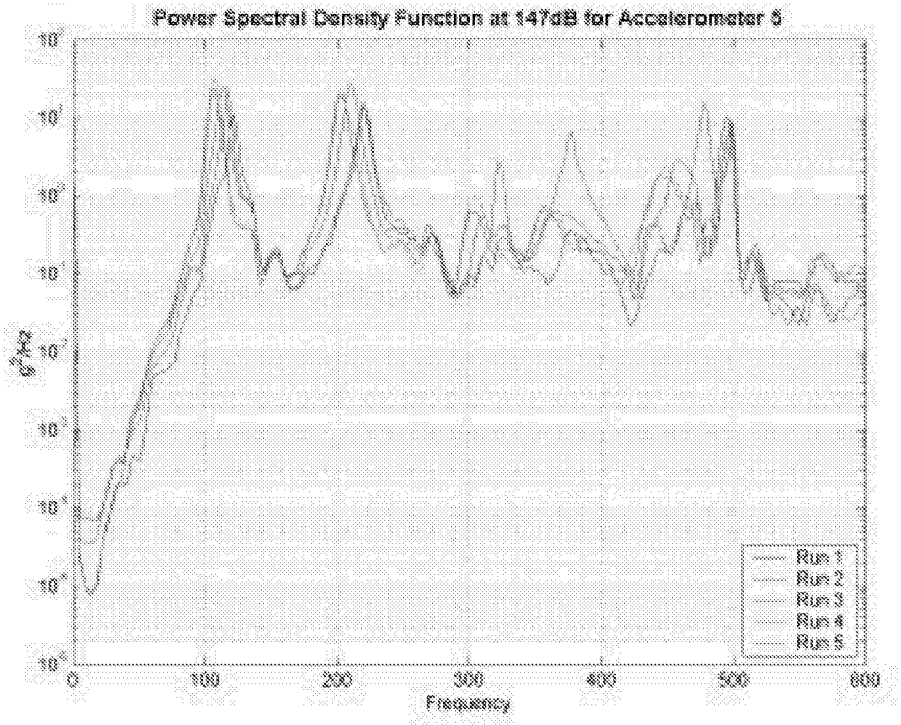

Figure A-31. PSD at 147dB for Accelerometer 5 and 0.125in thick plate.

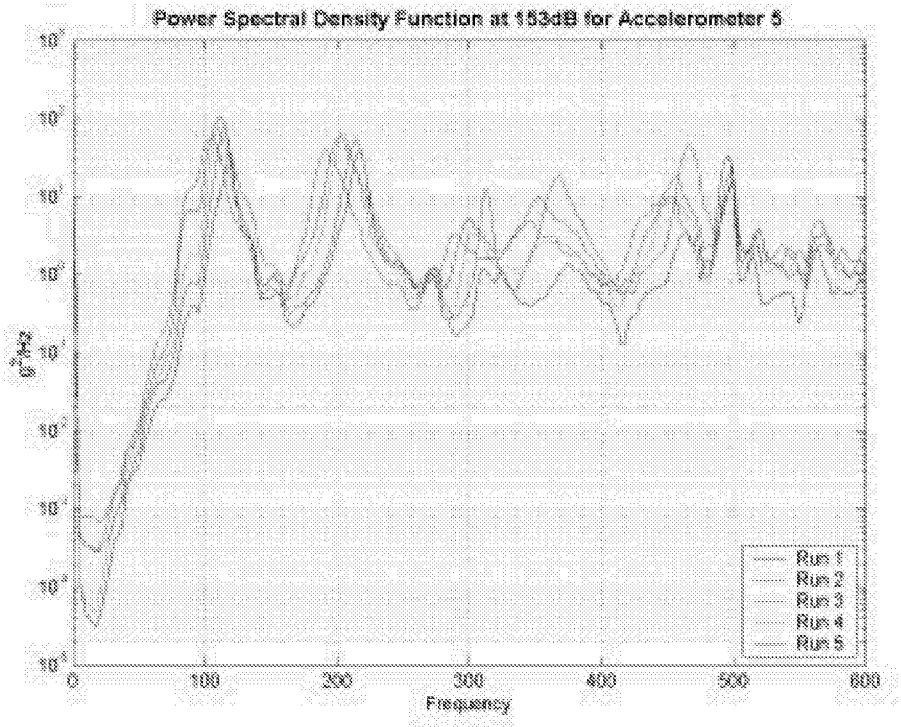

Figure A-32. PSD at 153dB for Accelerometer 5 and 0.125in thick plate.

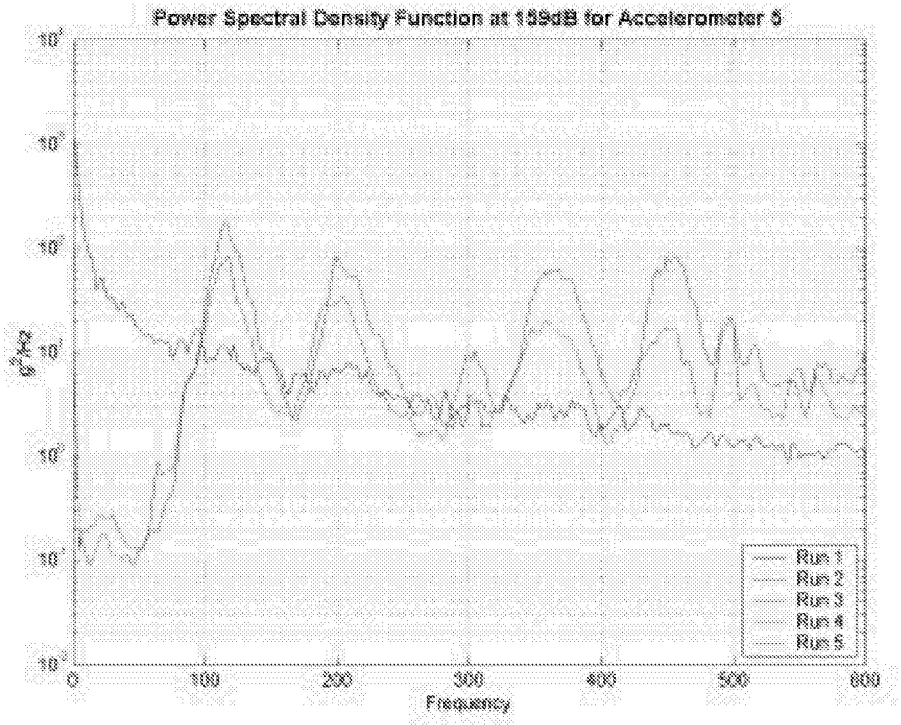

Figure A-33. PSD at 159dB for Accelerometer 5 and 0.125in thick plate.

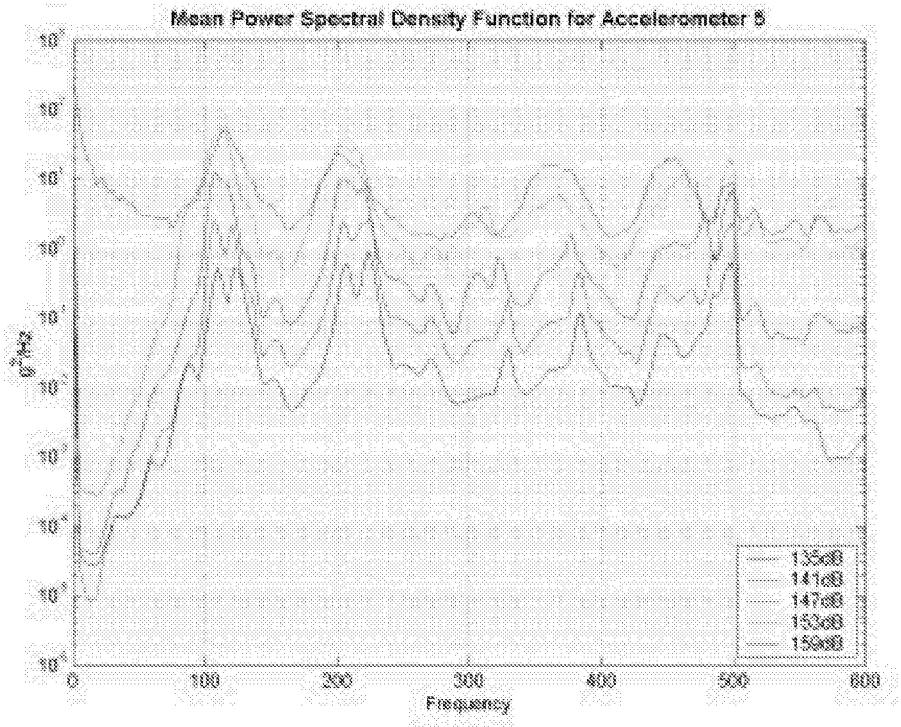

Figure A-34. Mean PSD for Accelerometer 5 and 0.125in thick plate.

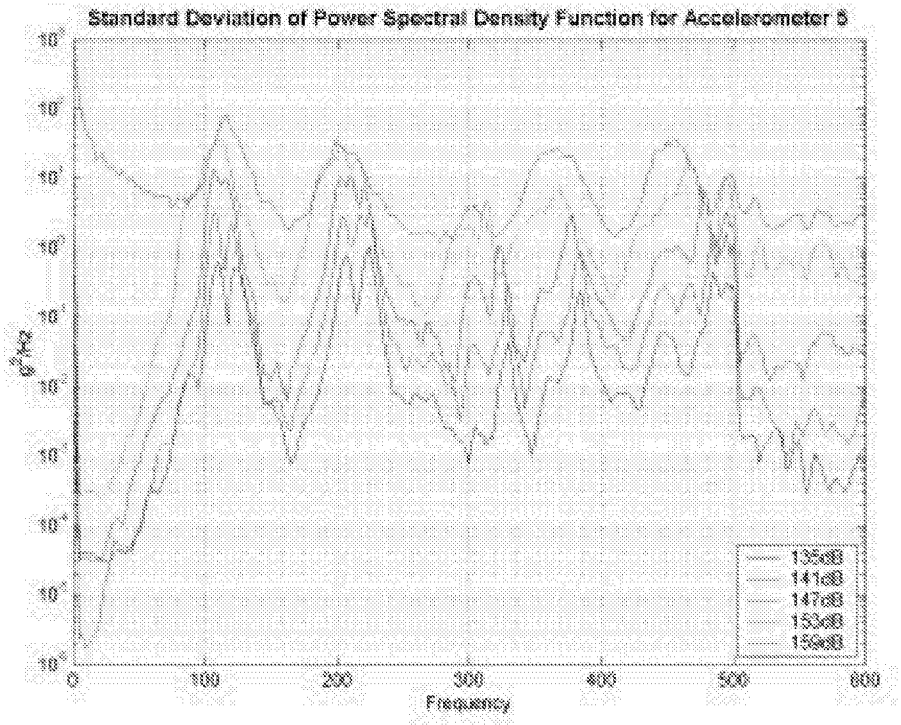

Figure A-35. STD of PSD for Accelerometer 5 and 0.125in thick plate.

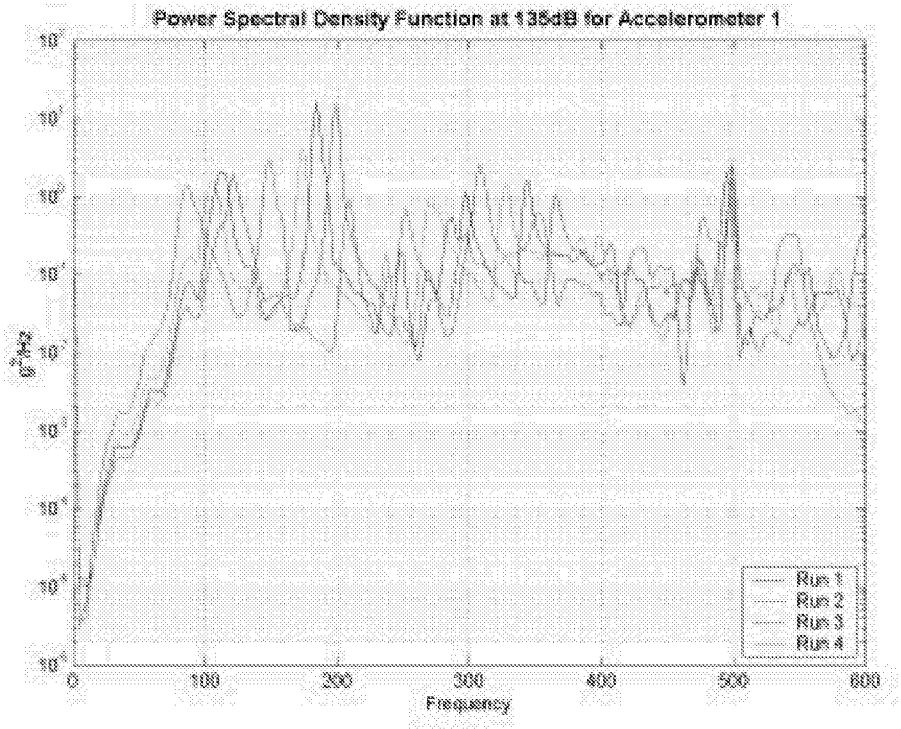

Figure A-36. PSD at 135dB for Accelerometer 1 and 0.062in thick plate.

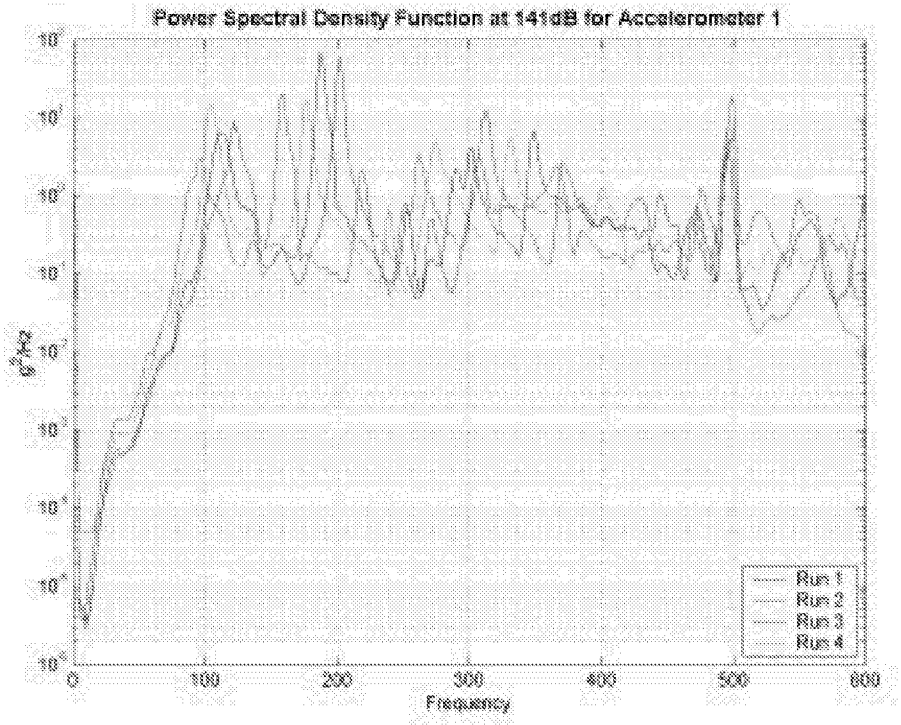

Figure A-37. PSD at 141dB for Accelerometer 1 and 0.062in thick plate.

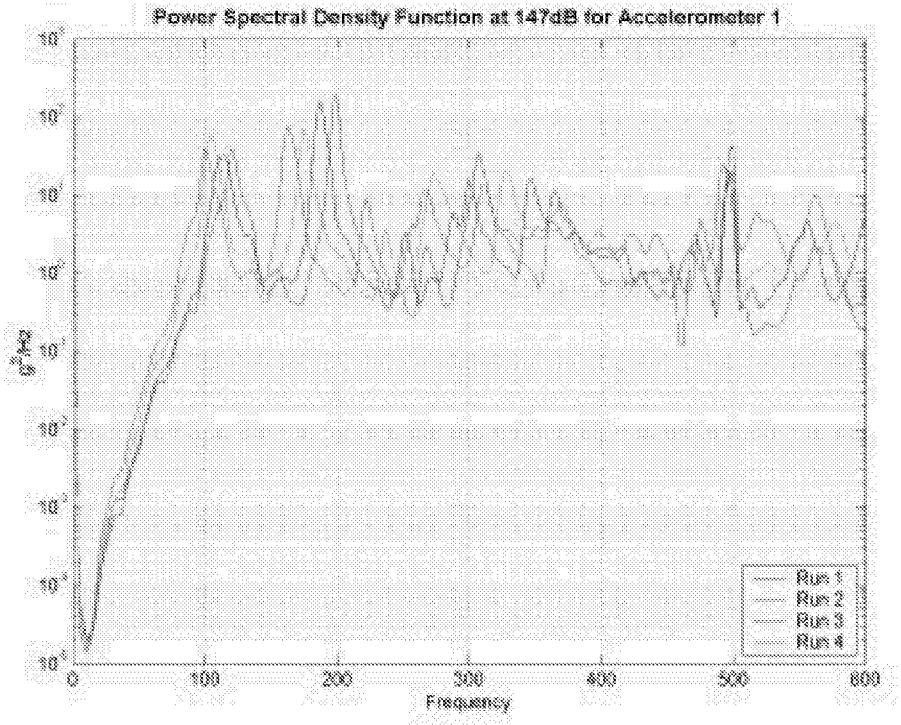

Figure A-38. PSD at 147dB for Accelerometer 1 and 0.062in thick plate.

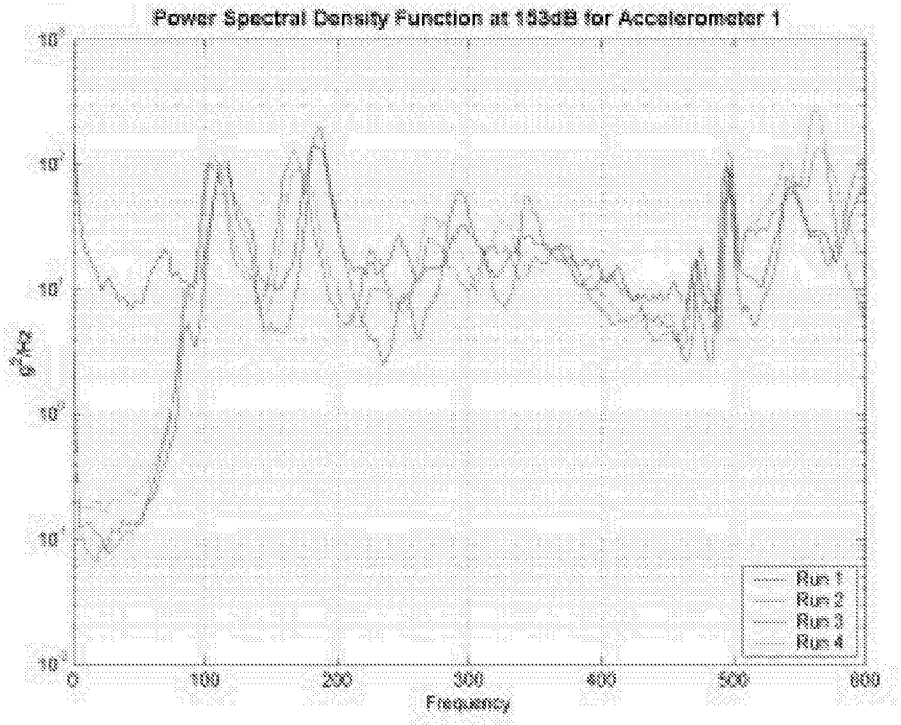

Figure A-39. PSD at 153dB for Accelerometer 1 and 0.062in thick plate.

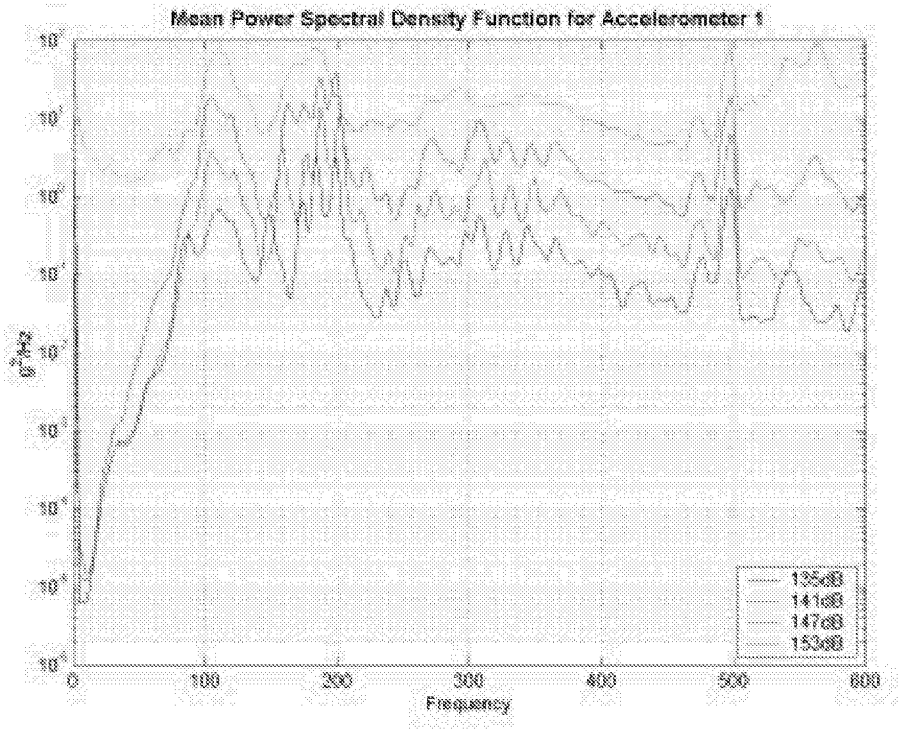

Figure A-40. Mean PSD for Accelerometer 1 and 0.062in thick plate.

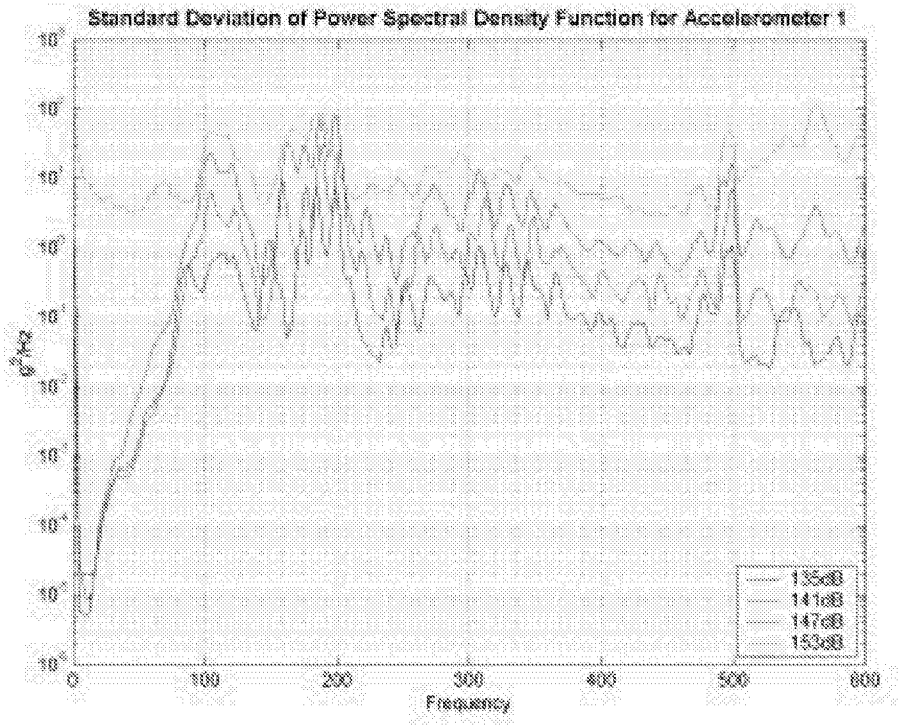

Figure A-41. STD of PSD for Accelerometer 1 and 0.062in thick plate.

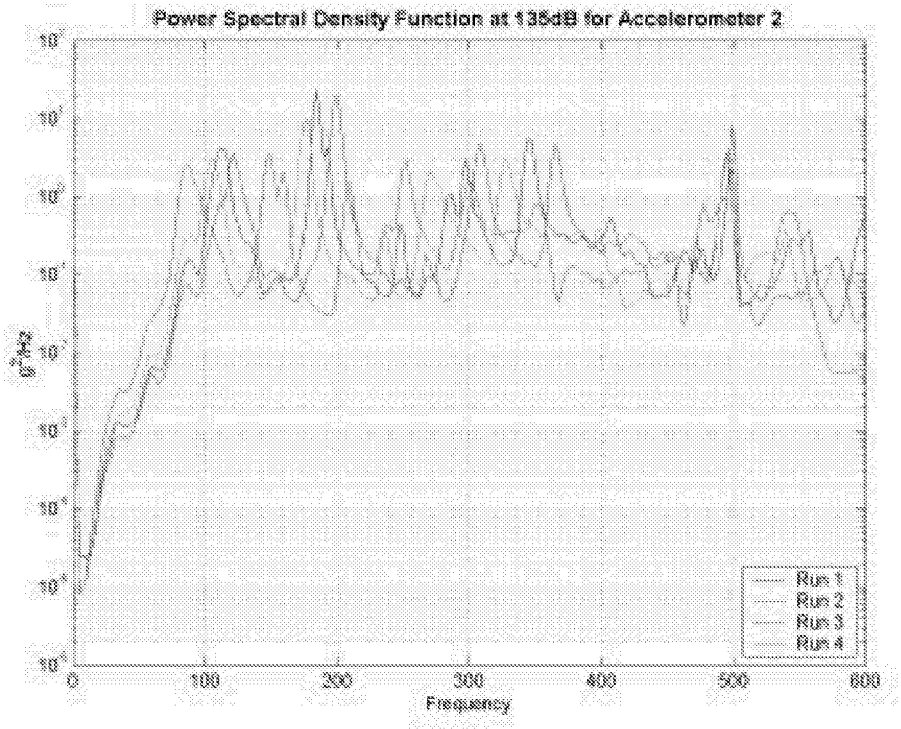

Figure A-42. PSD at 135dB for Accelerometer 2 and 0.062in thick plate.

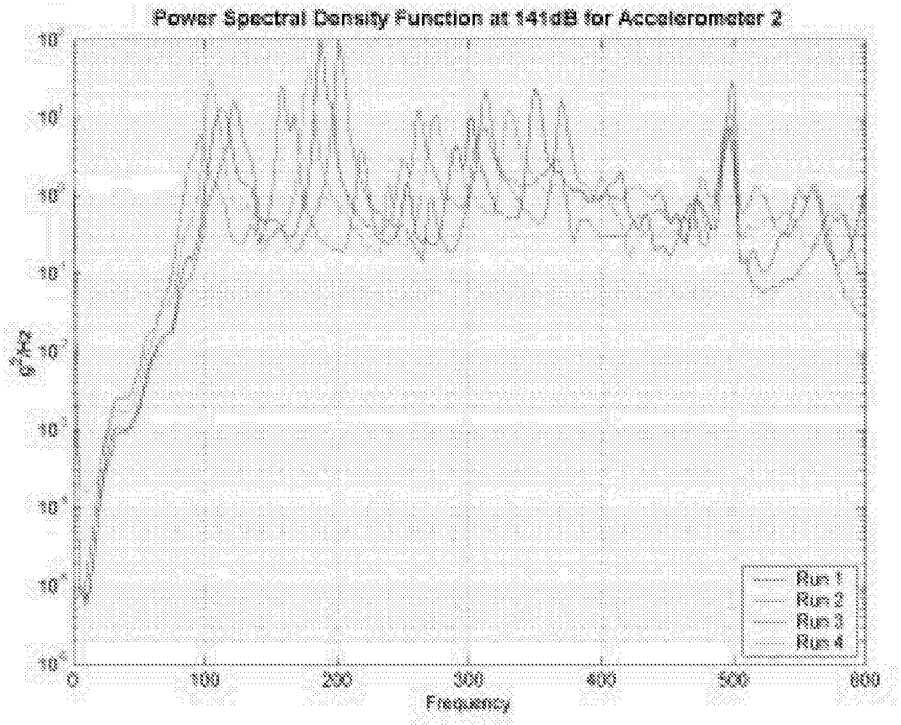

Figure A-43. PSD at 141dB for Accelerometer 2 and 0.062in thick plate.

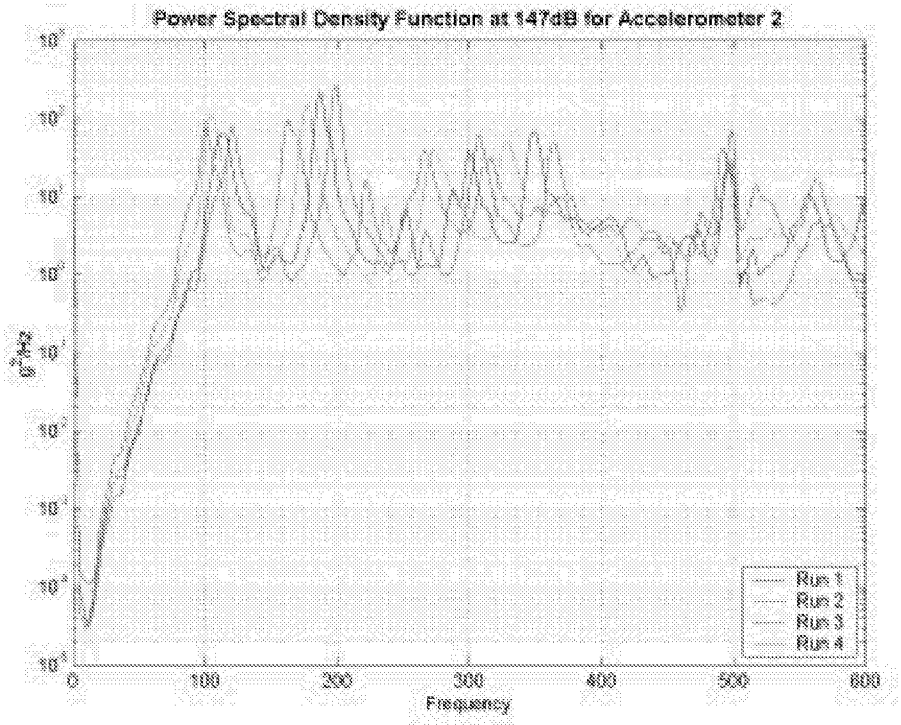

Figure A-44. PSD at 147dB for Accelerometer 2 and 0.062in thick plate.

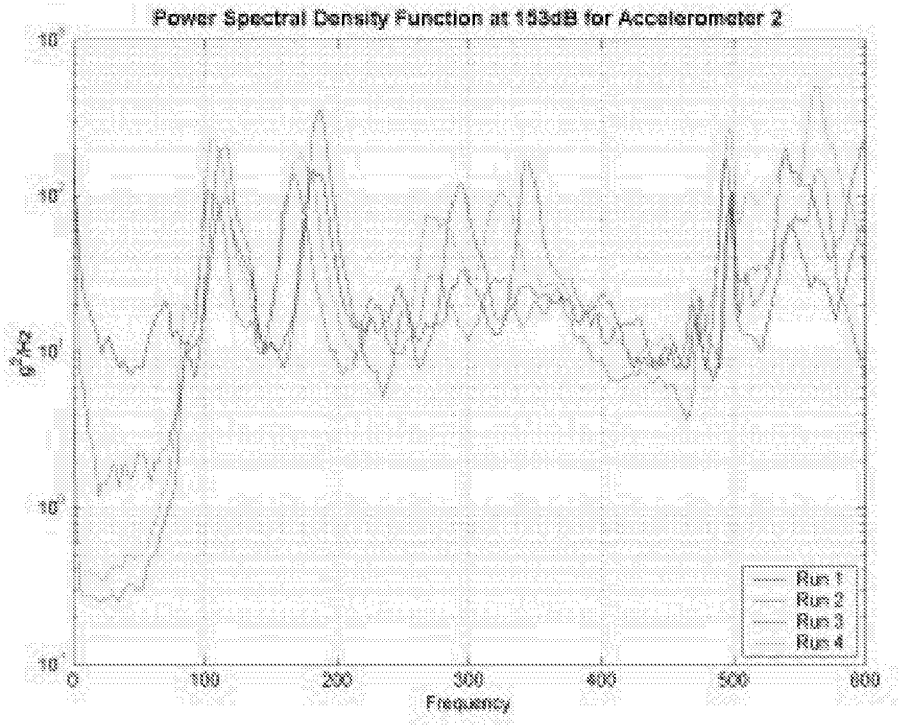

Figure A-45. PSD at 153dB for Accelerometer 2 and 0.062in thick plate.

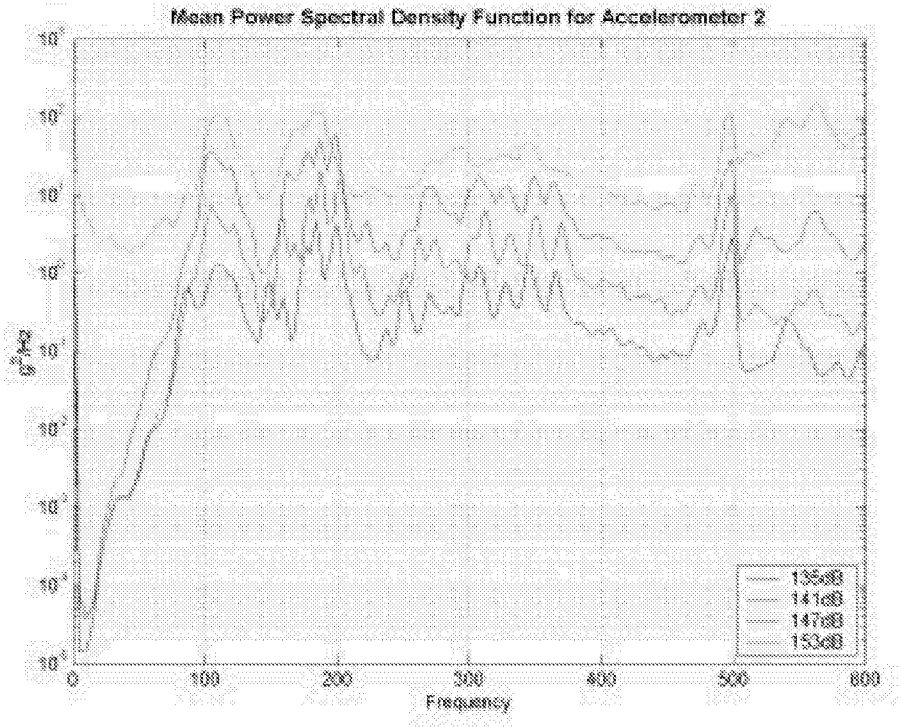

Figure A-46. Mean PSD for Accelerometer 2 and 0.062in thick plate.

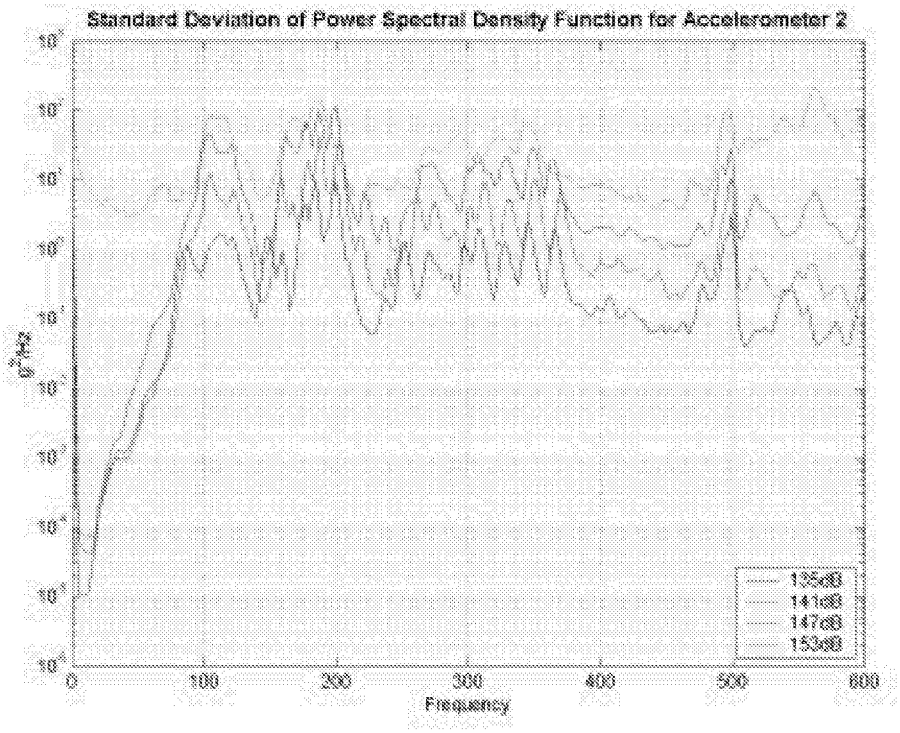

Figure A-47. STD of PSD for Accelerometer 2 and 0.062in thick plate.

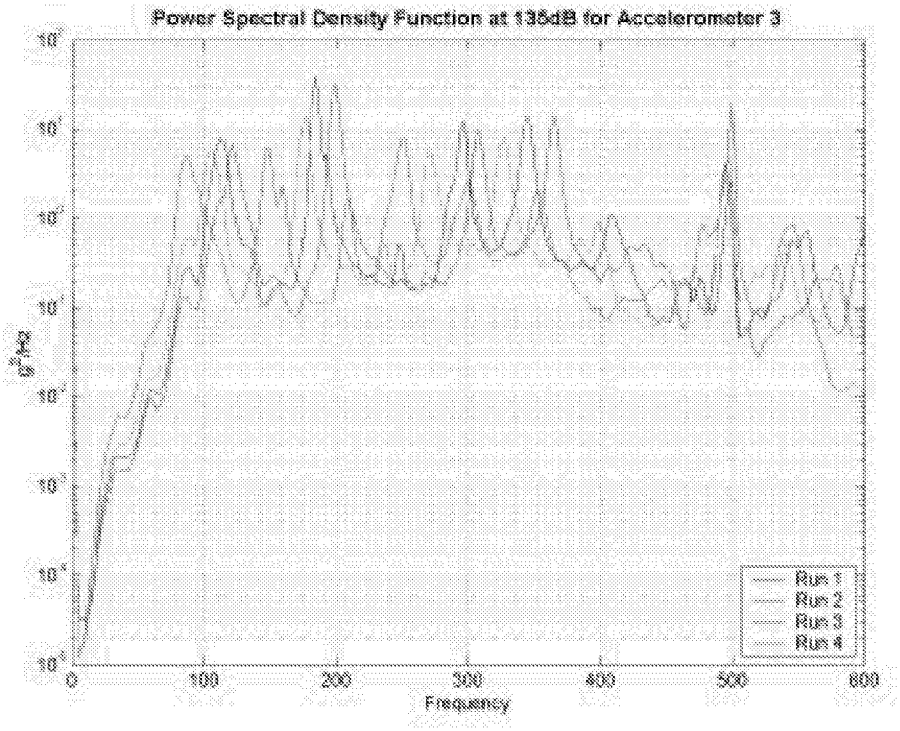

Figure A-48. PSD at 135dB for Accelerometer 3 and 0.062in thick plate.

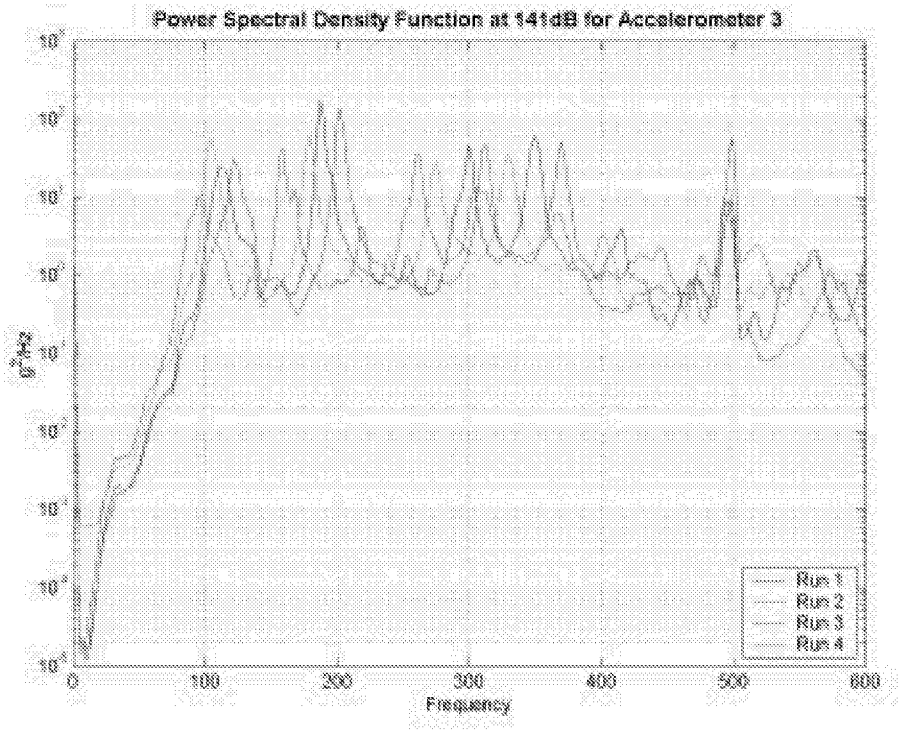

Figure A-49. PSD at 141dB for Accelerometer 3 and 0.062in thick plate.

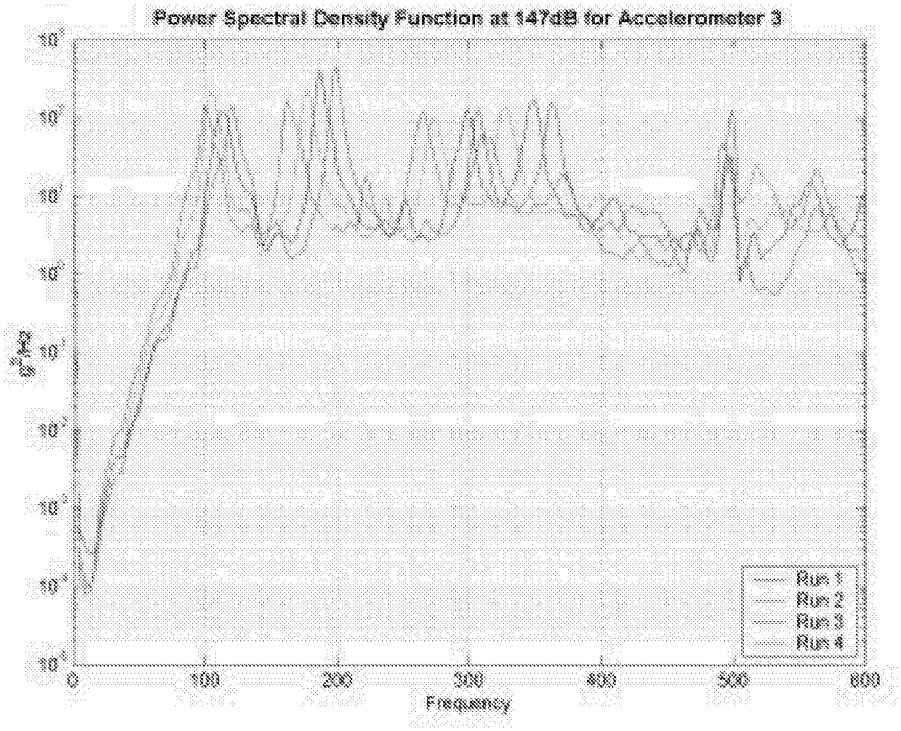

Figure A-50. PSD at 147dB for Accelerometer 3 and 0.062in thick plate.

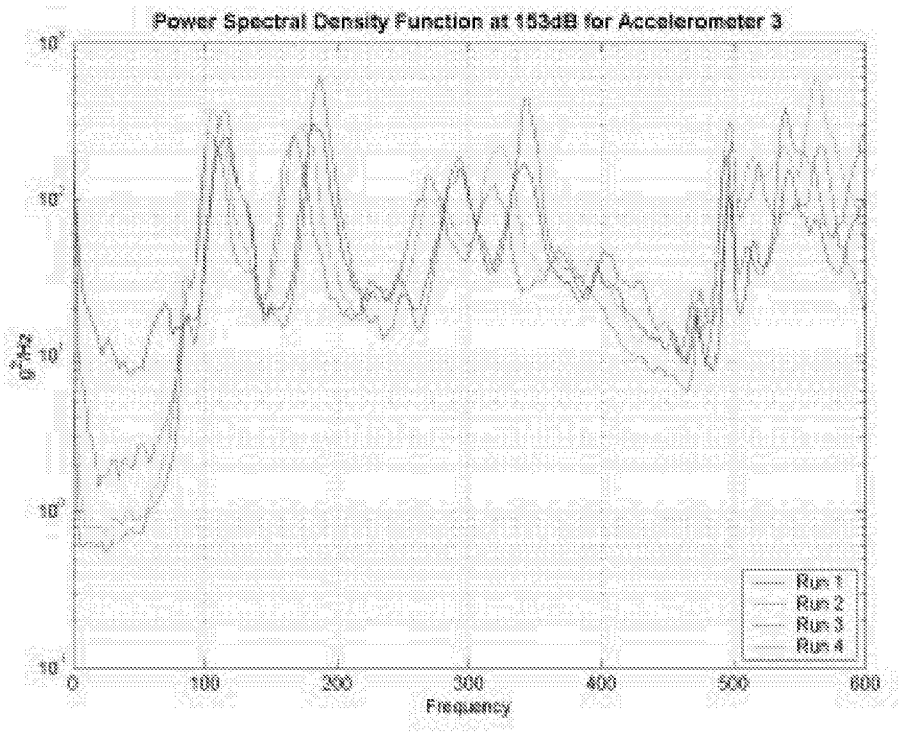

Figure A-51. PSD at 153dB for Accelerometer 3 and 0.062in thick plate.

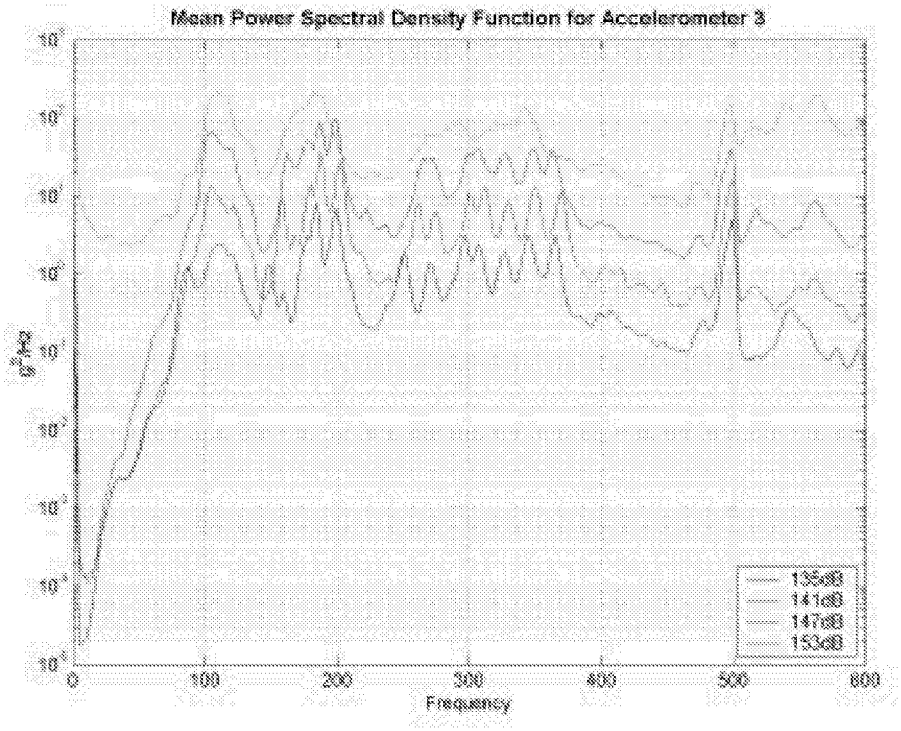

Figure A-52. Mean PSD for Accelerometer 3 and 0.062in thick plate.

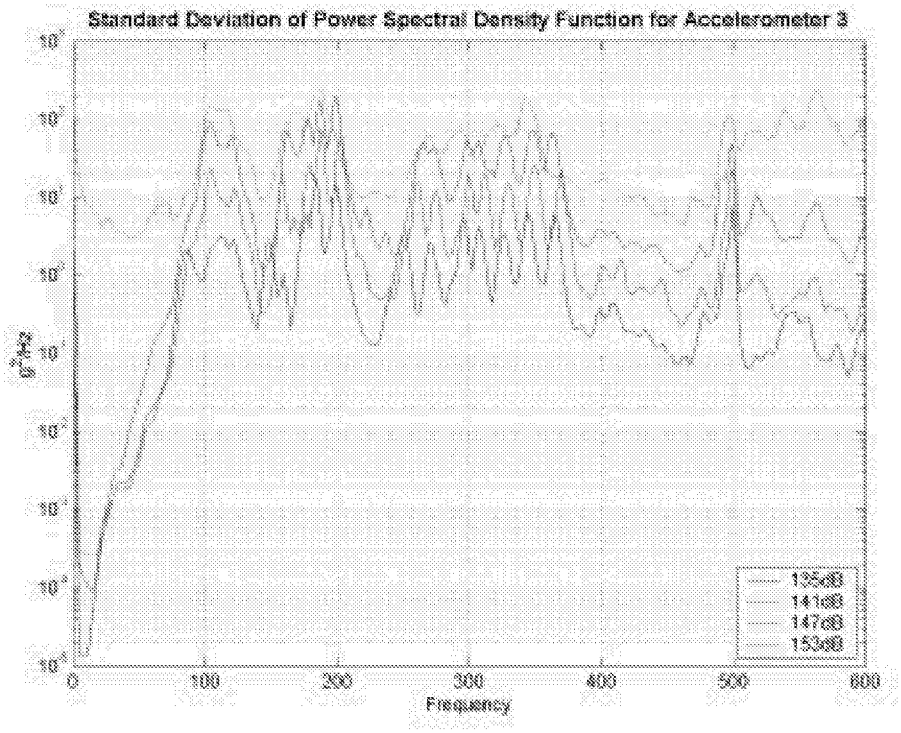

Figure A-53. STD of PSD for Accelerometer 3 and 0.062in thick plate.

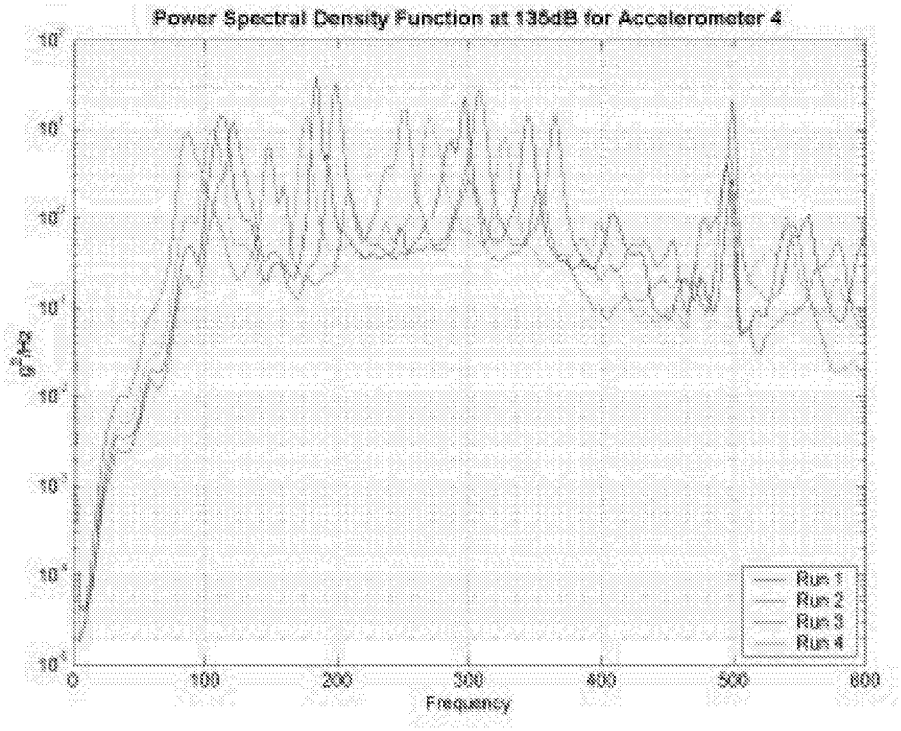

Figure A-54. PSD at 135dB for Accelerometer 4 and 0.062in thick plate.

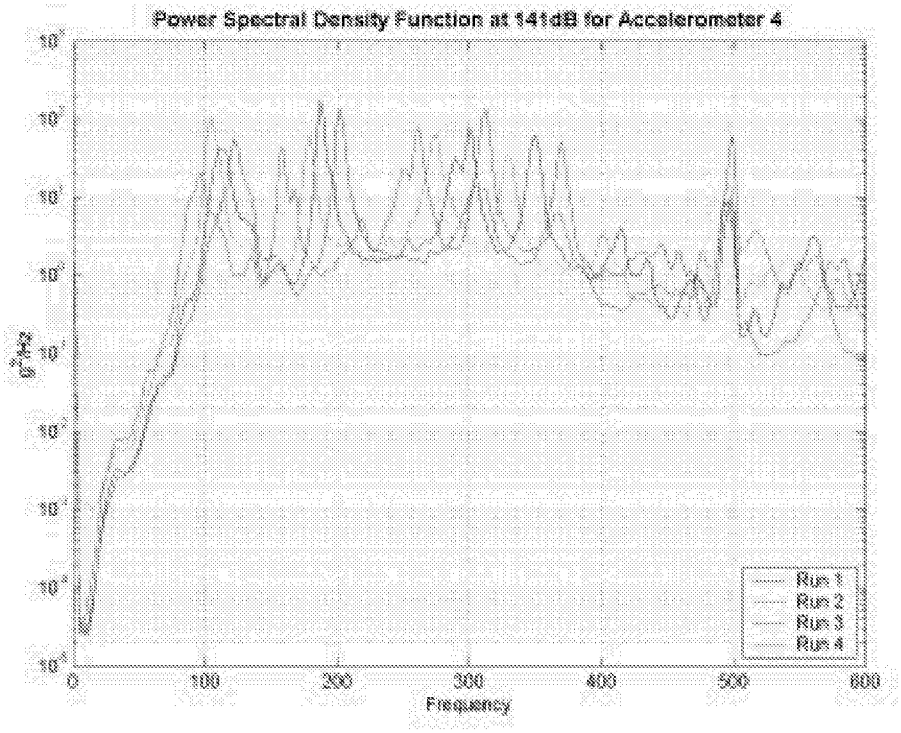

Figure A-55. PSD at 141dB for Accelerometer 4 and 0.062in thick plate.

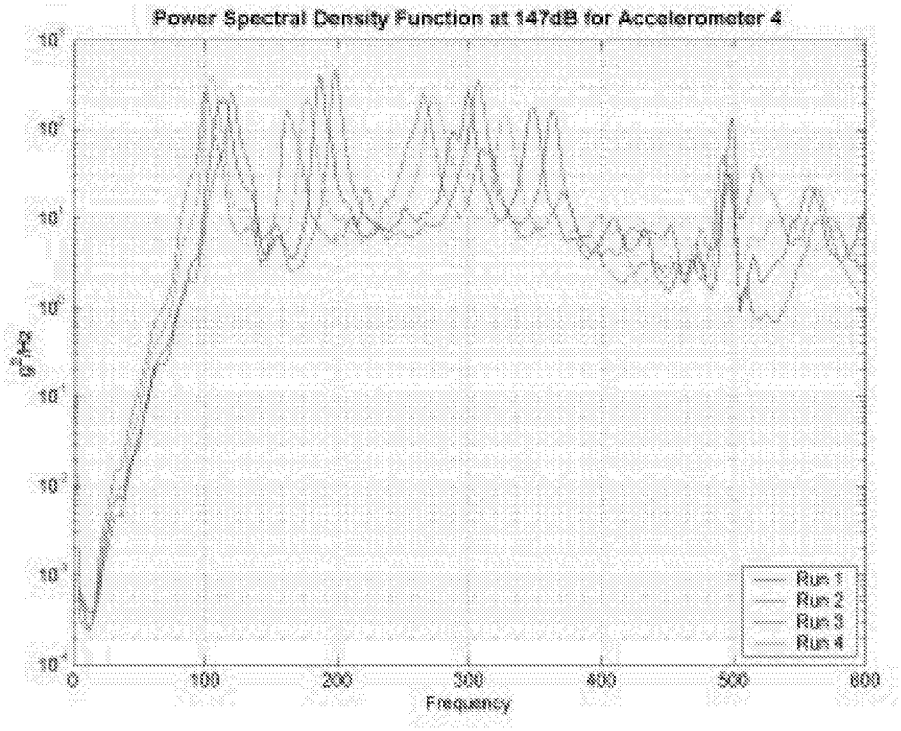

Figure A-56. PSD at 147dB for Accelerometer 4 and 0.062in thick plate.

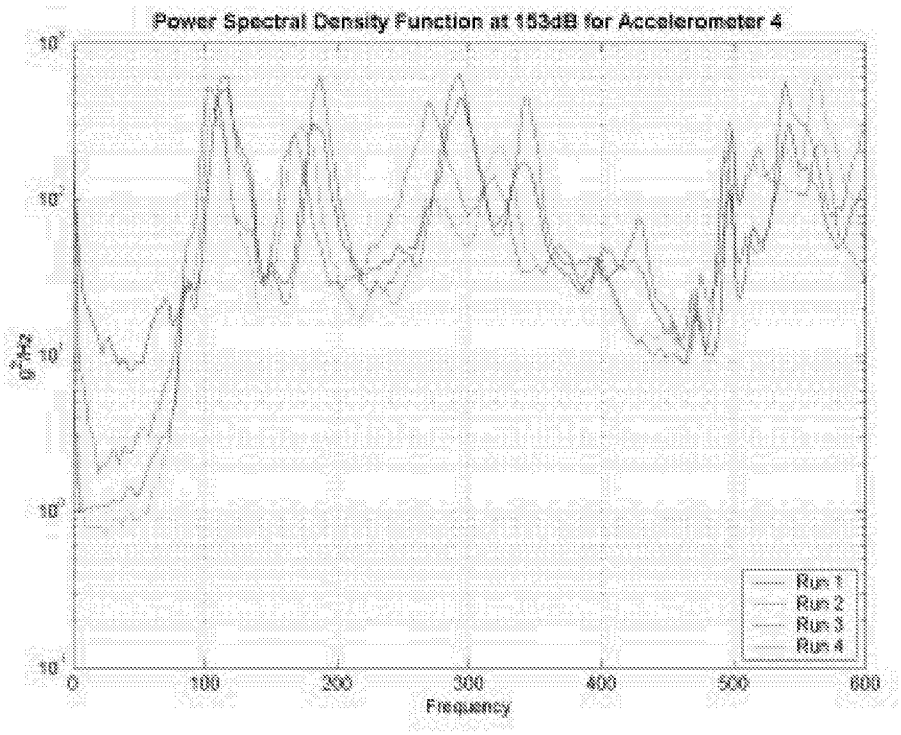

Figure A-57. PSD at 153dB for Accelerometer 4 and 0.062in thick plate.

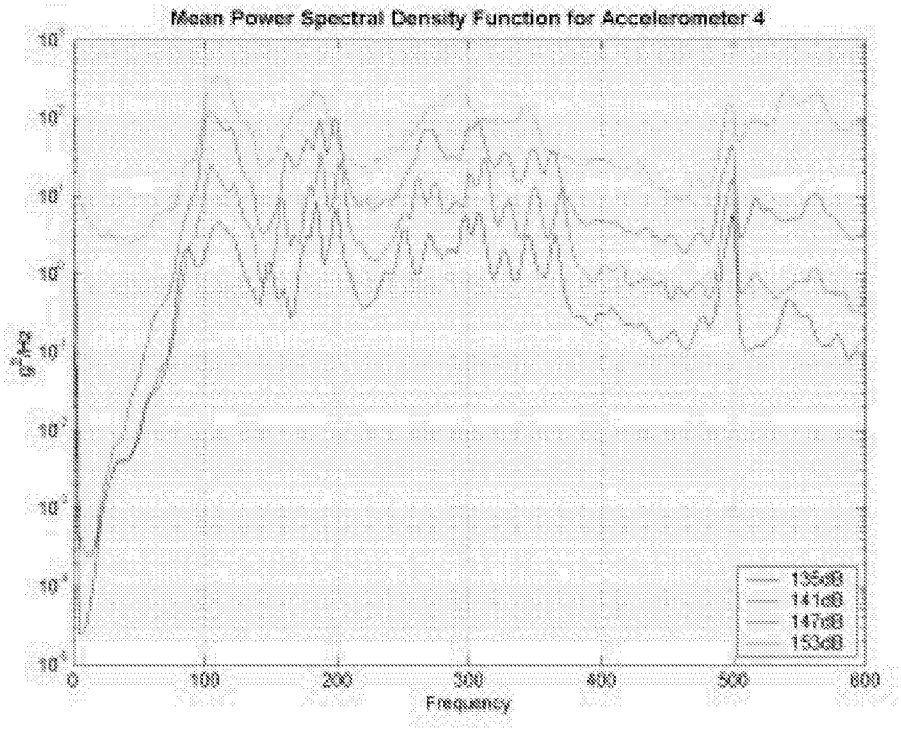

Figure A-58. Mean PSD for Accelerometer 4 and 0.062in thick plate.

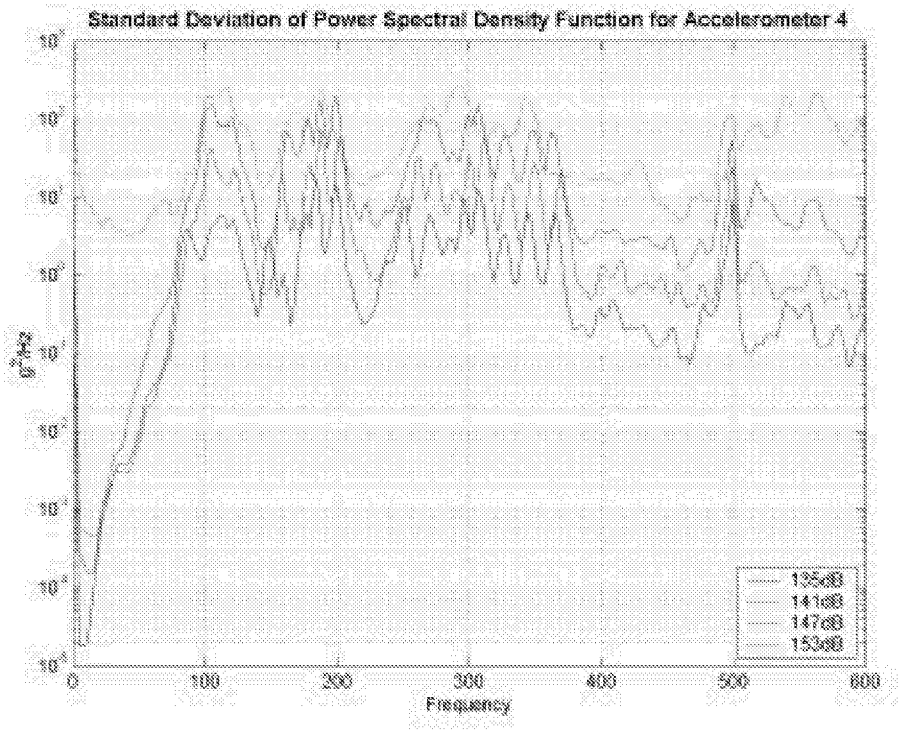

Figure A-59. STD of PSD for Accelerometer 4 and 0.062in thick plate.

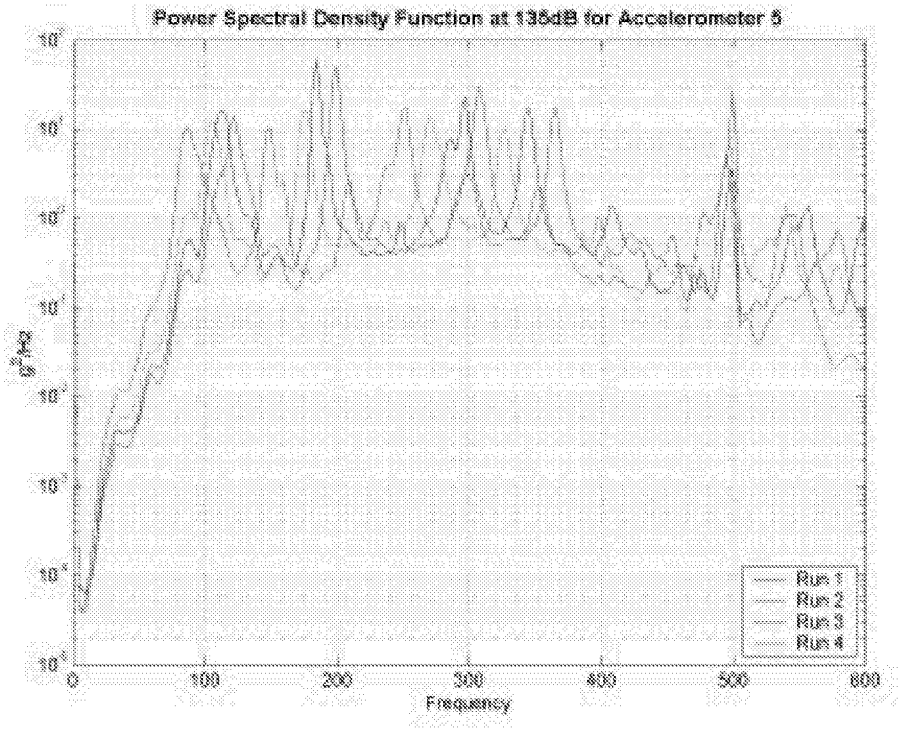

Figure A-60. PSD at 135dB for Accelerometer 5 and 0.062in thick plate.

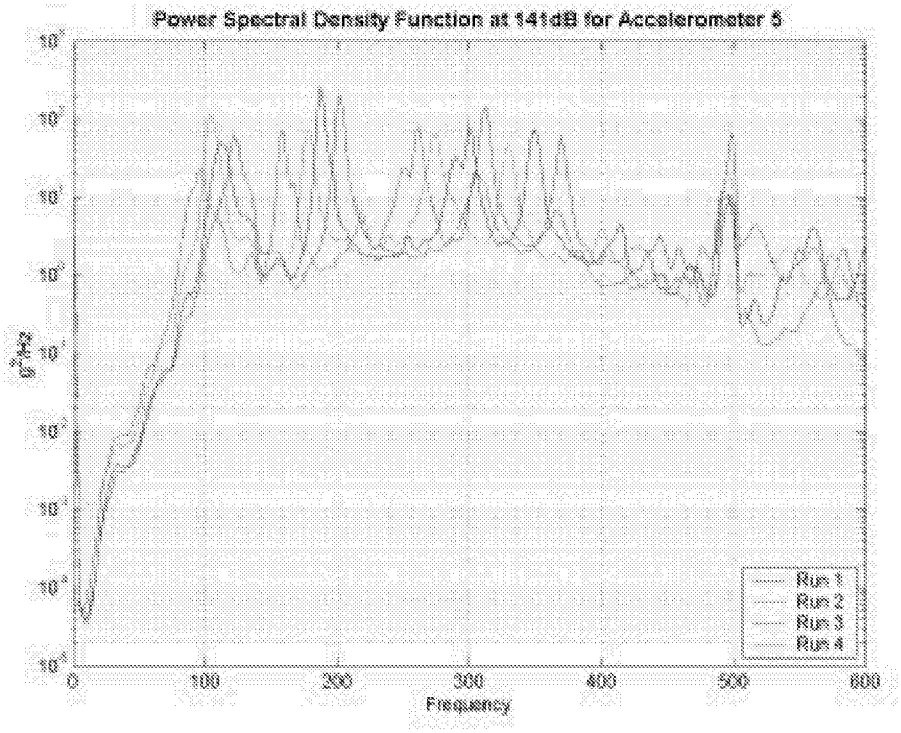

Figure A-61. PSD at 141dB for Accelerometer 5 and 0.062in thick plate.

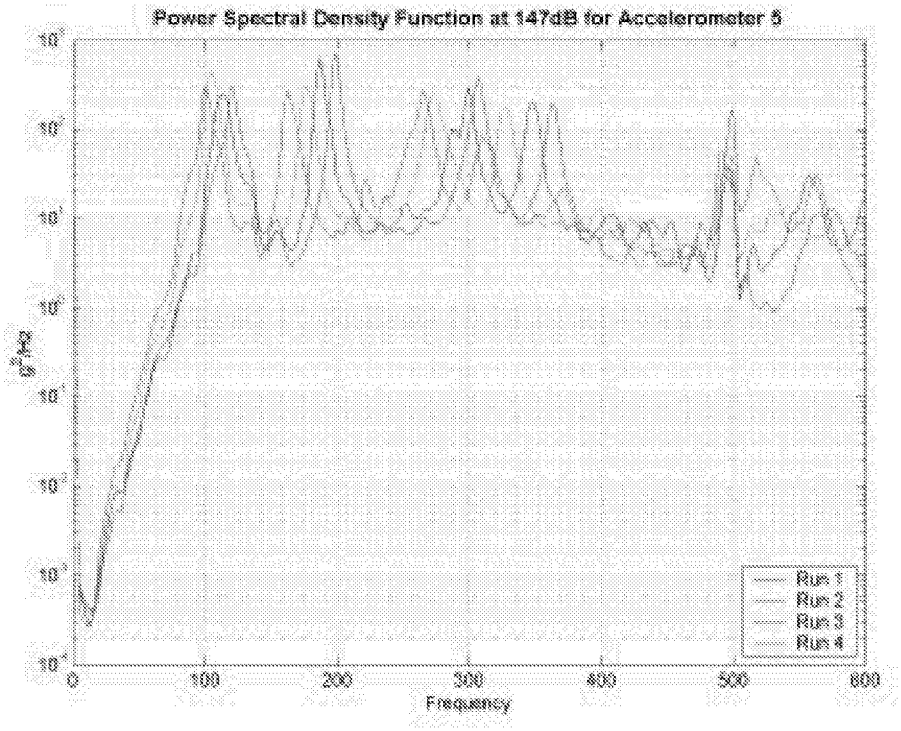

Figure A-62. PSD at 147dB for Accelerometer 5 and 0.062in thick plate.

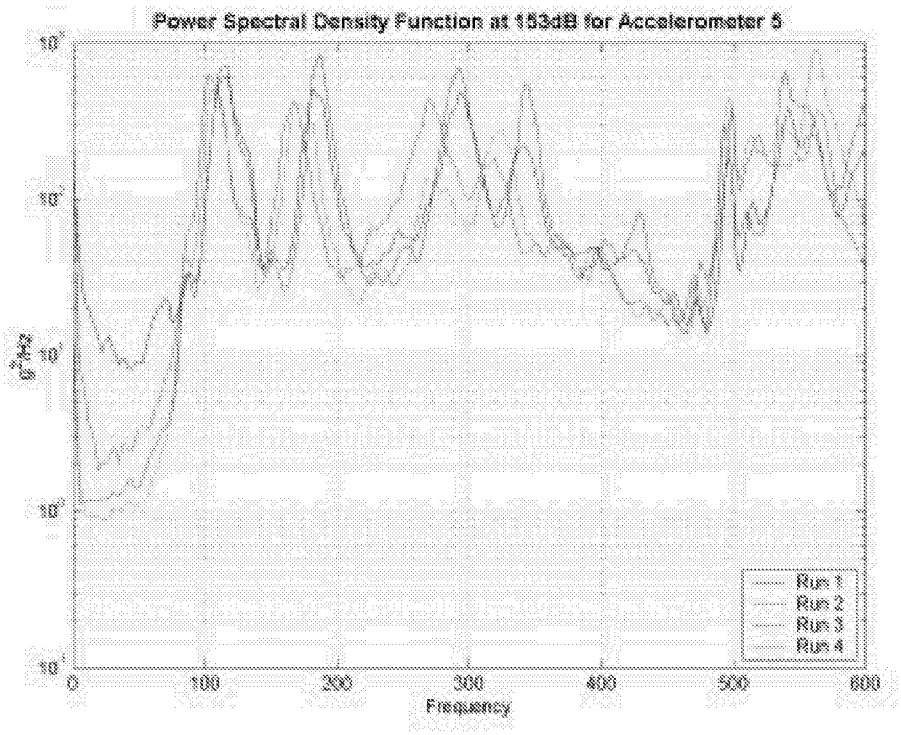

Figure A-63. PSD at 153dB for Accelerometer 5 and 0.062in thick plate.

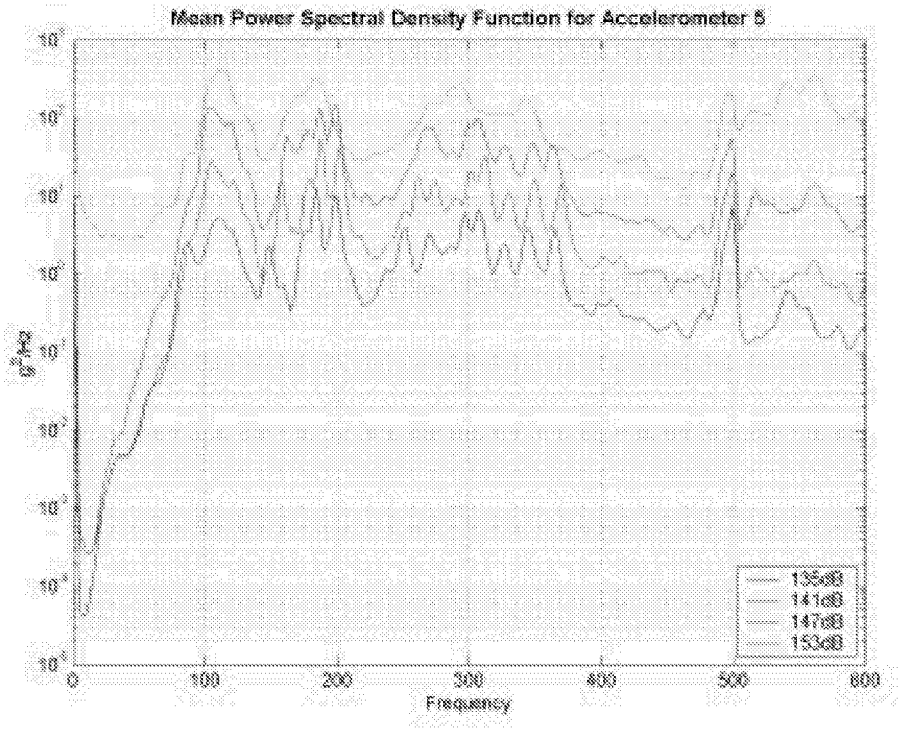

Figure A-64. Mean PSD for Accelerometer 5 and 0.062in thick plate.

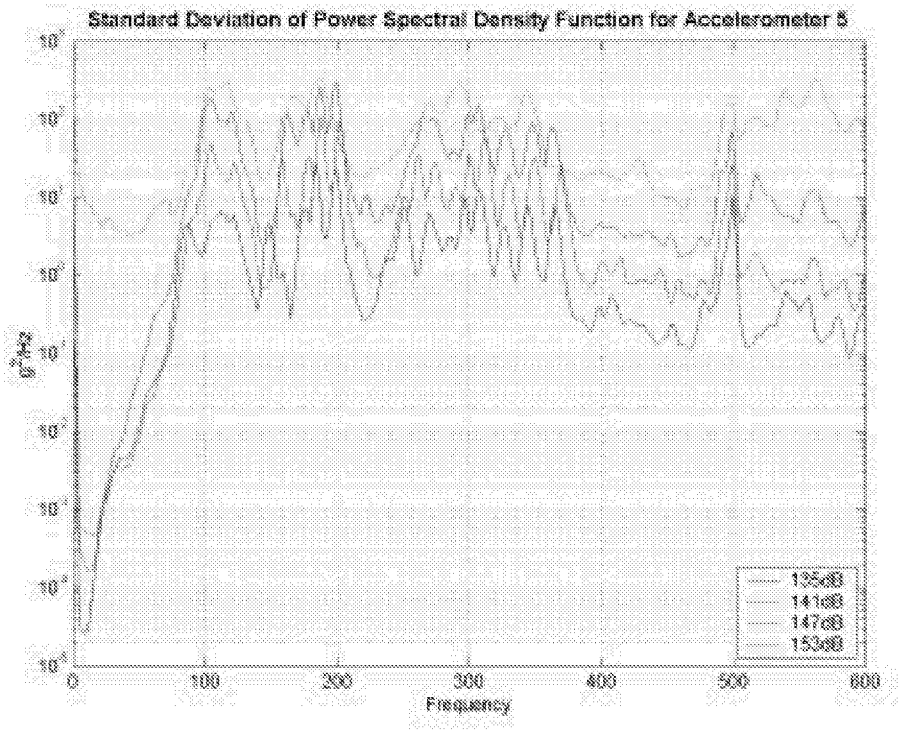

Figure A-65. STD of PSD for Accelerometer 5 and 0.062in thick plate.

Appendix B: Complete RMS Results

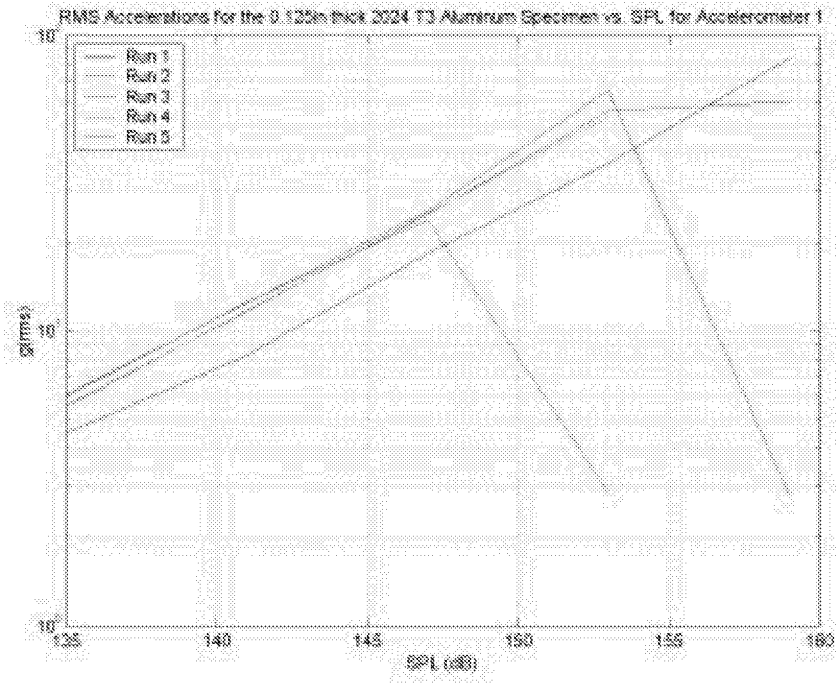

Figure B-1. RMS Accelerations vs. OASPL for Accelerometer 1 and the 0.125in plate.

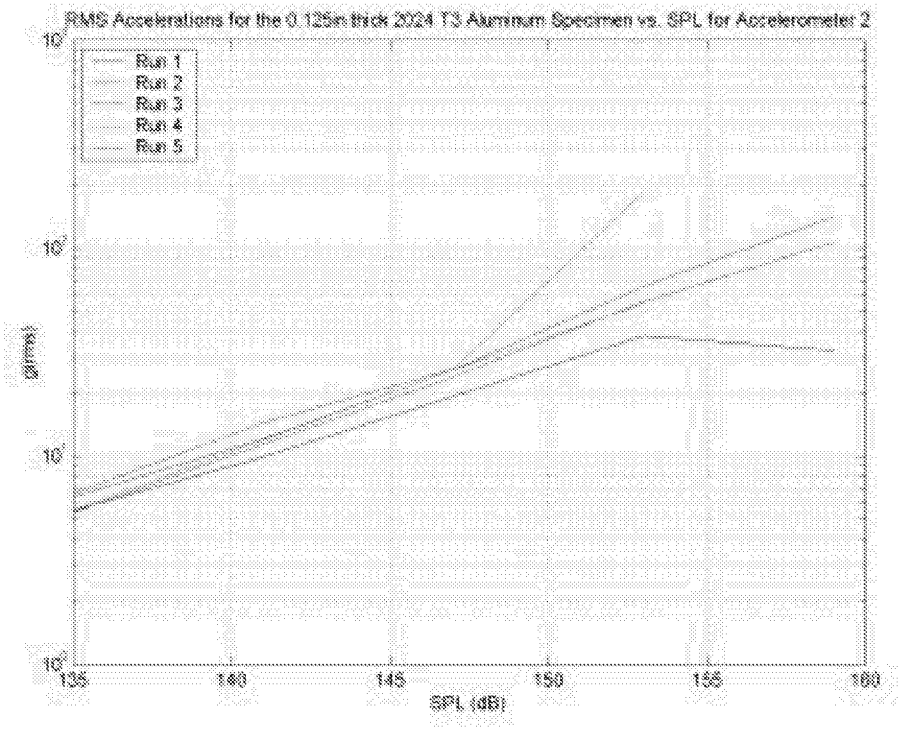

Figure B-2. RMS Accelerations vs. OASPL for Accelerometer 2 and the 0.125in plate

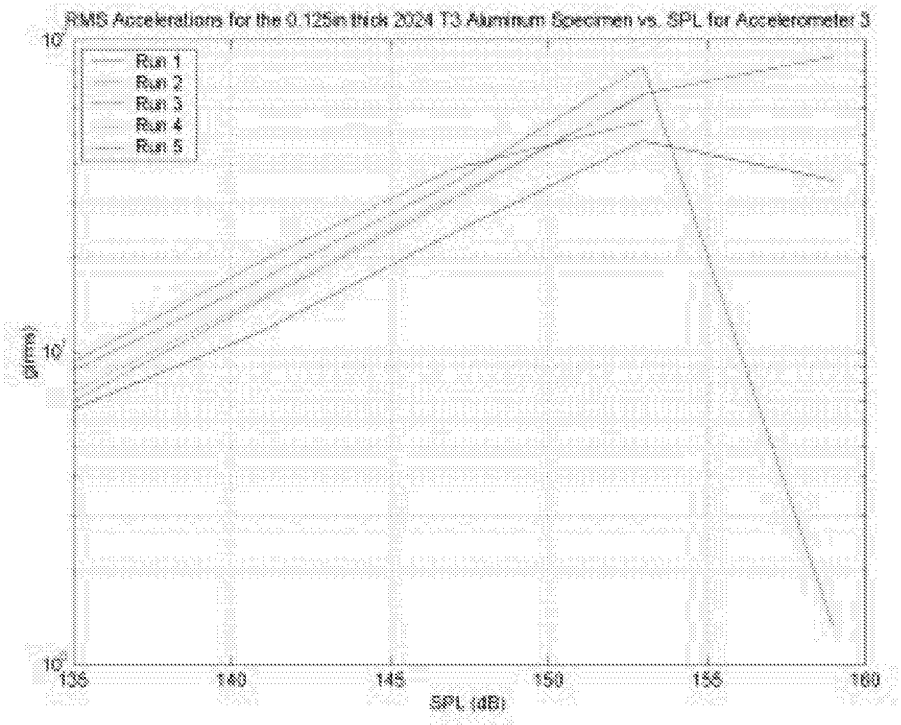

Figure B-3. RMS Accelerations vs. OASPL for Accelerometer 3 and the 0.125in plate

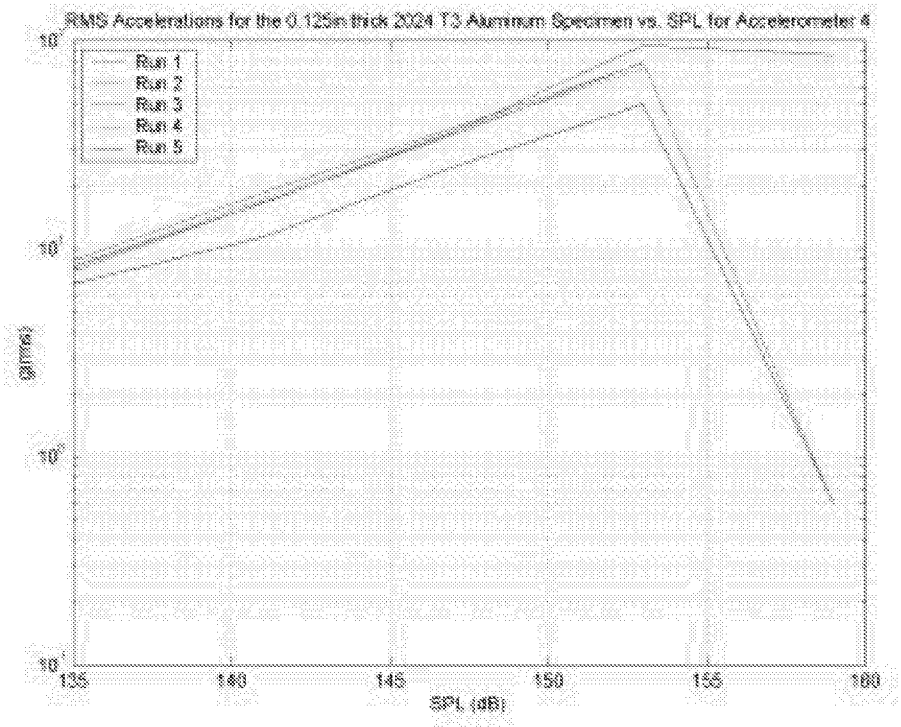

Figure B-4. RMS Accelerations vs. OASPL for Accelerometer 4 and the 0.125in plate

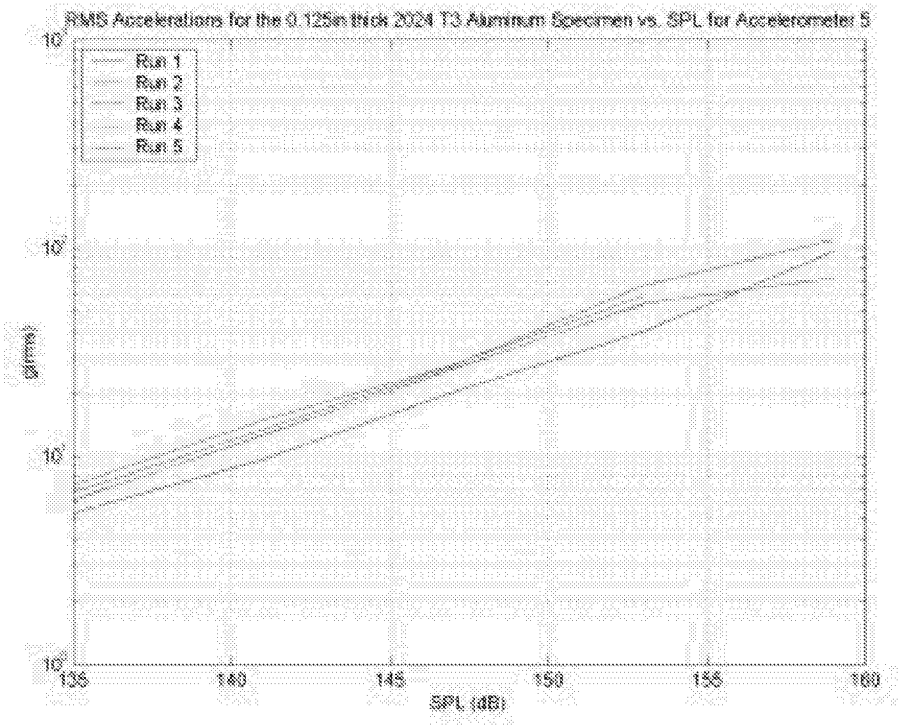

Figure B-5. RMS Accelerations vs. OASPL for Accelerometer 5 and the 0.125in plate

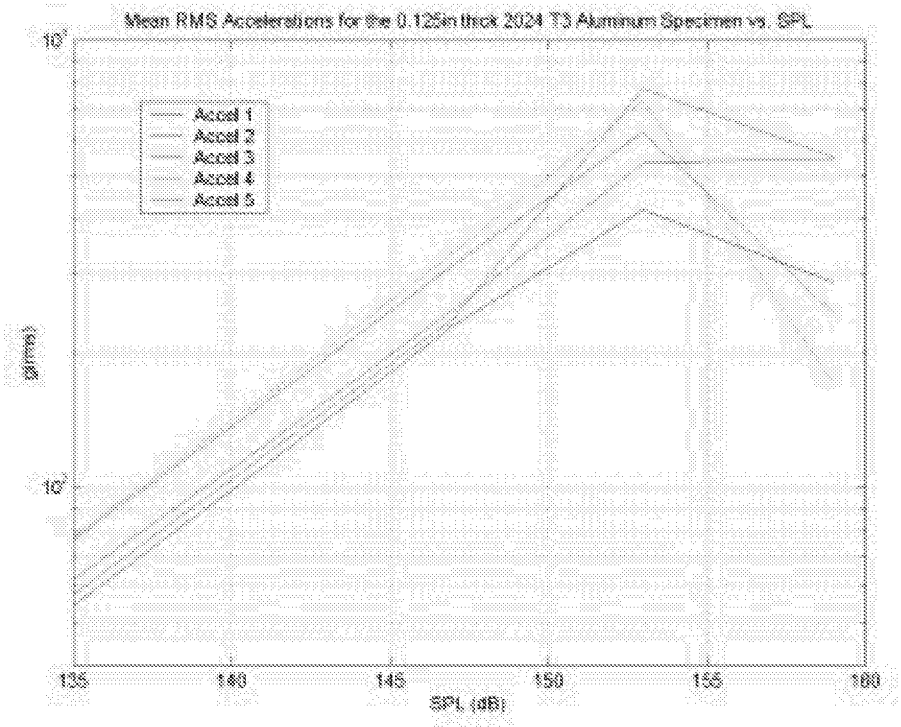

Figure B-6. Mean RMS Accelerations vs. OASPL for the 0.125in plate.

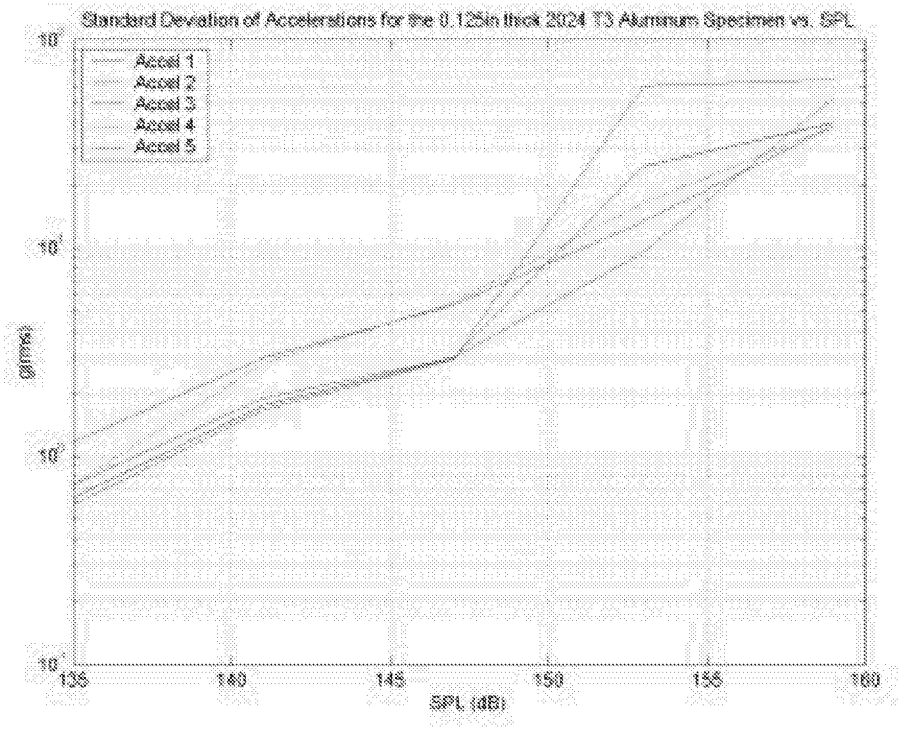

Figure B-7. STD of Accelerations vs. OASPL for the 0.125in plate.

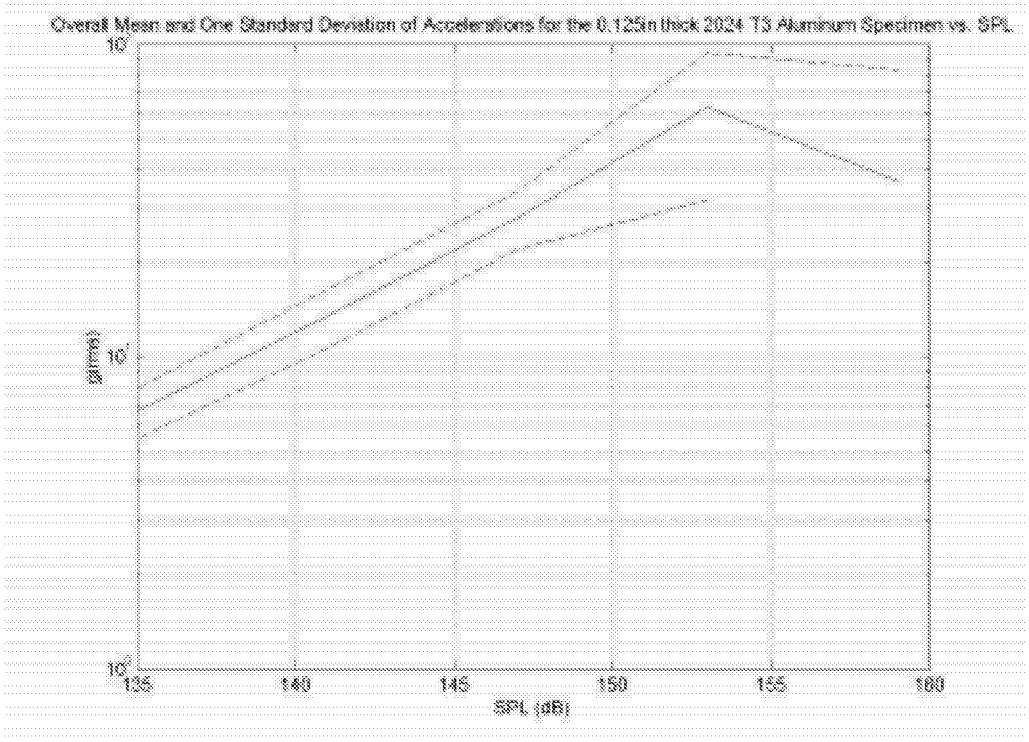

Figure B-8. Overall Mean and STD of Accelerations vs. OASPL for the 0.125in plate.

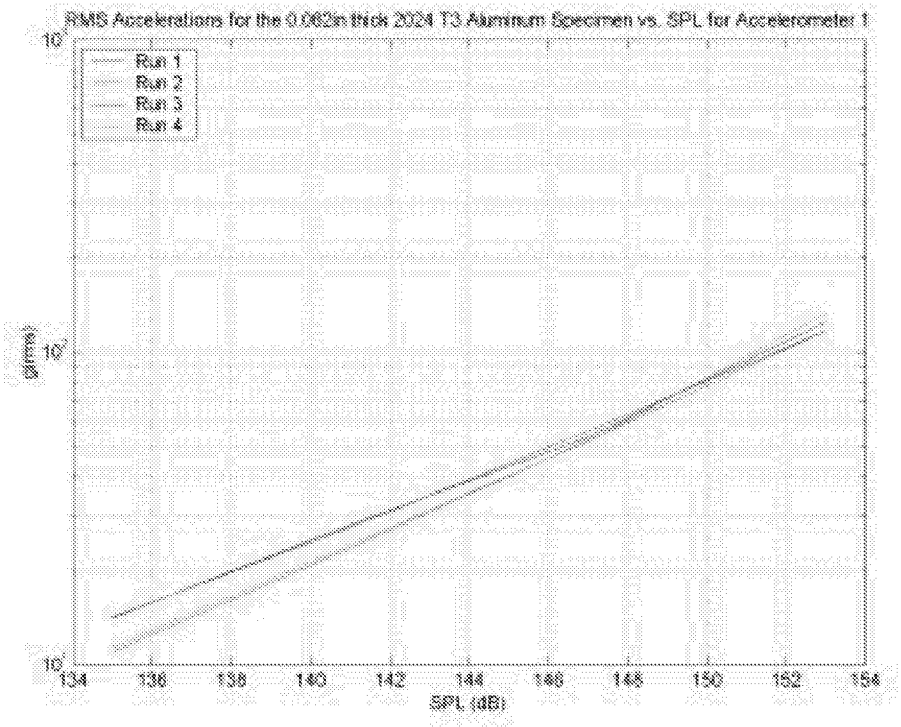

Figure B-9. RMS Accelerations vs. OASPL for Accelerometer 1 and the 0.062in plate.

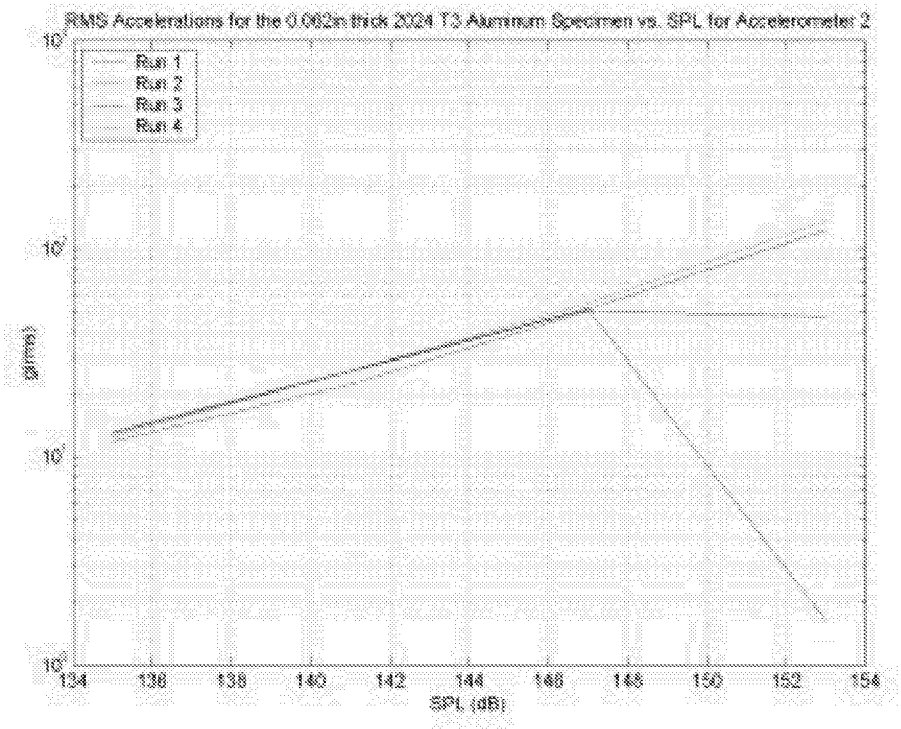

Figure B-10. RMS Accelerations vs. OASPL for Accelerometer 2 and the 0.062in plate.

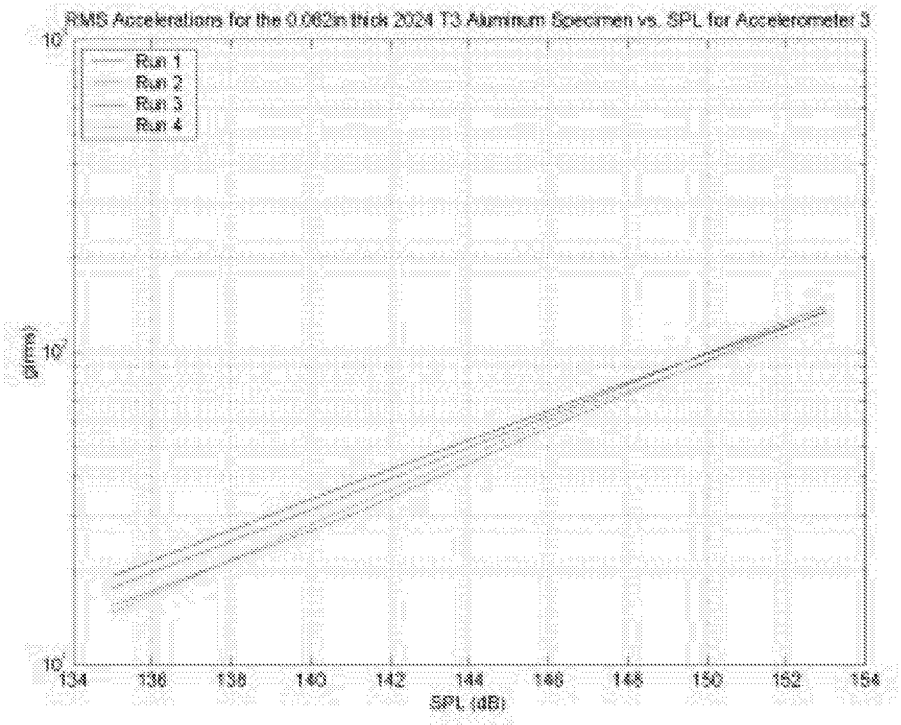

Figure B-11. RMS Accelerations vs. OASPL for Accelerometer 3 and the 0.062in plate.

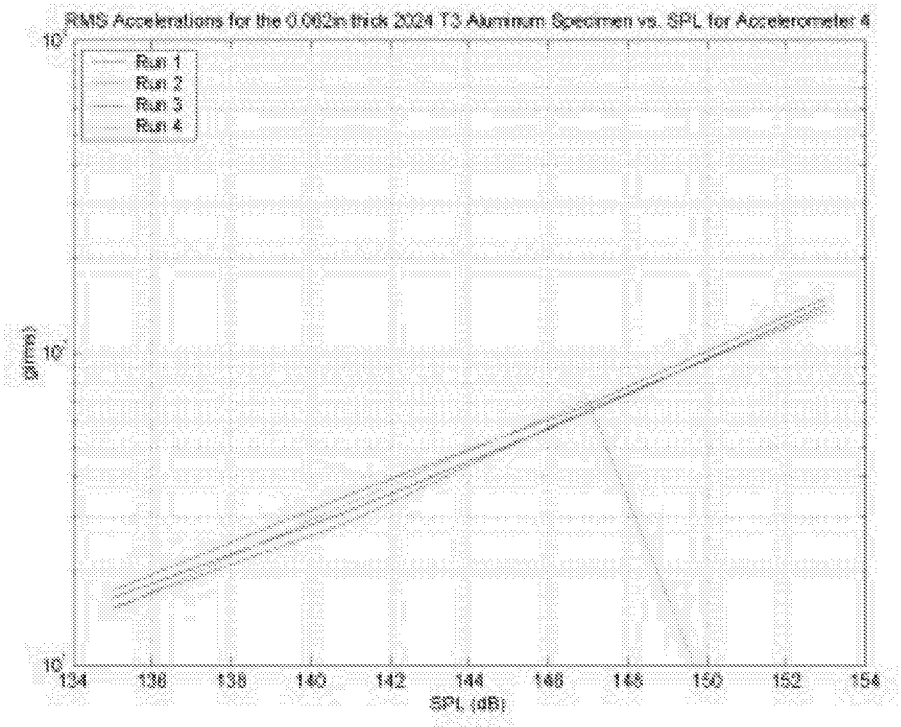

Figure B-12. RMS Accelerations vs. OASPL for Accelerometer 4 and the 0.062in plate.

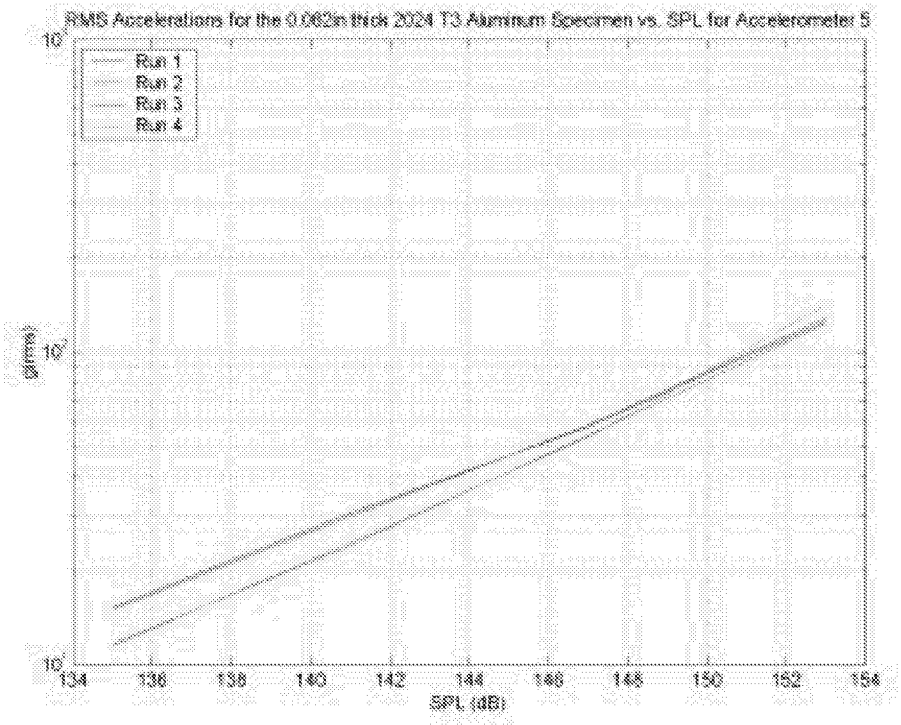

Figure B-13. RMS Accelerations vs. OASPL for Accelerometer 5 and the 0.062in plate.

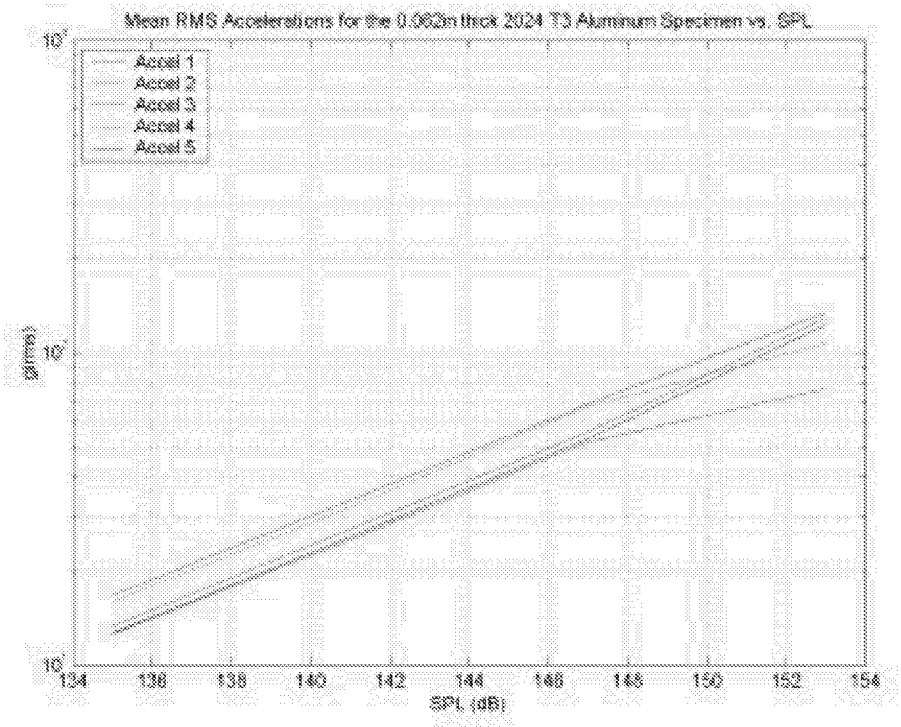

Figure B-14. Mean RMS Accelerations vs. OASPL for the 0.062in plate.

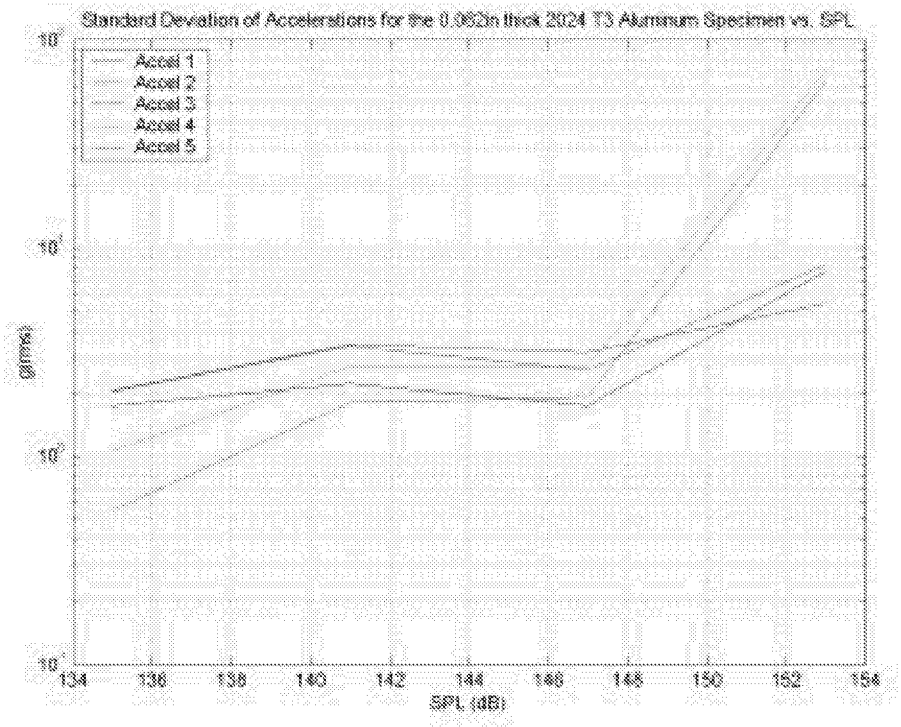

Figure B-15. STD of Accelerations vs. OASPL for the 0.062in plate.

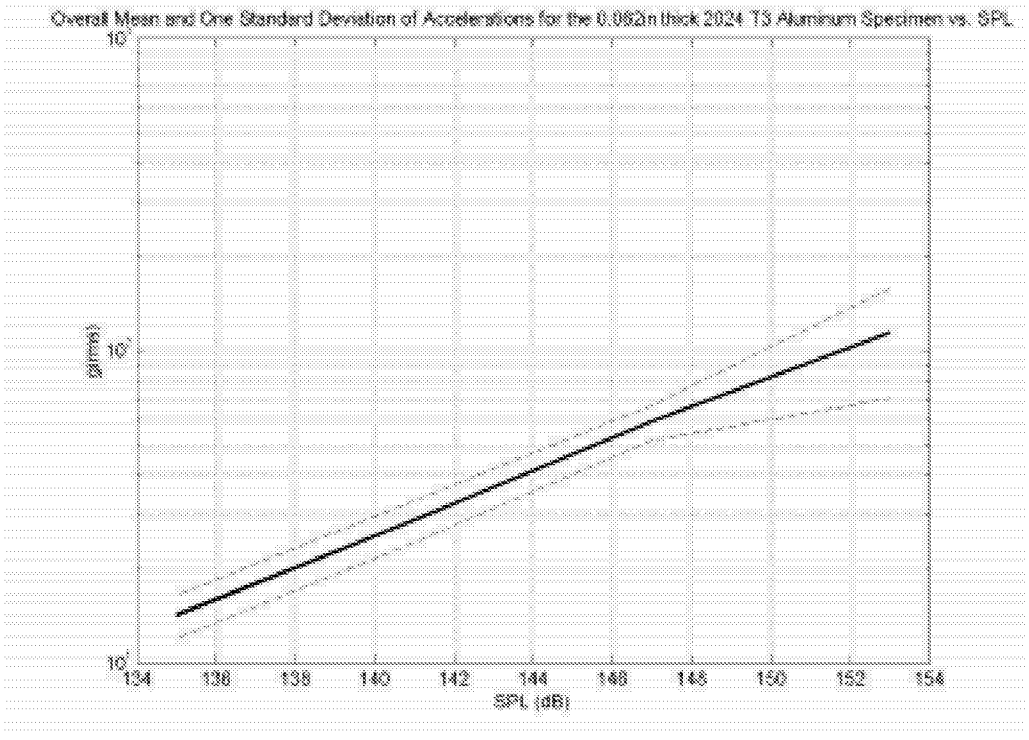

Figure B-16. Overall Mean and STD of Accelerations vs. OASPL for the 0.062in plate.

REPORT DOCUMENTATION PAGE

Form Approved
OMB No. 0704-0188

1. AGENCY USE ONLY (Leave blank)	2. REPORT DATE	3. REPORT TYPE AND DATES COVERED
	August 2001	Contractor Report

4. TITLE AND SUBTITLE
Experimental Structural Dynamic Response of Plate Specimens Due to Sonic Loads in a Progressive Wave Tube

5. FUNDING NUMBERS
C NAS1-00135
TA DF26
WU 706-63-71-81

6. AUTHOR(S)
Juan F. Betts

7. PERFORMING ORGANIZATION NAME(S) AND ADDRESS(ES)
Lockheed Martin Corporation
Langley Research Center, Mail Stop 371
Hampton, VA 23681-2199

8. PERFORMING ORGANIZATION REPORT NUMBER

9. SPONSORING/MONITORING AGENCY NAME(S) AND ADDRESS(ES)
National Aeronautics and Space Administration
Langley Research Center
Hampton, VA 23681-2199

10. SPONSORING/MONITORING AGENCY REPORT NUMBER
NASA/CR-2001-211045

11. SUPPLEMENTARY NOTES
This report was prepared for Langley Research Center by Lockheed Martin Corporation under subcontract to Swales Aerospace, Hampton, Virginia.
Langley Technical Monitor: Richard J. Silcox

12a. DISTRIBUTION/AVAILABILITY STATEMENT
Unclassified-Unlimited
Subject Category 71 Distribution: Standard
Availability: NASA CASI (301) 621-0390

12b. DISTRIBUTION CODE

13. ABSTRACT (Maximum 200 words)
The objective of the current study was to assess the repeatability of experiments at NASA Langley's Thermal Acoustic Fatigue Apparatus (TAFA) facility and to use these experiments to validate numerical models. Experiments show that power spectral density (PSD) curves were repeatable except at the resonant frequencies, which tended to vary between 5Hz to 15Hz. Results show that the thinner specimen had more variability in the resonant frequency location than the thicker sample, especially for modes higher than the first mode in the frequency range. Root Mean Square (RMS) tended to be more repeatable. The RMS behaved "linearly" through the SPL range of 135 to 153dB. Standard Deviations (STDs) of the results tended to be relatively low constant up to about 147dB. The RMS results were more repeatable than the PDS results. The STD results were less than 10% of the RMS results for both the 0.125in (0.318cm) and 0.062in (0.1588cm) thick plate. The STD of the PSD results were around 20% to 100% of the mean PSD results for non-resonant and resonant frequencies, respectively, for the 0.125in (0.318cm) thicker plate and between 25% to 125% of the mean PSD results, for nonresonant and resonant frequencies, respectively, for the thinner plate.

14. SUBJECT TERMS
Plates; Structural Dynamics; Acoustics; Progressive Wave Tube

15. NUMBER OF PAGES
97

16. PRICE CODE
A05

17. SECURITY CLASSIFICATION OF REPORT	18. SECURITY CLASSIFICATION OF THIS PAGE	19. SECURITY CLASSIFICATION OF ABSTRACT	20. LIMITATION OF ABSTRACT
Unclassified	Unclassified	Unclassified	UL